Magnetic Fabrics of granitic plutons and gneisses Northwestern Ontario

by

Lionel J.J. Charpentier

Lakehead
UNIVERSITY

OFFICE OF GRADUATE STUDIES

NAME OF STUDENT: Lionel J. J. Charpentier

DEGREE AWARDED: Master of Science

ACADEMIC UNIT: Geology

TITLE OF THESIS: Magnetic Fabrics of Granitic Plutons and Gneisses Northwestern Ontario

This thesis has been prepared

under my supervision

and the candidate has complied

with the Master's regulations.

Signature of Supervisor

2003/09/04

Date

Abstract

Specimens of plutonic granitic gneisses have been collected from different locations of the Superior Province. The study of their Koenigsberger ratio (related to natural remanent magnetization) and the theoretical Koenigsberger ratio (related to maximum artificial remanent magnetization) shows that the theoretical Koenigsberger ratio of the specimens is less dispersed than the Koenigsberger ratio. There is a power law relation between the remanent magnetization and induced magnetization for the Koenigsberger ratio and the theoretical Koenigsberger ratio and this power law relation is due to variation of amount of ferromagnetic minerals in the specimens.

A structural study of the McKenzie granite (NE of Thunder Bay), the Rice Bay dome and the Sawbill dome (NE of Fort Frances) have also been performed. The McKenzie granite magnetic fabrics cannot be used as kinematic indicators because of the non-coaxiality of the direction of the magnetic ellipsoid axes and also because a primary fabric has been overprinted by a secondary one. The Rice Bay dome fabrics are non-coaxial but are clearly related to the regional strain and mineral lineation: they may be related to the diapiric emplacement of the dome. Sawbill dome fabrics are not related to the diapiric emplacement of the dome but to a later event related to the southern border of the dome adjacent to the Quetico fault.

ACKNOWLEDGEMENTS

First, I would like to thank my supervisor Dr Borradaile for welcoming me in his laboratory, for his support and help during two years.

I also especially thank Sam Spivak, Ann Hammond, David Gauthier, Norihiro Nakamura for their technical and friendly help as well as everybody at the Department of Geology of Lakehead University. Ann Hamond prepared the core samples from oriented specimens.

I am also grateful to Dr Percival and Dr Pilkington for sending me their samples of the Minto Bloc and to Dr Borradaile for cores from the Trout and Barnum granites as well as those from Rice Bay and Sawbill Domes.

Lastly, I would like to thank my friends from the " Tennis de Table Frouzinois", especially Raymond Couzinou, from Pastel and my family for their support and their messages either by internet or by phone. I have a thought for Lucienne Darnatigues, Charles Krauth, Eva Darnatigues and especially Fernand Charpentier, whom I will not see again.

TABLE OF CONTENTS

Introduction

The genesis, transport and emplacements of granites and gneisses are intimately related to the regional stress and therefore their study can provide information about geological history of a region. Minerals lineation and foliations are sometimes very difficult to observe in granites but magnetic fabrics studies always define a magmatic petrofabric very precisely. In this study, magnetic anisotropy techniques are employed to study the emplacement and deformation of plutonic granites and gneisses and their emplacements and related internal structures. Specimens in Northern Ontario have been collected from different granitic and gneissic complexes and their magnetism as well as their structures have been studied.

I. Techniques

I.1. Specimen

Hand specimens have been collected from four different locations: the McKenzie granite, along the road between Atikokan and Ignace, the Rice Bay dome and the Southwestern area of Sawbill dome (figure I.1.).

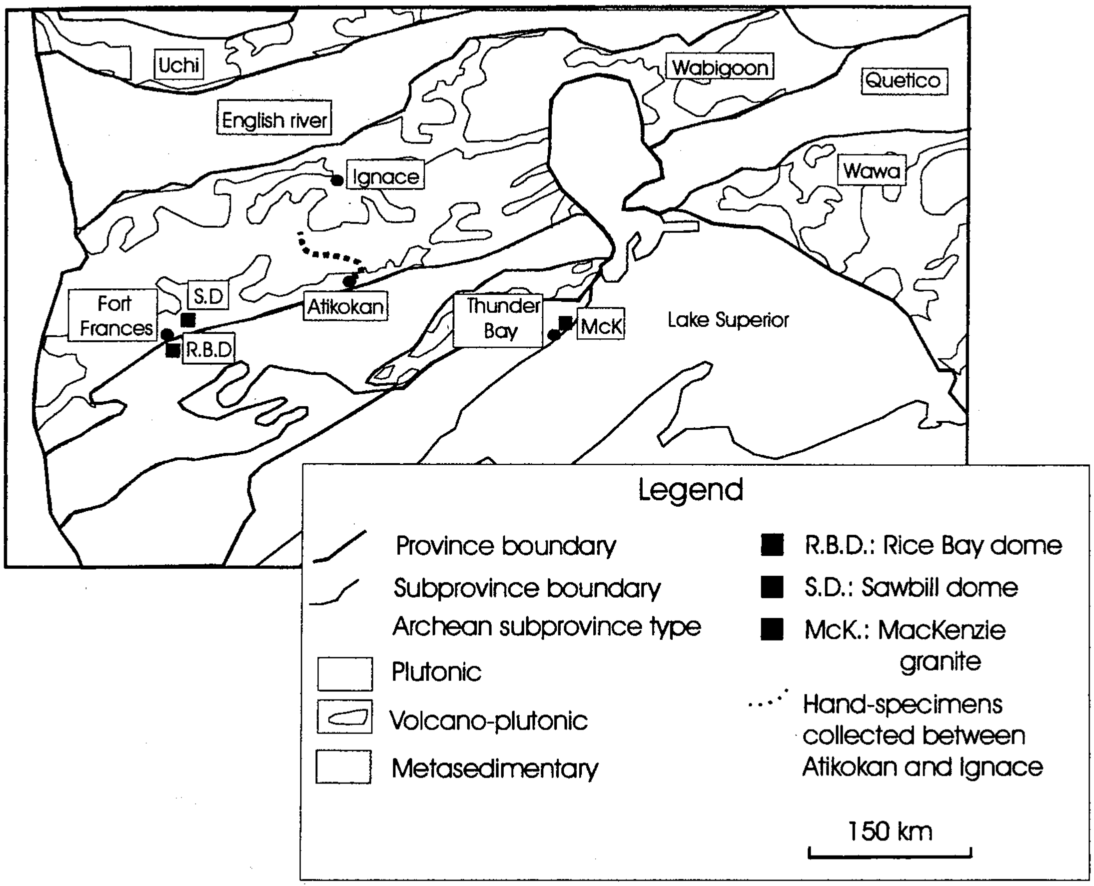

Figure I.1. Geological subprovinces of the Superior Province defined by Card (1990) with the locations of the different studied areas.

They were oriented and brought to the laboratory to be cut. In the laboratory, the specimen is first oriented in geographic coordinates and cut in order to have a horizontal base. Second, the specimen is drilled and the cylindrical portion is divided in cylinders of 10.55

cm^3 (2.5 cm diameter and 2.2 cm high). At least 2 cylinders have been cut from each specimen (figure I.2.).

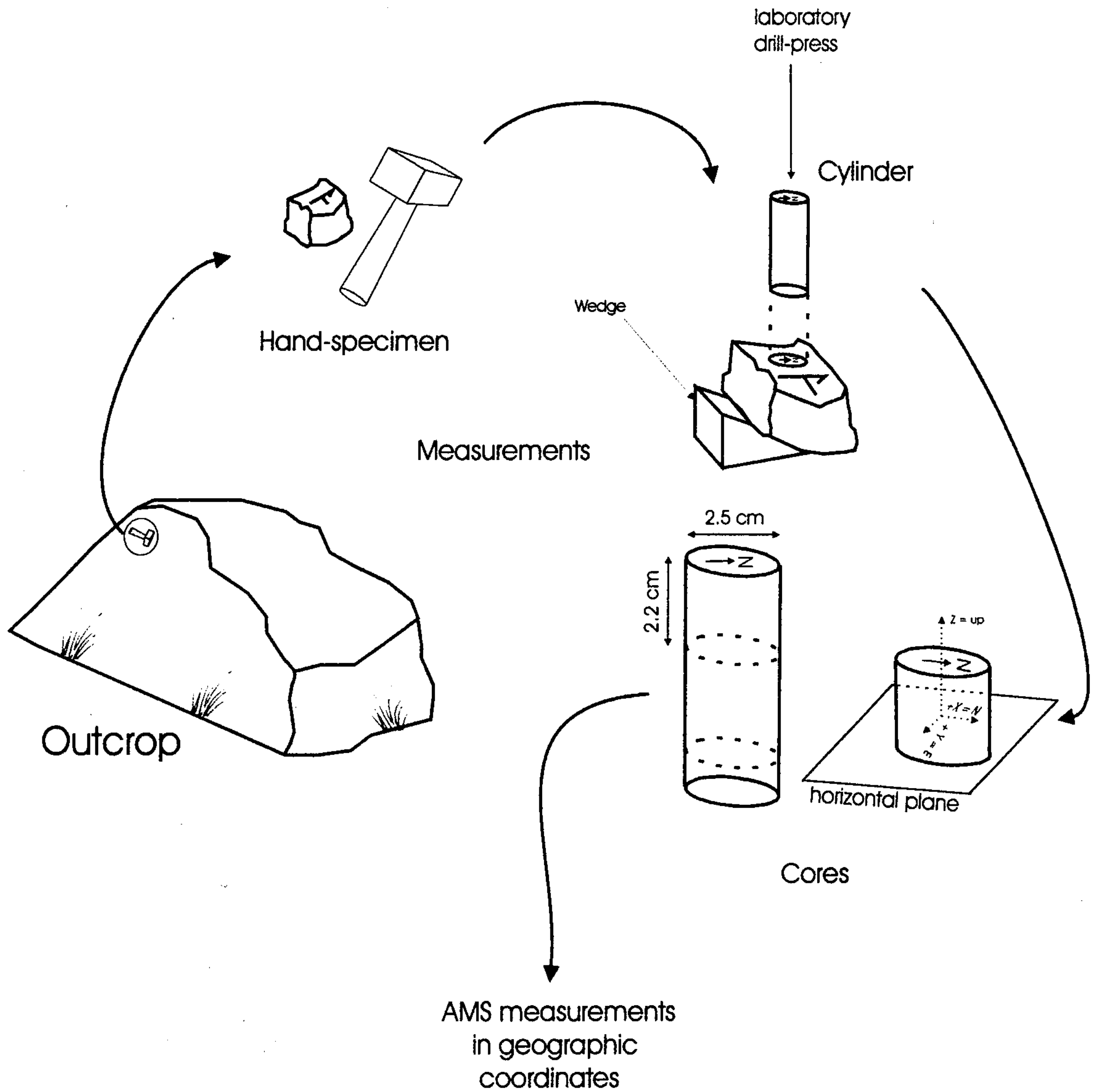

Figure I.2. Technique employed to collect specimens.

The NRM and AMS of each core have been measured and AARM of one core of each specimen too.

I.2. Anisotropy of magnetic susceptibility (AMS)

I.2.1. **Instrumentation**

AMS is measured in a field smaller of approx 0.1 mT (~ 1 Oersted). AMS was measured using a Canadian Sapphire Instrument SI-2 susceptibility meter with internal coil frequency of 19.2 kHz. The core is introduced into a coil. A specific orientation is given to the core according to the seven-orientation scheme (figure I.3.). These orientations are chosen in order to determine the magnetic susceptibility matrix as quickly as possible with the least manipulations and the easiest calculations. An electric field is applied in the coil, which induces a magnetic field into the coil. The cores introduced inside the coil will be magnetized proportionally to this magnetic field. This magnetization disappears when the magnetic field is turned off. The coefficient of proportion (the susceptibility) between the cores magnetization and the magnetic field is measured for each orientation. The calculations of variations of intensity of susceptibility in the 7 orientations are described by an ellipsoid. The shape parameter (Tj), the intensity of anisotropy (Pj), the bulk susceptibility (k_{MEAN}) and the orientations of the maximum, the intermediate and the minimum axes (according to the North) of the ellipsoid are calculated by a software called Si2 created by doctor Borradaile.

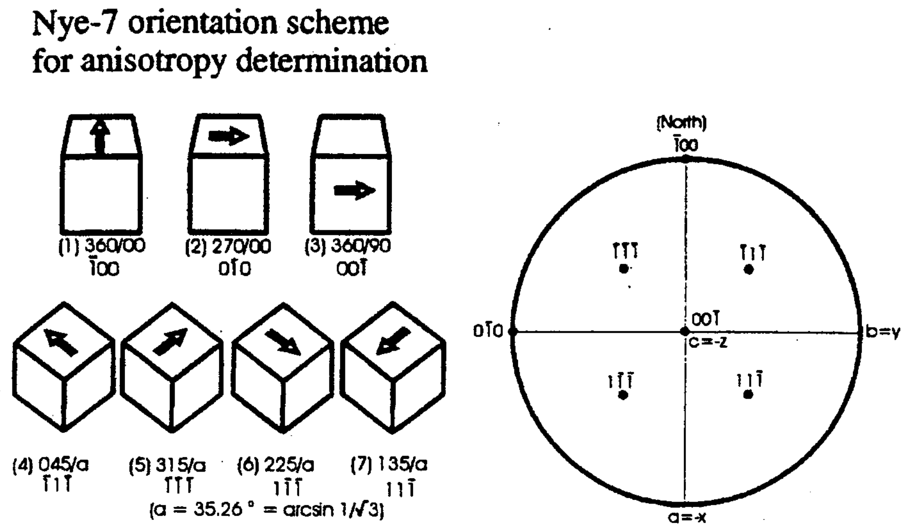

Figure I.3. Seven-orientation scheme used to determine the AMS ellipsoid and the AARM ellipsoid.

I.2.2. **Origin of AMS**

Undergoing a low magnetic field **H** vector (<1 mT), minerals magnetize. Their magnetization **M** vector will be related to the vector **H** by this relation:

$$\mathbf{M} = \mathbf{k} \times \mathbf{H}$$

where **k** is the second rank tensor of magnetic susceptibility. **k** is a tensor of second order and represented by an ellipsoid if all principal susceptibilities have the same sign. Susceptibility is dimentionless, but is measured on the basis of a sample, which is recorded in mass, volume or molecular weight. In this thesis and all structural work, the principal susceptibilities directions are most important. Therefore, we use a constant volume for cores (10.55 cm^3) and the susceptibility is reported in "units" of volume, thus µSI (vol.).

According to their bonds and their magnetic moments, minerals have different behaviors undergoing a magnetic field. They are classified according to the increase of intensity of their magnetic susceptibility:

Diamagnetic minerals (figure I.4.): every object on the Earth has a diamagnetic behavior. The diamagnetic response is opposite to the applied field and negative. The susceptibility is nearly constant at $-14*10^{-6}$ SI. Moments of electrons are opposite to the magnetic field.

The other induced response is paramagnetic (figure I.4.). This magnetic property of minerals is added to diamagnetic property of the same minerals. Undergoing a magnetic field, moments of electron of paramagnetic minerals tend to be parallel to the magnetic field and in the same sense. Paramagnetic minerals include a sub-group of minerals called antiferromagnetic (two spins of electrons are related but opposed) and in this sub-group, a group called ferromagnetic have the moment of electrons parallel to the magnetic field and both parallel to one another. Paramagnetic mineral magnetization stops when the magnetic field is turned off whereas ferromagnetic and antiferromagnetic minerals stay magnetized under magnetic Earth field conditions.

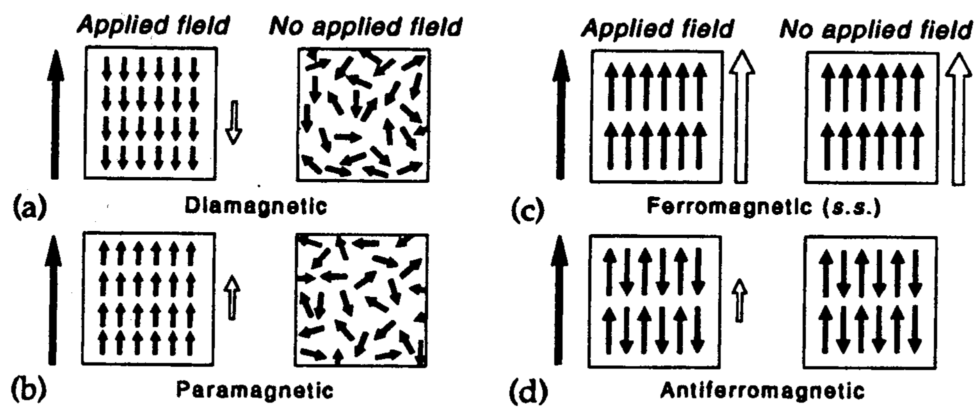

Figure I.4. Magnetic properties of minerals. The susceptibility is the coefficient of proportion between the magnetization of minerals and the applied field (modified from Tarling and Hrouda, 1993).

For one core, all these contributions can be added but they cannot readily be related to a specific mineral: the measured susceptibility corresponds to the magnetic response of the whole specimen.

Quartz, feldspar and calcite are diamagnetic minerals; all Fe-bearing magnetic silicate minerals (e.g. muscovite, biotite, pyroxenes, amphibole) are paramagnetic; hematite and ilmenite are antiferromagnetic; pyrrhotite and hematite are ferromagnetic minerals.

All these minerals show a crystalline anisotropy whereas magnetite shows a shape anisotropy because of its high susceptibility (Tarling and Hrouda, 1993). Magnetite behavior can be divided in three groups: monodomanial magnetite, pseudo-single domanial magnetite and multidomanial one. Magnetite grains having a diameter smaller than 1 μm will be monodomain magnetite whereas magnetite grains having a diameter greater than 5 μm are composed of several "grain" called magnetic domains: the magnetic poles of each domain tends to accommodate the external magnetic energy and their positive pole will be related to the negative pole of the nearby domain. The poles of the domains of a grain of magnetite will so describe a closed system called closure domain to reach equilibrium with the least possible magnetic energy. Some multidomain magnetite cannot reach this equilibrium due to crystal lattice imperfections and they consequently have the same behavior as monodomain magnetite: they are called pseudo-single domain magnetite.

I.2.3 **Influence of mineral fabric on magnetic fabric**

As AMS is defined by an ellipsoid (which shows the variations of intensity of magnetization with orientation with respect to the direction of the field), the susceptibility of rocks is function of the proportion of the different minerals in the core. According to the nature of granites, the ferromagnetic, paramagnetic and diamagnetic minerals content is different (see chapter II). As ferromagnetic minerals have the highest susceptibility, magnetic susceptibility is very sensitive to their presence, even in low proportion. But the presence of silicates such as quartz, feldspars, amphiboles, pyroxenes, biotite affects also the AMS ellipsoid.

The susceptibility of rocks is a function of the orientation of minerals. If some minerals are oriented in one direction and other minerals in another one, ellipsoid orientation will not reflect these variations but the orientation of the AMS axes will be the average orientation-distribution of the minerals in the core. Two cores having the same composition but with different minerals dispersion will not have the same susceptibility.

The susceptibility of rocks is a function of the composition. Even having without undergone any orientation mechanism, minerals show a magnetic ellipsoid, which is prolate or oblate (Borradaile, 1987) depending on the mineral. Thus, undergoing orientation mechanism, mineral is changing its shape and therefore, the AMS ellipsoid will be changed.

The susceptibility of rocks is also function of the number and the size of minerals. The more the number of minerals increase into the core, the more magnetic ellipsoid will correspond in some way to mineral alignment. This is especially true when mineral magnetic intensity is low.

I.2.4. **Relation between crystallographic minerals axes and magnetic ellipsoid directions**

As AMS is described by an ellipsoid as well as strain, it can be sometimes compared to it. AMS ellipsoid is related to lattice crystal symmetry; consequently, it will have the same relation with strain than this one.

If k_{max}, k_{min}, k_{int}, are the axis of the ellipsoid of magnetic susceptibility, then k_{max} will be parallel to X, the long crystallographic axis, k_{int} will be parallel to Y and k_{min} to Z, the short axis: this is true if minerals have a symmetry superior or equal to an orthorhombic symmetry. If the symmetry of the minerals is monoclinic, only one axis of the AMS ellipsoid will be parallel to one of the crystallographic axis and there will be no relation between AMS ellipsoid and crystallographic axes for triclinic minerals (figure I.5).

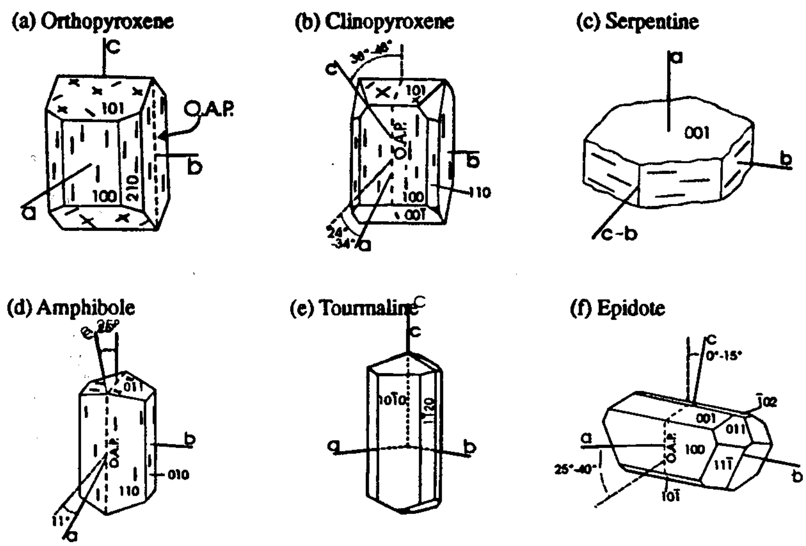

Figure I.5. Variations of angle between the crystallographic axes and the AMS ellipsoid axes for different silicates. (modified from Lagroix and Borradaile, 2000).

There are some exceptions:

Tourmaline, carbonates and goethite have their magnetic ellipsoid inverse to mineral fabric: k_{max} // Z, k_{int} // Y and k_{min} // X.

Thus, magnetic susceptibility intensity of magnetite is so high that directions of its magnetic ellipsoid are related to its shape. Monodomain magnetite (MD) shows also an inverse fabric, k_{min} will be parallel to maximum elongation. Indeed, MD magnetite is already saturated along its long grain axis so it will respond as k_{min} whereas its minimum grain axis will correspond to k_{max} in a low field (Stephenson *et al*, 1986). However, multidomain magnetite k_{max} will be parallel to the maximum elongation and k_{min} will be parallel to the maximum shortening.

Finally, presence of iron oxides tends to align the magnetic ellipsoid axis parallel or perpendicular to the cleavage of minerals (Borradaile and Werner, 1996).

I.3. Natural Remanent Magnetization (NRM) and Anisotropy of Anhysteretic Remanent Magnetization (AARM)

I.3.1. **Natural remanent magnetization (NRM)**

I.3.1.1. *Instrumentation*

The remanent magnetization is measured using a spinner magnetometer (Molspin). The vector declination and inclination is calculated by software called Spin created by G. Borradaile. With the Molspin, at least four measurements are needed to calculate vector intensity and orientation. The theoretical minimum number is three (e.g. JR5a Czech spinner).

I.3.1.2. *Definition of the NRM*

The NRM (mA/m) depends on the ferromagnetic content of the rock. Ferromagnetic minerals such as magnetite fossilize the geomagnetic field and geological processes during rock formation and during the history of the rock. NRM is divided in two parts: a primary NRM acquired during rock formation and a secondary NRM acquired after rock formation. The primary NRM is due to thermoremanent magnetization acquired during cooling of the rock when the temperature is becoming smaller than the Curie temperature of the ferromagnetic minerals, chemical remanent magnetization formed during the growth of the ferromagnetic minerals below the Curie temperature and detrital remanent magnetization acquired by sedimentary rocks. The secondary NRM is due to the alteration of ferromagnetic minerals or the exposure of rocks to another magnetic field such as lightning ones or a new geomagnetic field.

According to Butler (1992), NRM values are around 1 A/m for basalts, 0.1 A/m for granitic rocks, 0.01 A/m for nonmarine siltstones and 0.0001 A/m for marine siltstones.

The NRM intensity has been only used in chapter IV to calculate the Koenigsberger ratio of the studied granitoid rocks.

I.3.2. **Anisotropy of anhysteretic remanent magnetization (AARM)**

I.3.2.1 *Instrumentation*

Specimens are exposed to a weak direct current field (DC) during its demagnetization by an alternating field (AF). This process is repeated changing the orientation of the core. These orientations are the seven ones described by Nye (figure I.3.).

After each treatment of the core in one direction, the remanence of the core is measured using the spinner magnetometer (like the NRM measurement). The variations of intensity of remanence in each seven directions will be described by an ellipsoid.

The cores of the Mackenzie granite, the cores from the road between Atikokan and Ignace (Wabigoon province) and the ones from the Minto Block have been treated by an alternating field decreasing from 80 to 0 mT and a direct current field of 0.1 mT applied when the alternating field intensity ranges from 60 to 0 mT.

I.3.2.2. *Definition of the AARM*

The AARM (mA/m) is described also by an ellipsoid. It is due to the variations of maximum artificial magnetization of the core applied in the seven directions depending on particular technique. This magnetization is only fossilized by ferromagnetic minerals content of the core. Therefore, AARM ellipsoid will reflect the variations of remanent magnetization carried by ferromagnetic minerals in the core. The AARM will consequently reflect the shape anisotropy formed by ferromagnetic minerals.

The AARM ellipsoids variations will be studied using the same parameters as the AMS ellipsoid: the shape of the ellipsoid will be described by the Tj; the magnitude of the ellipsoid will be reflected by the Pj; the intensity of the ellipsoid will be the mean intensity (mA/m) and is the average of ARM values of the three axes of the AARM ellipsoid; the three ellipsoid axes will be oriented according to the North (declination and azimuth).

I-4. Parameters

Parameters have been already mentioned in chapters I.2.1 and I.3.2.2.. In this chapter, they will be defined by their relations:

Shape parameter Tj is:

$$Tj = \frac{\{[\ln (k_{INT} - k_{MIN}) / \ln (k_{MAX} - k_{INT})] - [\ln (k_{MAX} - k_{INT}) / \ln (k_{INT} - k_{MIN})\}}{\{[\ln (k_{INT} - k_{MIN}) / \ln (k_{MAX} - k_{INT})] + [\ln (k_{MAX} - k_{INT}) / \ln (k_{INT} - k_{MIN})\}}$$

where k_i represents the axis value of either the AARM ellipsoid or AMS ellipsoid.

Magnitude parameter Pj is:

$$Pj = \exp\sqrt{2[(\ln (k_{MAX}/ k_{MEAN})^2 + \ln (k_{INT}/ k_{MEAN})^2 + \ln (k_{MIN}/ k_{MEAN})^2]}$$

where k_i represents the axis value of either the AARM ellipsoid or AMS ellipsoid and k_{MEAN} is the mean susceptibility or the mean remanent intensity ($k_{MEAN} = (k_{MAX} + k_{INT} + k_{MIN})/3$).

I.5 Directions

AMS and AARM ellipsoids are also defined by the geographical direction of their axes. Directions of maximum, intermediate and minimum values of the AMS or AARM ellipsoids are plotted in stereonets. The directions of axes of ellipsoids will range from prolate to oblate. These directions related to crystallographic axes may coincide with strain ellipsoid axes (k_{max} // X, k_{int} // Y and k_{min} // Z). If the minerals orientation is only due to magmatic deformation, the orientation of the AMS and AARM axes of the cores according to their geographical position will reflect the magmatic flow of the magma during emplacement. If the magma takes place during regional deformation, the minerals alignment will correspond to magmatic deformation and high-temperature solid-state deformation and the AMS and AARM axes will reflect regional deformation during and after emplacement. If the magma takes place with or without regional deformation and undergoes a later deformation, a primary fabric will be due to magmatic and high-temperature solid-state (if the granite takes place during regional deformation) deformations and a second fabric will overprint the first one during a later regional deformation.

The AMS and AARM axes cannot be used as kinematic indicators when a primary fabric is overprinted by a secondary one (in the case of granite, magmatic fabrics may be overprinted by metamorphic ones) or when rocks contain minerals with inverse fabric (for example tourmaline) (chapter I.2.4.) or when the fabric accumulation is non-coaxial (Borradaile and Henry, 1997) or when the time of cooling of magma is not sufficient for minerals to accommodate magmatic or high-temperature solid-state deformations and to be perfectly aligned (De Saint Blanquat *et al*, 1999).

II. Granites and grey Gneisses: origin and nature

II.1 Granitoid rocks

II.1.1 **Nature of the granites.**

Granitic rocks *sensus lato* are composed of quartz + alkali feldspars + plagioclases and quartz, constituting 20 to 60 % of their sum. Rather than granite, the term "granitoid" is more appropriate because granite *sensus stricto* is the domain, which the percentage of quartz lays between 20 and 60 %, alkali feldspars between 35 and 90 % and plagioclases between 10 and 65 %. The Granite domain (*sensus stricto*) has been divided by Streckeisen in two parts: syenogranites and monzogranites (figure II.1.).

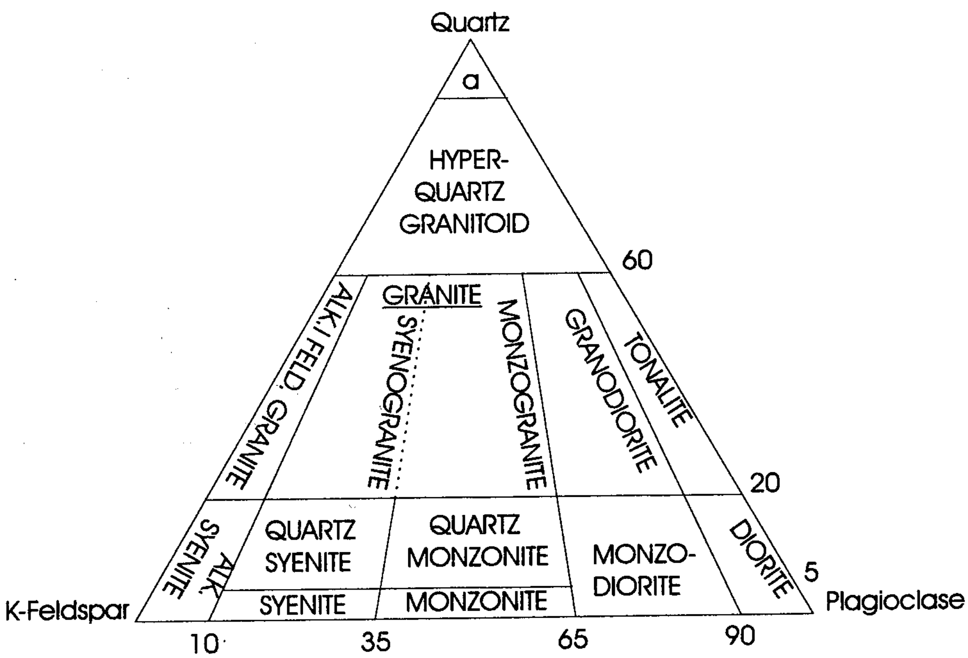

Figure II.1. QAP triangle for rocks saturated in silica. Letter a represents quartzolite domain. Quartz, Alkali feldspars and plagioclases are normalized to 100.

The processes of transport and emplacement can be extended to domains having a composition, whose the percentage of quartz is less than 20 % in the QAP diagram: these "granites" are included in felsic magmas family (e.g. Kehlenbeck and Borradaile, 1995).

This classification does not take into account the content of ferromagnesian minerals and does not reflect the difference of compositions due to the sources of the magmas. Nevertheless, this classification is easy to use, especially in the field. Since it is related to the content of quartz (silica), it reflects the partitioning of the granite after emplacement, magma becoming increasingly rich in silica.

Granites have been also classified according to their chemical composition by their major elements. The ratio A/CNK is the relation between alumina content of granite ($[Al_2O_3]$ = A) over the sum of concentration of calcium (C = [CaO]), of soda (N = $[Na_2O_3]$ and potassium (K = $[K_2O]$). This ratio reflects the nature of the granite but also has some petrological significance. If the ratio is less than 1, the alumina content is less than the sum of calcium, soda and potash concentration: the granitic magma is metaluminous. Common ferromagnesian minerals are pyroxene, hornblende and biotite. If the ratio is greater than 1, the alumina content is greater than the sum of calcium, soda and potash concentration: the granitic magma is peraluminous. Common ferromagnesian minerals are biotite, muscovite, cordierite, andalusite and garnet. Another group of magmas called peralkaline is defined. The relationship is $A<NK$ and the concentration of calcium is negligible. Petrology is characterized by aegirine, riebeckite and arfvedsonite. A/CNK = 1 corresponds to the composition of a granite having quartz and two feldspars only with feldspars having possibly a wide range of composition. This theoretical granite is called haplogranite (Bowen, 1922).

White and Chappell (1983) proposed to relate the differences of petrology with the sources of granites: granites having A/CNK < 1.1 are called I-type granites (I for igneous origin) and granites with a ratio A/CNK > 1.1 are called S-type granites (S for sedimentary origin) (figure II. 2).

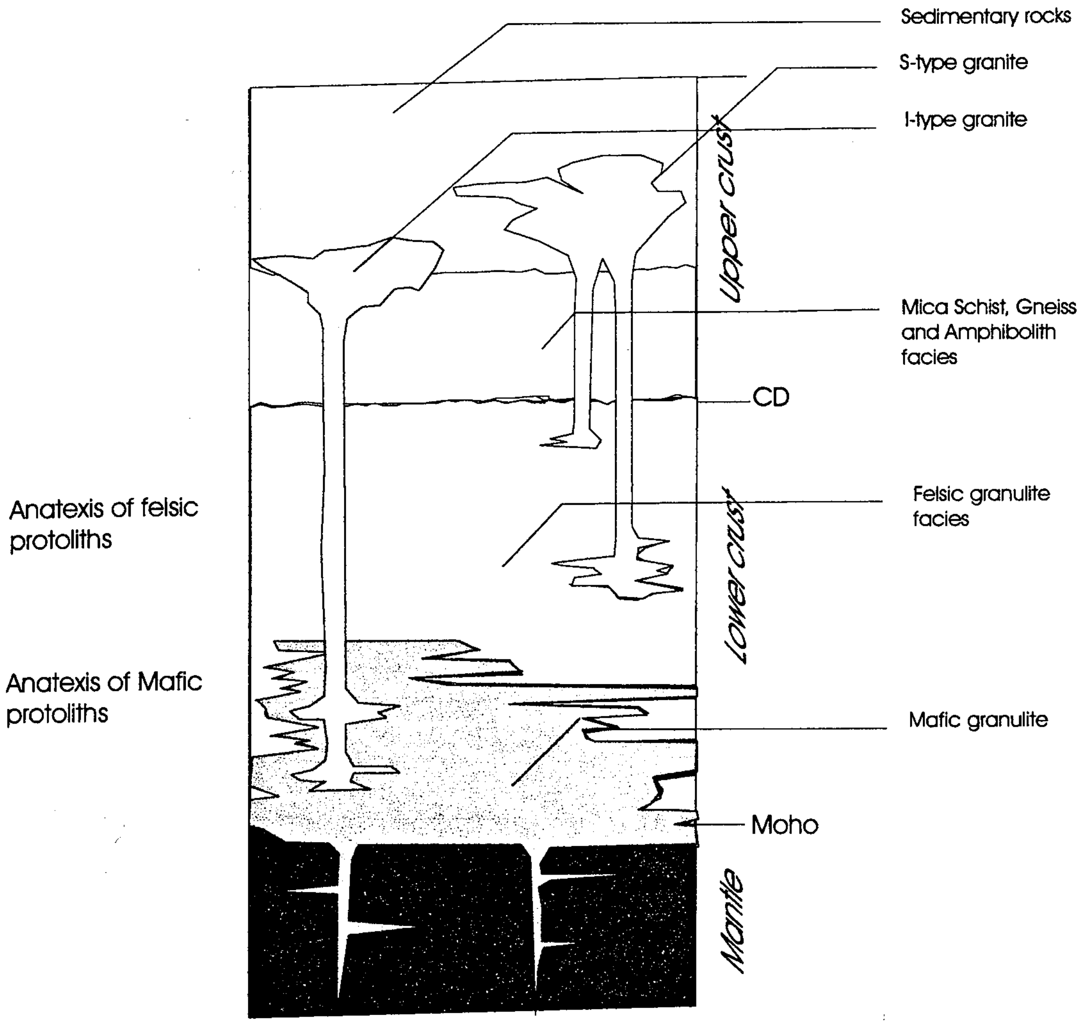

Figure II.2. Cross section of the continental crust. Explanations about crustal melting has been given in chapter II.2.1. An addition of continental crust and a high geothermal gradient must occur in order to the rocks to melt (modified from Johannes and Holtz, 1996).

These differentiations can be related to the previous classification with a different limit between peraluminous and metaluminous (A/CNK = 1) and between I-type and S-type granite (A/CNK = 1.1). Later, several different types of granites have been differentiated:

A-type granites (Creaser *et al*, 1991), M-type granites (Pitcher, 1982) and C-type magmas (Kilpatrick and Ellis, 1992). Whereas I-type and S-type magmas were related to the nature of the protolith, A-type, M-type and C-type magmas are influenced by tectonics. The petrology of A-type granites is similar to peralkaline magmas but A implies an anorogenic environment. As shown by Eby (1990), A-type granites are found in oceanic islands (Evisa in Corsica, Reunion and Ascension islands), in continental environments (Oslo grabben), attenuated crust (Yemen granite suite), intracontinental ring complexes (Nigeria) and postorogenic environments (Gabo, Mumbulla, Monga and Wangrah suites in southeastern Australia (Collins *et al*, 1982)). This classification simplifies and makes a good synthesis of possible behavior of granite but probably do not reflect the complexity of creation of felsic magmas: A-type magmas have the same origin as M-type magmas and granites are very often related to a mixing of continental crust or mafic mantle matter (Patino Douce, 1999). M-type is a too general term to be really meaningful. Thus, S-type granites are generated by different processes (Clarke, 1992). Two groups of S-type granites can be differentiated. The first one results from the dehydration-melting of muscovite schists. The second one is simply magmatic but is richer in lime and ferromagnesian components. Thus, granites are not usually related to just one source, mixing of several sources is common.

II.1.2 **Relation between nature, petrology and magnetism in granites.**

The nature of protolith inevitably affects the petrology of felsic rocks. Indeed, S-type, I-type and A-type will not have the same composition and mineralogy (Table II.1.).

Table II.1. Principal characteristics of metaluminous, peraluminous and peralkaline granites. (from Clarke (1992)).

The granitoid family			
QAP	60% > Quartz >20%	Alkali-feldspar/(Alkali-feldspar + Plagioclase) = 0-1	
	Peraluminous	Metaluminous	Peralkaline
Definition (Shand, 1947)	A> CNK	CNK > A > NK	A < NK
Characteristic Minerals	aluminosilicates, cordierite, garnet, topaz, tourmaline Spinel, corundum	orthopyroxene, clinopyroxene, cummingtonite, hornblende, epidote	fayalite, aegirine, arfvedsonite riebeckite
Other common Minerals	biotite, muscovite	biotite, minor muscovite	minor biotite
Oxide minerals	ilmenite, tapiolite	magnetite	magnetite
Accessory Minerals	apatite, zircon, monazite	apatite, zircon, titanite, allanite	apatite, zircon, Titanite, Allanite, Fluorite, Cryolite, Pyrochlore.
Other Chemical Features	F / Cl > 3	–	Low CaO, Al_2O_3, H_2O Ba, Sr, Eu. High SiO_2, Fe / Mg, Na + K, Zr Nb, Ta, ΣREEs, Y F / Cl < 3
Typical Mineral Deposits	aplite, pegmatite greisen; ploymetallic Sn, W, U, Mo, Cu, Be, B, Li, P	porphyry Cu, Mo	Sn, W, U, Mo and rare metal (Nb-Ta) greisens
General tectonic	continent-continent	subduction related	post-tectonic or anorogenic

As shown previously, S-type granites (White and Chappell, 1988) are peraluminous granites in Shand classification (1947) and are characterized by ilmenite. These "ilmenite-series" granites, defined by Sasaki and Ishihara (1979) due to their low content of magnetite suggests, they are sometimes called "paramagnetic" granites (Bouchez, 1997), but of course that term can only strictly apply to a monoclinic material. I-type granites (Chappell and Stephen, 1988) are metaluminous according to Shand classification and are characterized by magnetite as well as A-type granite. They are consequently "magnetite-series" granites (Sasaki and Ishihara (1979)) and ferromagnetic granites (Bouchez, 1997). This has of course consequences on the AMS and the AARM (see chapter I).

II.2. Nature of grey gneisses

II.2.1. **Petrology of grey gneisses**

Grey gneisses are overlain by mafic to ultramafic volcanic rocks and intruded by late granites, which composition is variable from granodiorites to syenites (see figure II.1.). In the QAP diagram, grey gneiss composition is in the tonalitic domain.
It is composed of quartz, plagioclase, biotite and other minerals can also be found such as green hornblende, microcline (Martin, 1994). Accessory minerals are epidote, allanite, sphene, zircon, apatite, ilmenite and magnetite.

Poulsen *et al* (1980) called the Rice Bay dome a paragneiss. Many other authors (e.g. Martin (1994), Condie (1997), Arkani-Hamed and Jolly (1989) and Defant and Kepezhinskas (2001)) suggest that grey gneisses are orthogneisses and consequently are partly plutono-magmatic origin.

The geological division in subprovinces from Card and Ciesielski (1985) of the Superior Province (Ontario) and the succession of metasedimentary subprovinces and volcano-plutonic subprovinces suggest to many scientists (e.g. Condie (1997), Kimura et al (1993), Martin (1994)) that continental crust and grey gneisses are produced by accretion and subduction of provinces. Thus, Percival and Williams (1989) suggested that the Quetico subprovince is an accretionary prism. In the Superior Province, Wabigoon, Quetico and Wawa subprovinces may have collided with one another in a dextral transpressive context (Hudleston *et al* (1988), Borradaile *et al* (1988), Williams *et al* (1992)) and in the case of the Quetico belt (Werner and Borradaile, 1996), during one long tectonic episode.

II.2.2. **Theories of petrogenesis**

Many authors (e.g. Petford (1995), Defant and Kepezhinskas (2001) and Martin (1994)) have related the genesis of grey gneisses with the mantle. Martin (1994) summarizes different theories:

(1) Arth et al (1978) proposed a basaltic source with at least 75 % of basaltic melt by fractional crystallization to produce trondhjemitic melt but trondhjemite-tonalite-gneiss suites are not genetically directly related to mafic magmatism.

(2) A direct melting of the mantle (Stern and Hanson, 1991) but according to Martin (1994), REE and the La/Yb ratio of Archean trondhjemite-tonalite-gneiss suites do not corroborate this hypothesis.

(3) A partial melting of Archean greywackes (greenstones) (Arth and Hanson, 1975) but major elements and some trace-elements behavior in trondhjemite-tonalite-gneiss suites do not concur.

(4) Partial melting of quartz eclogite (Rapp *et al*, 1991). Eclogites are not found in Archean terranes and therefore, this theory is improbable.

(5) Partial melting of garnet amphibolite (Nédélec *et al*, 1990). Martin (1994) proposed creation of trondhjemite-tonalite-gneiss suites melt by two processes of partial melting: a first partial melting of the mantle creating a tholeiite melt, which is changed into tonalitic magma by partial melting.

Some new hypothesys have been proposed. Defant and Kepezhinskas (2001) argue that Cenozoic adakites are the analog of trondhjemite-tonalite-gneiss suites in the uniformitarian principle. Adakites have SiO_2 > 56 wt %, Al_2O_3 > 15 wt % and Na_2O > 3.5 wt % and are the results of partial melting of subducted young oceanic crust. Such rocks are found in Kamchatka, in Mount St Helens, Panama and Costa Rica. Whereas Smithies (2000), using major elements comparison, thinks that adakites do not correspond to trondhjemite-tonalite-gneiss suites. The principal observation made by Smithies (2000) is about the content of Mg in gneisses and in adakites. Mg is a very important component to know whether mantle interact during the genesis of gneisses. According to Smithies (2000), trondhjemite-tonalite-gneiss suites SiO_2 around 70 %, Al_2O_3 > 15 % and more importantly Mg# ($Mg\# = Mg^{2+}/(Mg^{2+} + Fe^{total})*100$) maximum around 50 whereas adakites have SiO_2 between 60 and 65 %, Al_2O_3 > 15 % and Mg# around 60. Smithies think that trondhjemite-tonalite-gneiss suites more closely match with Phanerozoic Na-rich granitoids and trondhjemite-tonalite-gneiss suites genesis would be generated by melting of hydrous basaltic material at the base of thickened crust. This model would be appropriate during early Archean time and mantle interaction would only occur during late Archean time.

II.3. Classification of studied complexes

The Mackenzie granite is a granite *sensus stricto* according to the QAP diagram and is composed of plagioclase (oligoclase), quartz, alkali feldspar and biotite with accessory sphene, apatite and opaque minerals (Rogers, 1979). It is an I-type granite according to White and Chappell classification (1983)

Trout lake and Barnum lake granites are porphyritic quartz monzonite, quartz syenite to a lesser extent and locally quartz monzodiorites in the QAP diagram. They are composed of potassium feldspars phenocrysts in a coarse-grained matrix of oligoclase, quartz and biotite. They are also I-type granites. Drill core was provided by Dr Borradaile from an earlier study.

Sawbill dome and Rice Bay dome are tonalitic gneisses in the QAP diagram. They are composed of quartz, plagioclases and biotite. The Sawbill dome is more altered than the Rice Bay dome and can have locally a granodioritic composition. They cannot be classified with the S-I-A-M classification from White and Chappell (1983) because they are not granites but gneisses. Drill core was provided by Dr Borradaile from an earlier study too.

These plutons are plotted in the QAP diagram in figure II.3. and the granitoid plutons are classified into Table II.2. in the S-I-A-M classification.

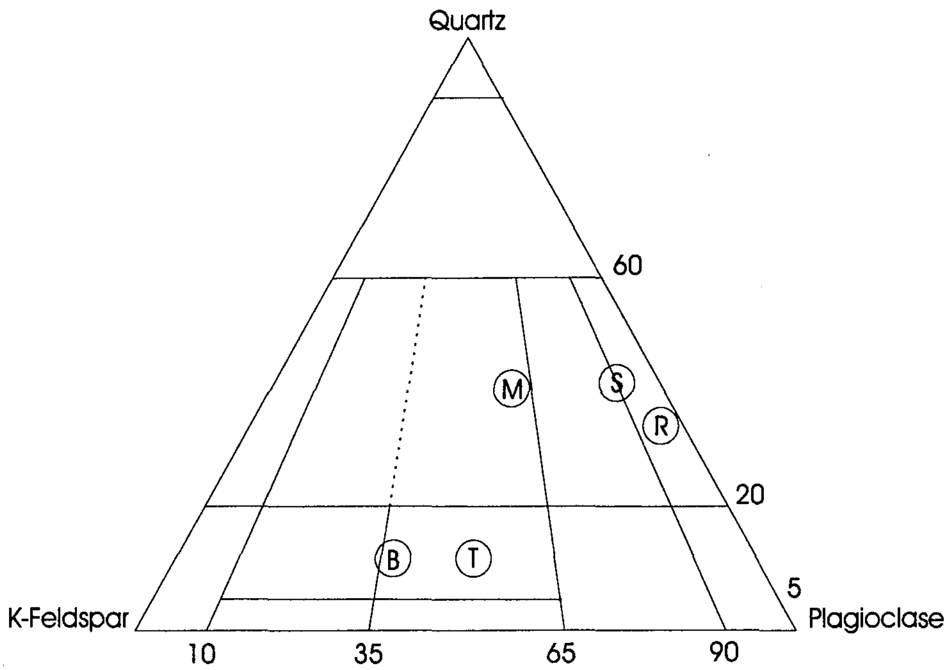

Figure II.3. QAP triangle. M represents the Mckenzie granite composition. S and R are the compositions of Sawbill and Rice Bay domes. B and T are the compositions of Barnum lake and Trout lake granites.

Table II.2. S-I-A classification of granites.

Distinctive characteristics of the the four major types of granites	"I-type" granites	"S-type" granites	"A-type" granites
Origin or tectonic relation	Igneous rocks	Sedimentary rocks	post-orogenic or anorogenic
[Al2O3] / { [Na2O]+[K2O]+[CaO] }	< 1.1	> 1.1	< 1.1 A / NK
Principal ferromagnetic minerals	Magnetite	Ilmenite	Magnetite
Principal paramagnetic minerals	Biotite Hornblende	Biotite Muscovite Titanite	Fayalite Aegirine Arfvedsonite Titanite
Deposits	Cu, Mo, Ni, Zn, Ti	Sn, W, Be, B, Li	F, Y, Nb, Ga, Zr, Ta
Examples of granite	Trout lake granite Barnum lake granite Mckenzie granite		

III. Granites emplacements and their associated structures.

Granites emplacement can be classified into two groups: concordant or syntectonic plutons and discordant or anorogenic or post-tectonic plutons.

III.1 **Syntectonic emplacement or concordant plutons (Castro, 1987)**

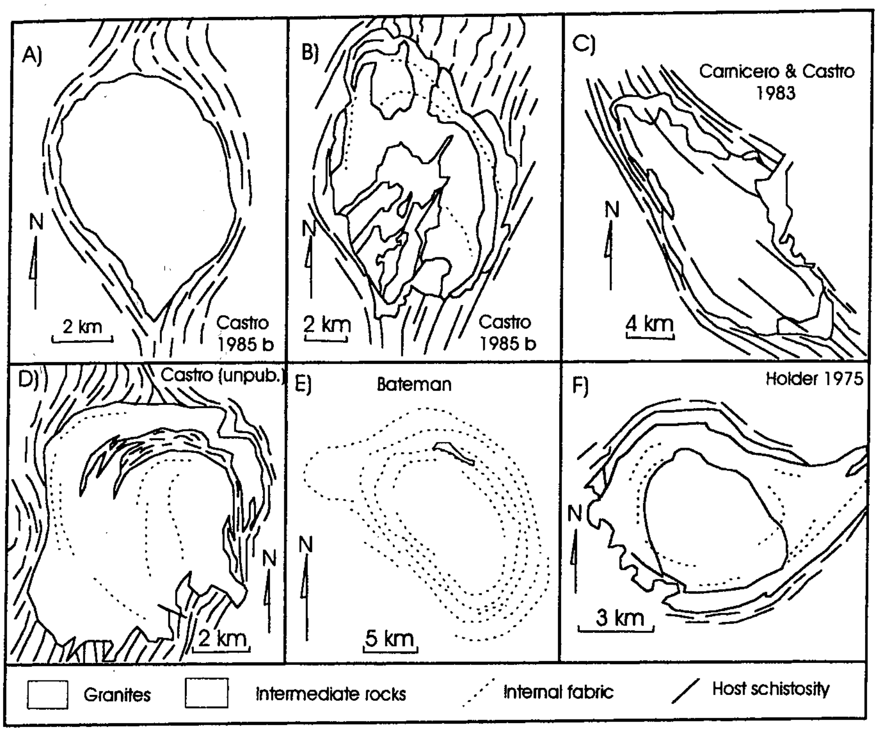

Figure III.1. Some examples of concordant plutons from Spain and Ireland: (a) Plasenzuela; (b) Trujillo; (c) Higuera-taliga; (d) Zarza; (e) Cannibal creek; (f) Ardara (from Castro, 1987).

The magmas emplaced in tectonic context accommodate the stress. Their internal structures fossilize at the magmatic stage and also in the solid-state stage due to regional tectonism. Internal structures in granitoids emplacements are more or less parallel to internal structures of the host rocks. The granites' shapes will also reflect regional tectonic (e.g. Olivier *et al*, 1997). This is the reason why these granites are called "concordant" plutons.

As regional tectonic stress accumulates non-coaxially, granite emplacements are commonly non-coaxial. They will be limited by faults and expand parallel to these faults (figure III.2). Foliations and lineations continue to develop progressively during magmatic and solid-state processes. There may be a gradation between country rocks near the granitoid and the regional assemblage of rocks. The plutons are elongated with a shape geometry related to active fault zones. As these granites are also affected by solid-state deformation, they will be deformed and develop at the same time in the country rocks. These relations are true if solid-state deformations are in continuity with magmatic ones and therefore, the deformation is high-temperature solid-state one.

III.1.1. *Transcurrent shear zones*

III.1.1.1. Emplacement in transtensive context

Space creation in extensional context permits the magma to rise more easily.

According to Sanderson and Martini (1984), the consequences of transtension in transtensive basins are:

" - *constrictional (prolate) strain (L>S),*

- *horizontal stretching, with steep or flat cleavage,*
- *folds and thrusts at high angle to the zone,*
- *extensional structures at a low angle and*
- *crustal thinning, subsidence and basin development.*"

Plutons are elliptical or tabular with their long axis parallel to the fault zone. These granites are compositionally heterogeneous over short distance. In brittle zones, the magma may rise into conduits or uses tectonic fractures (inverse flower structures).

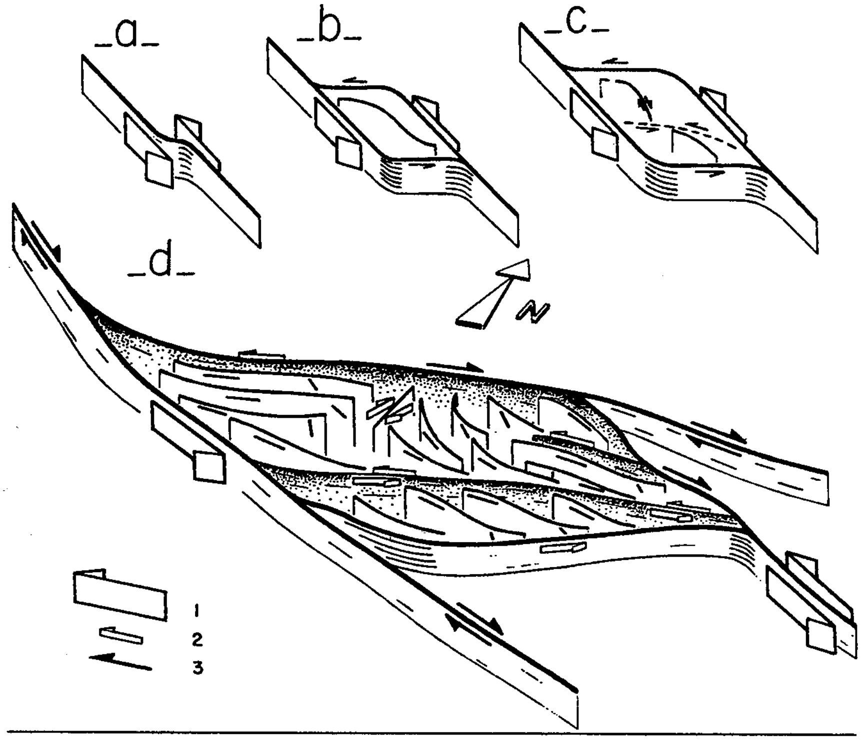

Figure III.2. Crustal opening and creation of a transtensive area in a shear zone by a sinistral transcurrent fault: (a-b-c) history of the granitic filling in created space. (d) the present structure of the Mortagne pluton: 1- synemplacement main crustal transcurrent shear; 2- synemplacement secondary transcurrent shear; 3- late perigranitic shear (Guineberteau et al, 1987)

III.1.1.2. <u>Emplacement in transpressive context</u>

According to Sanderson and Martini (1984), transpressive consequences are:

" *- flattening (oblate) strain (S>L),*

- steep cleavage and a stretching lineation, which may be either vertical or horizontal,

- folds and thrusts at small oblique angle to the zone,

- normal faults, dykes, veins and other extensional structures at high angle to the zone,

- crustal thickening and vertical uplift."

To understand more easily the rise of magma in transpressive context, De Saint Blanquat *et al* (1998) wrote: " *...using an automotive analogy, a pre-existing void in the crust is similar to having a reserved parking space in Toulouse: no such thing exists in Toulouse, they are created by the person who needs to park.*" In fragile-ductile zone (Clemens and Mawer, 1992), the magma may be rising into conduits as in the brittle zones of the crust (catazone and epizone). The magma may be helped to rise by preexisting faults (flower structure) but the magma may also develop flower structure during its rise (forceful emplacement).

III.1.1.3 Synthesis of possible structures in shear zones

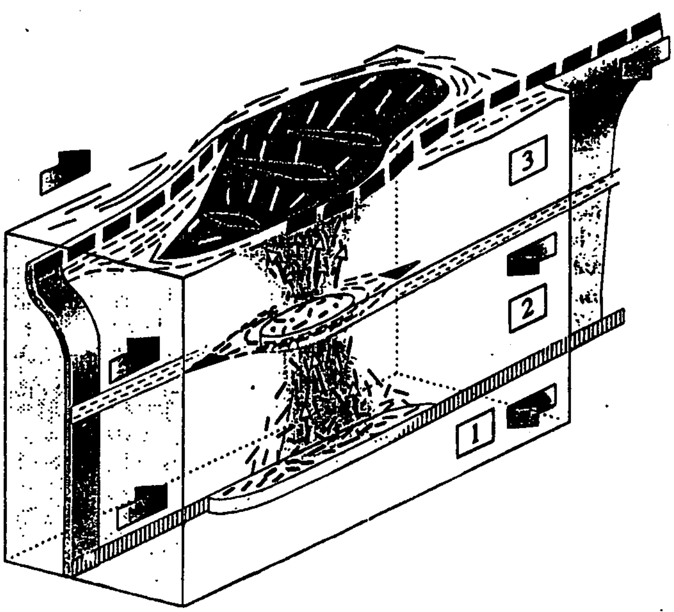

Figure III..3. Schematic draw showing three different structures created in shear zones and linked with the relative depth of level of erosion (Bouchez, 1997).

Bouchez (1997) has suggested that, in shear zones, lineations may be classified as follows:

- Part 1 (figure III.3.), lineations are parallel to the shear directions, planar in the shear zone. These plutons are very elongated with subvertical foliations parallel to the shear zones.

- Part 2 (figure III.3.), lineations are vertical and show rise of granite. According to Ramberg (1981, p 254), this level is between the source level (part 1) and the end of rise of granite (part 3) and could be called the trunk of the batholith. This part of the granite could disappear (if the host rocks are ductile).

- Part 3 (figure III.3.), the upper zone of granites: the directions of fabrics are less well defined. If the host rocks are brittle, there is a multiplication of roots (or conduits) and so a batholith may have several sources: contacts between magma bodies are sharp as in polydiapirs in Maladetta pluton according to Leblanc *et al* (1994) (figure III.4.)

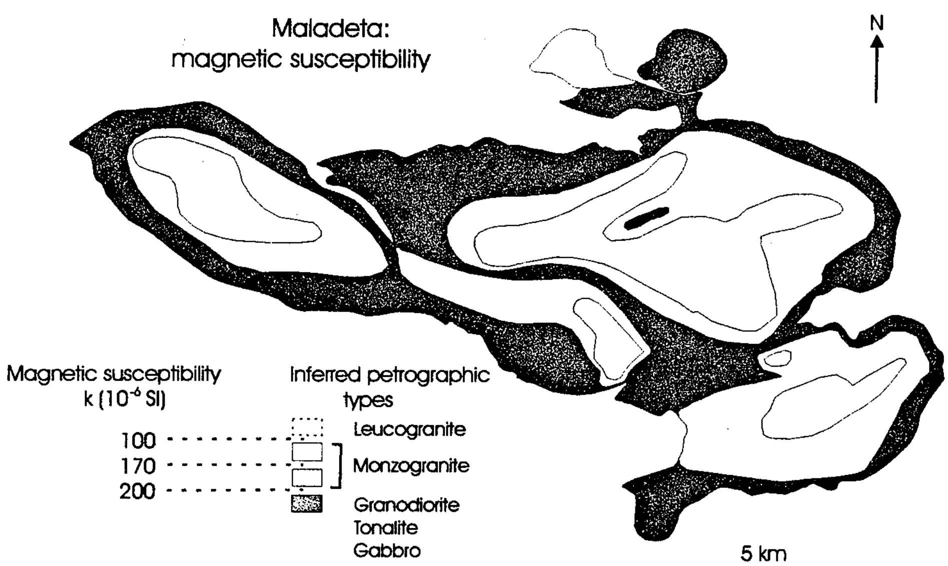

Figure III.4. Map of magnetic susceptibility of the Maladeta massif (modified from Leblanc et al, 1994). White areas represent the more acidic magma composition and are related to the places where the magma came in (roots): four different roots can be discriminated.

The mechanism of emplacement is highly dependent on the depth of emplacement. Transcurrent tectonics are coupled with transport mechanisms. Transport mechanisms are either diapirism in mesozone and conduits in catazone and epizone.

In epizone, magma expands horizontally above a resistant layer through which the magma rises and a less competent layer, which accommodates and is deformed by the rise of the magma. Such formations are called laccoliths (Roman-Berdiel *et al*, 1995) when the formation and the rise of magma form an antiform and are called lopoliths when the formation and the rise of the magma form a synform.

III.1.2. *Granites diapirs*

Spheroidal granites usually show neither visible fabrics nor clear compositional zoning, few xenoliths, sharp discordant margins and narrow contact aureoles with static fabrics. Granitic diapirs are placed in ductile zone and crustal stress does not affect them very significantly according to Clemens and Mawer (1992). The principal property of diapirism is the very high proportion of melt (greater than 30 %) and the high degree of temperature. Magma needs to convect with a squeezing chamber with a pronounced vertical extensional lineation (Cruden, 1988) (figure III.5). The magma is not differentiated while the internal movement of the fluid is extremely intense. The kinematic and internal fabrics are consistent with internal convection. The rise of diapir stops very rapidly due to the rapid loss of heat. The fabrics are consequently different according to the level of erosion of the diapir: lineations are more or less horizontal at the base and the top of the granite and vertical in the middle of the granite. The host rocks are ductile (e.g. Miller and Paterson, 1999; England, 1990; Marsh, 1982), affected by the rise of the granite (concentric metamorphic aureole) with a foliation parallel to the margin of the granite and lineation steep on sides, shallow near roof).

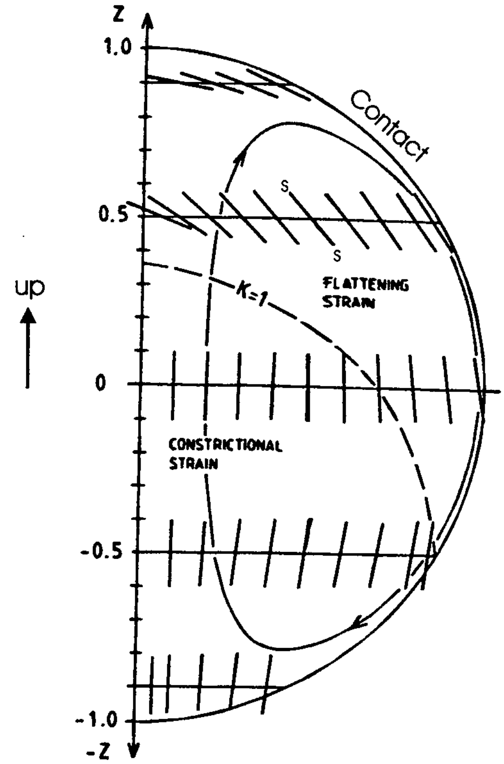

Figure III.5. One theoretical possible behavior of fabrics into "hot" Stoke's diapiric conditions (fluid sphere after rising 2 radii). The lines represent the orientation of the long axis of foliation. Fabrics are supposed to be symmetrical: only one half of the fluidal sphere is represented (modified from Cruden, 1990).

The mineral-elongation directions are oblique or subperpendicular to the regional extension direction in the adjacent greenstone (Schwertdner et al, 1983). The displacement of the magma is compensated by the displacement of the country rocks: whereas magma is rising, country rocks are sinking. This sinking is tracked by fabrics, which tend to be steep (Schwertdner et al, 1983). Sinking rim-synclines can close the root of the magma. The frequency of the domes can create interferences between one another with horizontal shortening (Castro, 1987). This interrelation is called synkinematic doming. But synkinematic doming can only occur if magma has first risen by diapirism. Bouhallier *et al* (1995) theoretical model shows the expected development of magma rising diapirically (figure III.6.).

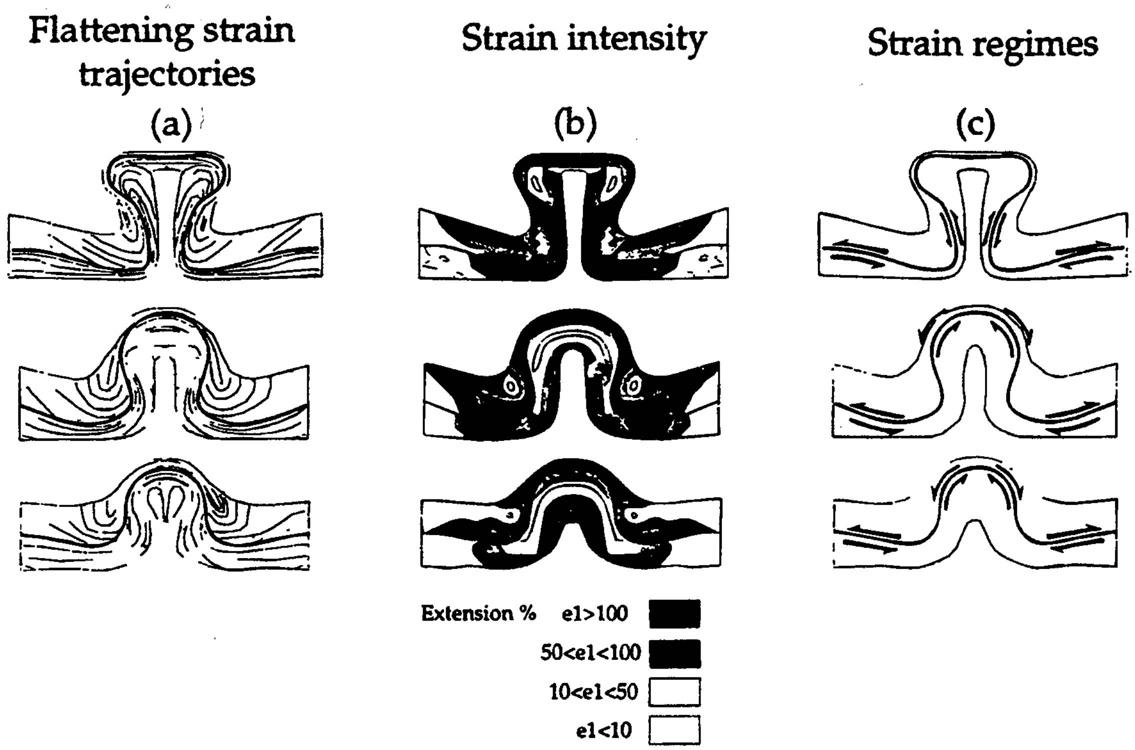

Figure III.6. Evolution of strain according to the degree of maturity of the diapir: maximum extension e1 correspond to the percentage of finite principal extension. (from Bouhallier et al, 1995).

III.1.3. *Ballooning*

Paterson, in two articles (1989 and 1995), enumerates the signs of ballooning emplacement:

"

(a)- concentric zoning of the pluton,

(b)- development of foliations in the aureole parallel to the pluton margin (also showing the syntectonism of the granite emplacement),

(c)- synkinematic growth of porphiroblast in the aureole,

(d)- foliations in the pluton that are parallel to foliations in the aureole and that increase in intensity towards the pluton margin.

(e)- evidence that final emplacement took place by bulk heterogeneous flattening (e.g. lack of stretching lineations or presence of 'millipede' structures).

(f)- folding of aplitic dykes originating from the core of the pluton with foliations in plane.

(g)- solid state deformation associated with the foliations in outer portions of the granitoid."

The five first notes could also go on for diapirs. The contact between the host rocks and magma is sharp. Ballooning emplacement can be divided into two stages during emplacement: the first one is the rise of the magma, which can only occur by diapirism. Then the sinking of the country rocks closes the trunk. Therefore, ballooning is only an ultimate stage of diapirism (England, 1990). Thus, it is very difficult to distinguish balloons from diapirs while they have the same tectonic context and their minimum stress direction is circa vertical.

III.1.4. Pulses of magma.

In some case, such as the Andean Cordillera or the Ardara pluton of Ireland, the flow is irregular and contacts between the late flow and the new one are sharp because the late flow is partly crystalline. If the late flow is partially magmatic, it may be mixed with the new one. The example of Andean granite is interesting: in this case, Petford and Atherton (1991) show that granite's emplacement occurred during an extensional regime and the later granite is also filled by magmatic flow during a later compressional event (figure III.7.) According to Clemens and Mawer (1992), conduits, which can be 40 km long according to Castro (1987), are too long to have a regular flow and, as usual, conduits open and close several times causing a disrupted flow and, consequently, granites with sharp internal contacts.

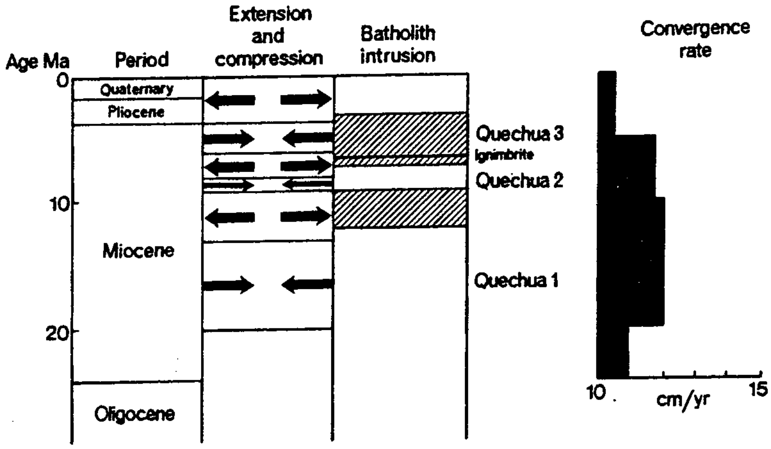

Figure III.7. Compressional and extensional periods from the Miocene Andean granite pluton, and their relation to batholith intrusion and volcanism. (Petford and Atherton, 1991)

III.2. **Discordant or post-tectonic plutons.**

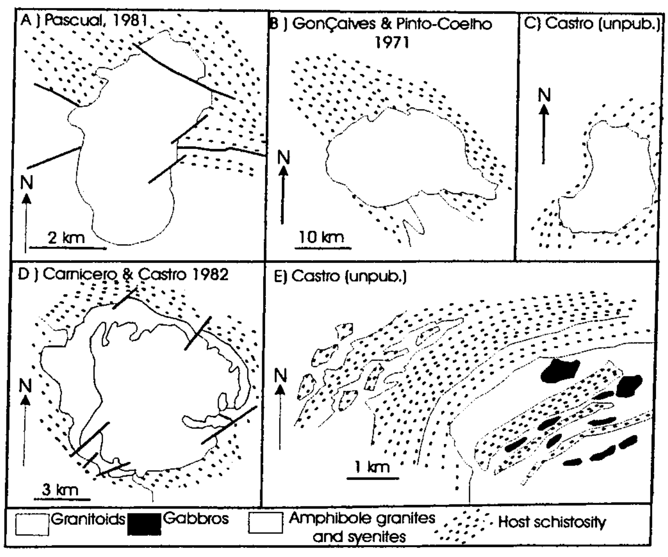

Figure III.8. Some examples of discordant plutons (Spain): (a) Arenales; (b) Santa Eulalia; (c) Zorita; (d) Barcarrota annular complex; (e) detail of the Northern border of the late granodiorite near Puente del Congosto. (Castro, 1987)

Two emplacement processes can be distinguished: stoping or cauldron. These granites tend to be non-foliated. They do not have a well-defined shape; their contacts are irregular and host rocks are sometimes fractured by the magma and their blocks integrated in the magma (little stoping phenomena). The foliations of granites "cut" foliations of host rocks.

Magma rises by conduits or diapirism and accumulates in the brittle crustal levels.

As Park (1983, p.88) says (figure III.9.), this is passive or permitted emplacement. The H_2O content of magma helps the fracturing of rocks having a higher density. They sink in the magma and the magma can rise higher around them. This kind of propagation is not really effective.

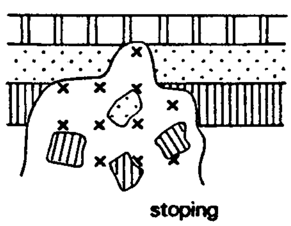

Figure III.9. Schematic draw showing a passive emplacement: stoping. (Park, 1983)

If the temperature is not sufficiently high to melt them, the host fragments sinking may fill the trunk or the conduits, and consequently interrupt the rise of the magma.

Cauldron emplacement as read in "Anorogenic Complex" from Bonin (1982) is only a special mechanism for mafic ascent, e.g., hotspot or rift volcanism in extensional zones (figure III.10.). There are segregation of acid magma and basic magma; this acid magma rises into conduits and fractures in the host brittle crust. A piece of this crust sinks in the convective magma and during this sinking, magma crystallizes near the borders of the magmatic chamber towards the core; this forms an annular complex with acid rocks near the sides of the magma becoming more and more basic towards the core.

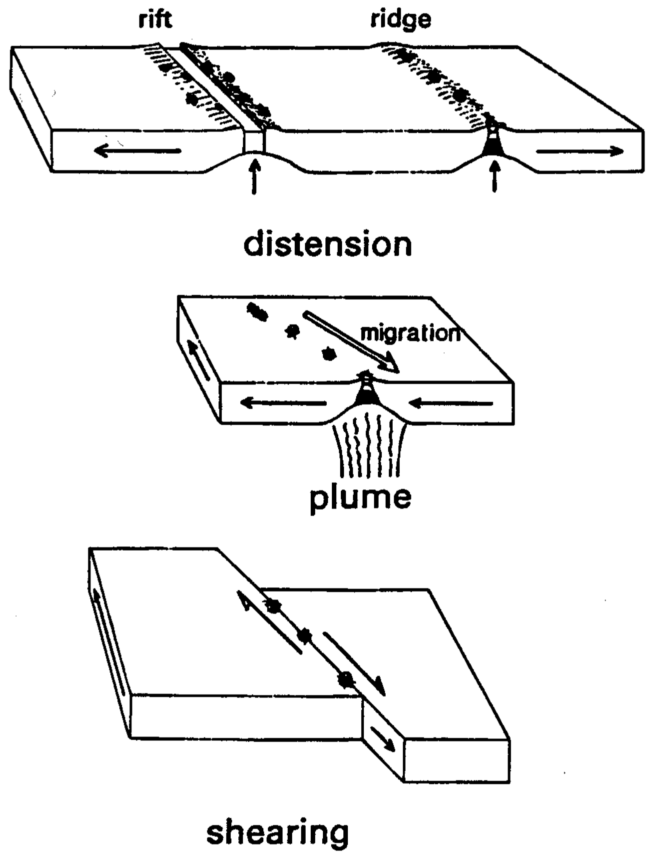

Figure III.10. Three possibilities to account for the distribution of the anorogenic complexes: a- Distension and formation of a rift or ridge. b- Hot-spot above a plume. c- Lithospheric shearing. (Bonin, 1982)

However, according to Castro (1987), if the same type of magmas rises in a regional context, different kind of emplacement can coexist. In the region of the Olivenza-Monesterio batholith, which is a balloon, *"cauldrons and balloons appear to be associated spatially"*.

In post-tectonic granites, the process of segregation, transport and emplacement of such kind of granites is poorly understood. The internal fabrics are not related to the fabrics of the country rocks and stoping is also a property of such kinds of granites.

Post-tectonic granites might be emplaced as diapirs while there is no regional tectonism and their emplacement is only related to fluidal properties of the felsic magma.

III.3. Conclusion

According to Marre (1986, p.20), each fabric based on flat or elongated minerals from the granitic plutonic rocks can be matched to an ellipsoid type (see figure III.11.):

Linear fabrics (L) result from a deformation by elongation represented by a L-strain ellipsoid, with axial symmetry (positive uniaxial).

Plano-linear (L-S) fabrics are the result of intermediate deformation by elongation and flattening, and are expressed by L>S, L=S or L<S ellipsoids with orthorhombic symmetry.

Planar fabrics (S) result from a deformation by flattening and are expressed by a S ellipsoid with axial symmetry (negative uniaxial).

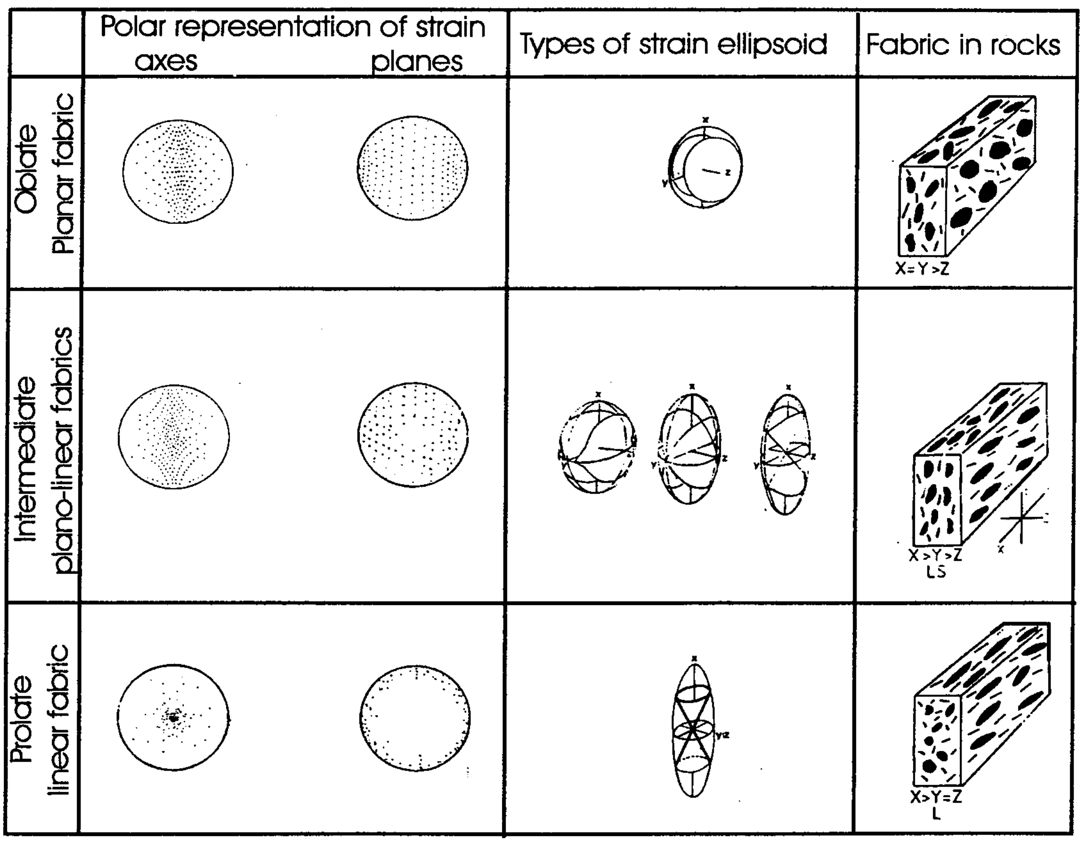

figure III.11. synthesis of strain of minerals defined by Flinn (1956) (modified from Marre (1986) and Hutton (1988)).

IV. Relation between induced magnetization and remanent magnetization

IV.1 Definitions

IV.1.1 The Koenigsberger ratio (Q)

The Koenigsberger ratio is the ratio of natural remanent magnetization over the induced magnetization.

$$Q = NRM / (k^*H_e)$$

NRM is the natural remanence of rocks in mA/m,

k is the susceptibility in SI units,

and H_e is the present earth magnetic field in mA/m.

H_e varies with the latitude and the longitude but its variations are very small. An approximately constant value may be assumed for our purposes ($H_e = 79.58$ mA/m).

Q varies consequently according to NRM and k.

As defined previously (see definition of AMS), the susceptibility of a rock depends on its nature (diamagnetic, paramagnetic and ferromagnetic components) and its anisotropy (the alignment of these minerals).

Here the susceptibility k will be the bulk susceptibility as usually done.

$k = (k_{max} + k_{int} + k_{min}/3)$

The induced magnetization (k) disappears when the magnetic field is suspended. k has no relation with the history of the rock: it only reflects its intrinsic physical properties.

The NRM (natural remanent magnetization) depends on the nature of the rock, its formation and also on the history of magnetization. NRM is always divided in two parts: the primary NRM resulting of the formation and the nature of the rock (especially the "ferro"-magnetic content of the rock) and the secondary remanence. The secondary remanence results from alteration of ferromagnetic minerals in the matrix (as defined by Rochette, 1987) and secondary magnetic fields due to a lightning (Butler, 1992).

Even though two rocks have the same nature and the same primary remanence, they can have a different secondary remanence and consequently their NRM and their Q will be different.

IV.1.2 - The theoretical Koenigsberger ratio (Q_{th})

The ARM (anhysteretic remanent magnetization) is an artificial permanent magnetization given by laboratory magnetic field. The previous magnetization (NRM) is firstly erased using an alternating field and the rock is demagnetized. The rock is secondly remagnetized with the simultaneous application of a small DC field and a large decaying AF. The ARM is consequently only related to the nature of the rock and not to its history.

We defined the theoretical Koenigsberger ratio (Q_{th}) as:

$$Q_{th} = ARM / (k*H_e)$$

Q_{th} reflects consequently only the nature of the rock and the variations due to the maximum possible remanence.

Here the remanent magnetization A will be the sum of AARM axes divided by three:

$A = (A_{max} + A_{int} + A_{min}/3)$

IV.2. - Applications

This study is namely on granites (*sensus lato*). Pilkington and Percival (1999) showed that for most of the samples, the induced magnetization of samples contribution is more important than remanent magnetization (for 92 % of samples). The figure IV.1. shows the same proportion with most of samples having a Koenigsberger ratio between 0.01 and 0.1.

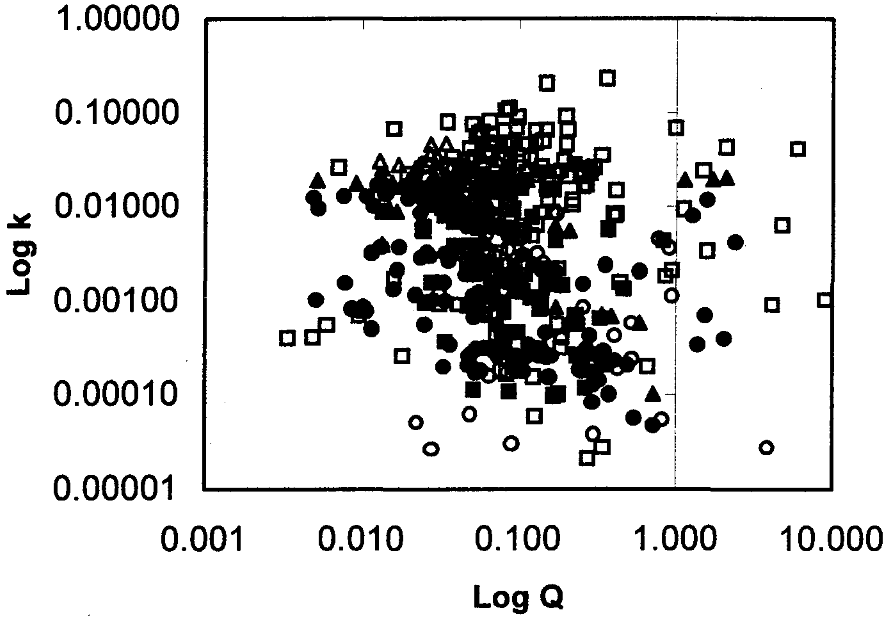

Figure IV.1. Relationships between the susceptibility (k) and the Koenigsberger ratio (Q). Samples show clearly a relation and show also the importance of contribution of induced magnetization. The relation between the susceptibility and Q and NRM cannot be defined using this figure because the susceptibility is expressed in the x axis and in the y axis (Q is dependent on k). The triangles represent post-tectonic granites: the black triangles represent the Trout lake samples (n =51), the white triangles represent the Barnum lake samples (n = 30). The squares represent granitoid samples: the black squares are samples from the Wabigoon province (n = 99), the white squares are samples from the Minto block area (n = 130). The black circles are the Mckenzie granite samples (s.s) (n = 170) and the white circles represent the Sawbill dome samples (n = 35).

The differentiation of the granites is more apparent from the susceptibility axis than the Koenigsberger axis. The distribution of samples from the Wabigoon Subprovince and the Minto Bloc province is large due to the wide variation of composition of the samples (from tonalites to syenites).

The post-tectonic granites (Barnum lake and Trout lake intrusions) are composed of monzonitic rocks with orthoclase phenocrysts. Their susceptibility values are large and due to the ferromagnetic component (Borradaile and Kehlenbeck, 1995) but their Koenigsberger ratio do not show any differences with the other granitic rocks: only their susceptibility permits us to differentiate them to the Mckenzie granite samples (composed of granitic rocks s.s.) and the Sawbill dome samples (composed of tonalitic rocks alterated into granodiorite in some places).

The same relation has been used between the susceptibility (k) and the theoretical Koenigsberger ratio (Q_{th}) (figure IV.2.).

It can be consequently concluded, comparing the figure IV.1. and the figure IV.2. that the theoretical Koenigsberger ratio (Q_{th}) shows a less dispersed range of values than the Koenigsberger ratio (Q). This is due to the secondary remanence, which depends on the history of the rock and which have been erased during the determination of Q_{th}.

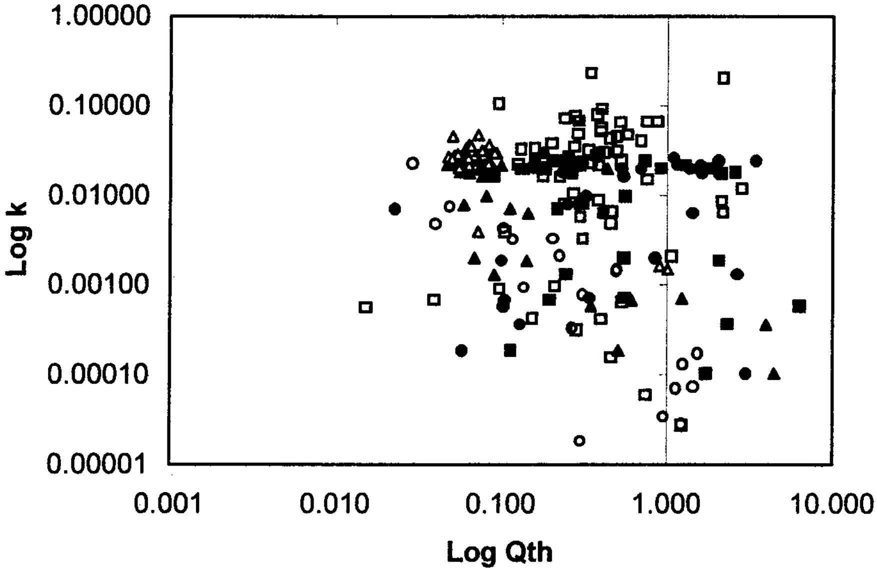

Figure IV.2. Relationship between the theoretical Koenigsberger ratio (Qth) and the susceptibility (k). The legend is the same in this figure than in figure 1. The location of the triangles (Barnum lake, n = 29 and Trout lake, n = 30), especially for Barnum lake, is better defined than in figure 1. This is the case for all the samples of the Minto block (n = 60) and Wabigoon province samples (n = 43) still showing a wide range of susceptibility, have a shorter range of theoretical Koenigsberger ratio). The values of the theoretical Koenigsberger ratio are also less dispersed. (Mckenzie granite, n = 67 and Sawbill dome, n = 19).

The induced magnetization data versus remanent magnetization data have been plotted in order to understand their relations and consequently, the behavior of the Koenigsberger ratio (figure IV.3.). The Mckenzie granite is taken as example. The Mckenzie granite is a monzogranite intruded during the Kenoran event (circa 2500 Ma)

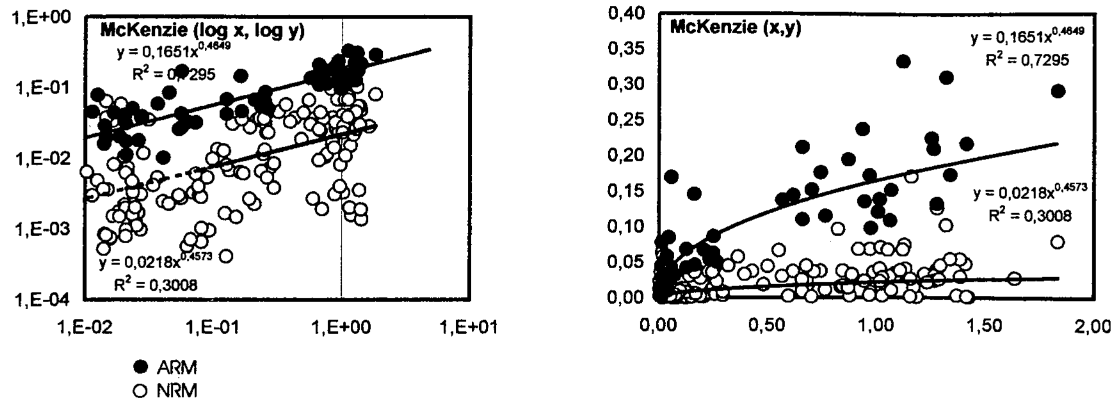

*Figure IV.3. – relationship between the induced magnetism (k*79.58) versus the remanent magnetism (NRM or ARM). The left figure has a logarithmic scale but represent the same data: the power laws are changed to lines in a logarithmic scale.*

The intensity of the ARM data is bigger than the NRM ones. Both relations with the induced magnetization (and especially the susceptibility k, since the Earth's magnetic field (H_e = 79.58 mA/m) is considered constant) may be more or less fitted by a power law. The remanent magnetization increases firstly rapidly when the induced magnetization is low. The point of inflexion of the curves varies: its emplacement is located near k*79.58 = 0.2 for the relation with the ARM and lower (k*79.58 < 0.1) for the relation with the NRM. After this point of inflexion, the remanent magnetization increases less rapidly. It seems that before this point of inflexion, the slope of the two curves was greater than 1 and consequently, the remanent magnetization increases more rapidly than the induced magnetization. After this point of inflexion, the slopes seem inferior to 1: the remanent magnetization increases slower than the induced magnetization increases. This affects the Koenigsberger ratio and the theoretical Koenigsberger ratio, which tend to a maximum value when the remanent magnetization increases more rapidly than the induced magnetization and then Q and Q_{th} decreases slowly when the remanent magnetization increases less rapidly than the induced magnetization.

The coefficient of regression R^2 of the NRM versus k*79.58 curve is smaller than R^2 for the ARM: this is due to the number of data for the NRM (n = 170) being greater than the number of data for the ARM but this is also due to the dispersion of the data being larger for the NRM data than the ARM data. This can be seen in figure IV.3 and it is compatible with the results shown by the comparison of the figure IV.1 with the figure IV.2.

The same relations (remanent magnetization versus induced magnetization) have been found for the post-tectonic granites (Trout lake and Barnum lake), the two different provinces granitoid rocks (Wabigoon province and the Minto bloc area) and Sawbill dome. The figure IV.4 shows the same relation in a logarithmic scale.

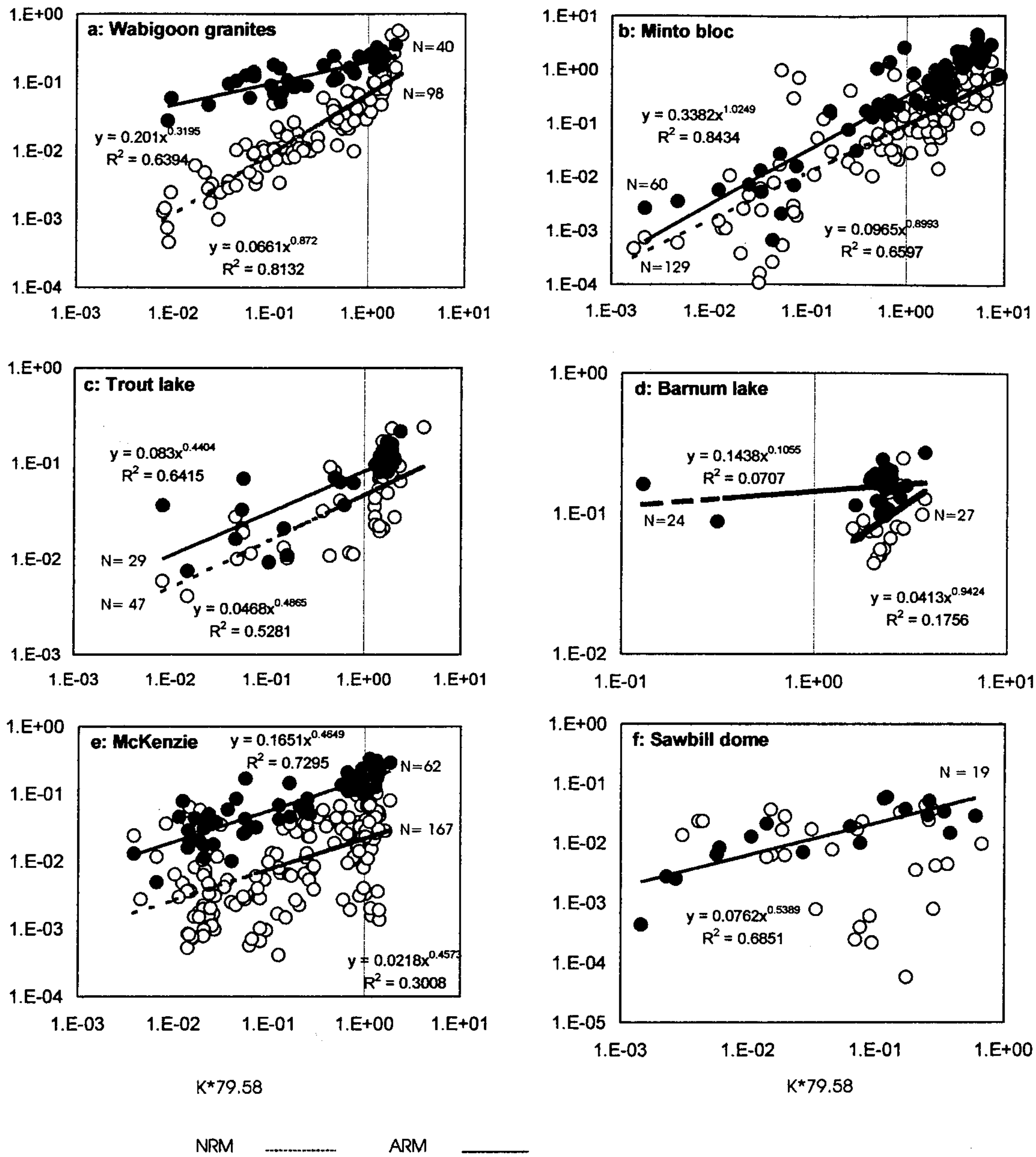

*Figure IV.4. – Same relation as figure IV.3. All granites show a power law relation between the remanent magnetization (NRM or ARM) versus the induced magnetization (k*79.58). The white dots correspond to NRM data and the black dots correspond to ARM data. (a) Wabigoon province: n = 43 for ARM data and n = 99. (b) Minto bloc: n = 60 for ARM data and n = 130 for NRM data. (c) Trout lake: n = 30 for ARM data and n = 51. (d) Barnum lake: n = 29 for ARM data and n = 30 for NRM data. (e) Mckenzie granite: n = 67 for ARM data and n = 170 for NRM data. f- Sawbill dome: n = 19 for ARM data.*

For all the granites, the ARM intensities are larger than NRM intensities data and their dispersion is less noticeable. (table IV.1).

Table IV.1

	NRM					ARM						
Location	(n)	A	B	R	sign. 95%	(n)	A	B	R	sign. 95%	k mean	standard error
Barnum lake	24	0.041	0.942	0.42	yes	27	0.144	0.106	0.27	no	0.027439	0.001192
MacKenzie	167	0.022	0.457	0.55	yes	62	0.165	0.465	0.85	yes	0.015344	0.000477
Minto bloc	129	0.097	0.899	0.81	Yes	60	0.338	1.025	0.92	yes	0.027780	0.003051
Sawbill dome	37	none	none	none	no	19	0.076	0.539	0.83	yes	0.002591	0.000653
Trout lake	47	0.047	0.487	0.73	yes	29	0.083	0.440	0.8	yes	0.015049	0.001193
Wabigoon	98	0.066	0.872	0.9	yes	40	0.201	0.320	0.8	yes	0.007887	0.000701

Table IV.1. - Results from figure IV.4.: n is the number of samples, a and b are coming from the equation of each curve ($y = a*x^b$), R is the correlation coefficient, R^2 is the cofficient of regression for each curves and there are also the answer whether the equations are significant at 95 % for each granite. The mean susceptibility (k mean) and its standard error is also added.

All the curves of figure IV.4. are significant according to the value of their coefficient of regression except Barnum lake ARM versus induced magnetization curve. In Wabigoon province case, the curves of ARM versus induced magnetization and NRM versus induced magnetization intersect one another in high-induced magnetization (induced magnetization greater than 1) whereas in the Minto block and Mckenzie granite case, the curves intersect one another in the low-induced magnetization area (induced magnetization smaller than 1).

For every granite or granitoid plutonic province, the factor a in the relation between NRM and the induced magnetization relative to the Koenigsberger ratio is smaller than 0.1. The exponent b is smaller than 1 also. No relation can be seen between these factors and the susceptibility: the biggest factor a is given by the Minto block data, which have the biggest mean susceptibility (k mean = 27780 ± 3051 μSI, n = 129) but the second biggest factor a is given by the Wabigoon data, which has one of the lowest susceptibility (k mean = 7887 ± 701 μSI, n = 98). The same thing can be seen for the exponent b. It would be logical that a relation between the remanent magnetization of rocks (related to the ferromagnetic content of rocks) and the induced magnetization (related to the susceptibility of rocks and consequently to their ferromagnetic content, especially for granite having a susceptibility superior to 2000 μSI) could be seen but it is not the case. This might be related to the differences of ferromagnetic minerals (e.g. hematite, magnetite) or the differences of structures of magnetite (single domain, pseudo-single domain or multi-domain magnetite) or their proportions. According to these different structures, the magnetite magnetization may respond differently undergoing a magnetic field.

The same remarks can be made for the relation of the ARM and the induced magnetization (theoretical Koenigsberger ratio relation Q_{th}) proving that the previous remarks are not related to the emplacement or the solid-state deformations undergone by the granites or the granitic provinces but to their nature. Indeed, in comparison with the Koenigsberger relation, a increases but is still smaller than 0.5 and b is variable: it increases with most of the granites except for Trout lake data and Wabigoon data.

The post-tectonic granites Barnum lake and Trout lake having the same nature and the same history as shown by Borradaile and Kehlenbeck (1995) do not show the same characteristics using the Koenigberger relation and the theoretical Koenigsberger relation.

The relation of the k versus NRM (Koenigsberger ratio) and of k versus ARM (theoretical Koenigsberger ratio) does work for each intruded body (except Barnum lake) (figure IV.4.) but also for granites from the same block as shown by the results of the Wabigoon samples and the Minto block samples. The cause of the relation between the remanent magnetization and the induced magnetization is unknown but it has been proved there is one.

IV.3. – Relations between remanence and susceptibility in granites

The Koenigsberger ratio is the remanent magnetism versus the magnetic susceptibility (k) (see previous chapter) multiplied by the Earth's magnetic field, giving Q and Q_{th}, dimensionless. ARM versus Ms relation as shown by King *et al* (1982) can only be considered. King et al (1983) show that the relation between ARM and AMS is linear. Nevertheless they assumed that in natural rocks, some complications could occur. In figure IV.5., three figures have been plotted showing the same data from McKenzie granite and showing three possible interpretations fits that we can attempt to interprete.

The figures IV.5.a and IV.5.b show the relation between the bulk remanent intensity A and the bulk susceptibility k with the same data (n = 74) of the McKenzie granite. In figure IV.5.a, the relation is linear using the interpretation of King *et al* (1983) and in figure IV.5.b, the relation is a power law following the results between the remanent magnetization and the induced magnetization as shown previously. The regression coefficient R^2 of figure IV.5.b. is slightly larger than the R^2 of figure IV.5.a.: this suggests that the figure IV.5.b relation would be more appropriate.

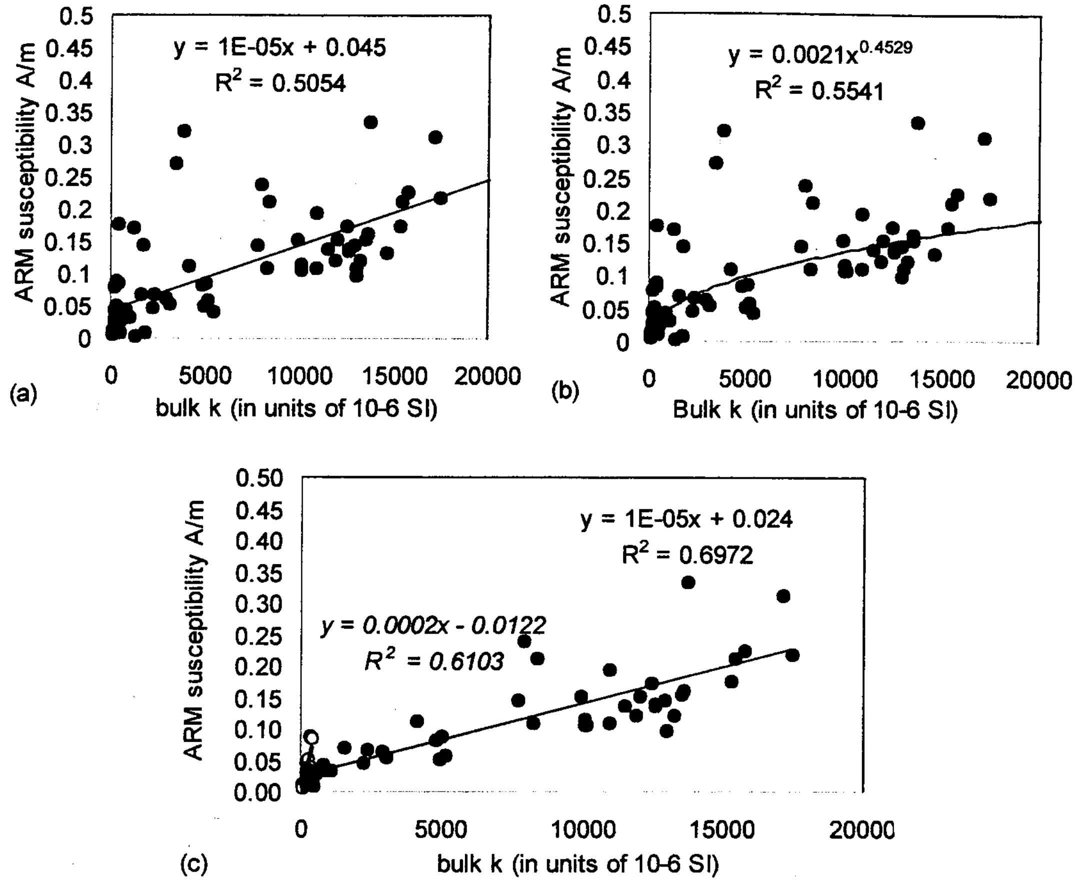

Figure IV.5. Three different fits of the ARM susceptibility A and the bulk susceptibility k of the McKenzie granite samples (n = 74 in figures a and b). Specimens relation between ARM and bulk susceptibility in figure IV.5.a of the McKenzie granite follow the classical linear relation from King et al (1983) for the whole specimens. In figure IV.5.b, The relation between remanent intensity and the bulk susceptibility of the same specimens is a power law. In figure IV.5.c, specimens ARM and bulk susceptibility relation is also linear but two groups of samples have been discriminated: a first group of specimens is represented by the white circles and their ARM and bulk AMS relation is linear with its italic equation on the left side of the figure (k<500 μSI, n = 15). The second group of specimens (0<k<20000 μSI, n = 47) is represented by black circles and their ARM and bulk AMS relation is linear too and its equation can be seen on the right side of the figure.

King *et al* (1982) have suggested that the absence of linear relation between remanent intensity and bulk susceptibility of specimens could be due to superparamagnetic (SP) magnetite grains, the effect of magnetite interactions, or to the effect of shape anisotropy in magnetite and the shifting of the x-axis of non-magnetic matrix.

The shifting of non-magnetic matrix cannot explain McKenzie specimens' behavior because the linear relation of the remanent intensity and the bulk susceptibility crosses the x-axis before –14 μSI, which is the minimum magnetic possible susceptibility value for every object undergoing a low magnetic field.

The effects of magnetite's structures variations (single, pseudosingle and multidomain magnetite) cannot be the cause of this inflexion in the case of the McKenzie granite because the frequency-distribution of mean susceptibility of the McKenzie granite show a structural difference of magnetite circa 6000 μSI (see figure V.2.).

The power law relation of the ARM intensity and k is not attributed to a heterogeneous mineralogy of McKenzie granite since the other granites (Trout lake and Barnum lake granites) show the same relation and the inflexion of ARM vs. k is consequently a general property of granitoid rocks. Despite their rather high regression coefficients R^2 values, the two groups that we can differentiate using two linear fits in figure IV.5.c., no petrological variations of McKenkie specimens have been found to explain this differentiation and therefore, such differentiation is meaningless.

The ARM, the maximum magnetic saturation of the rock in every direction, is strictly related to the ferromagnetic content of the specimens. This inflexion of the ARM-k curve at ~ 410 μSI could be due to the difference in magnetite content: in samples with

$k < \sim 410$ μSI in the case of the McKenzie granite, the magnetite grains may not numerous and close enough to interact magnetically. At large k values, the amount of magnetite grains may be sufficient for magnetite grains to interact. The same phenomenon has been proposed to explain the relation between the AMS Pj (AMS anisotropy degree) and the bulk magnetic susceptibility by Archanjo (1993). Grégoire *et al* (1995) proved that such interactions between magnetite's grains do exist consistently with the theoretical laws. The ARM versus k does not follow one proportional law but two different ones attributed to the amount hence average distance of ferromagnetic minerals.

IV.4. Conclusion.

(a) As shown by Pilkington and Percival (1999) in different magmatic rocks, the induced contribution is larger than the remanent one.

(b) The susceptibility is not directly proportional to ferromagnetic content of rock as currently thought, consequently the relation of King should not be used in granitoid rocks.

(c) The Koenigsberger ratios increase rapidly when the induced susceptibility is low, then decreases gradually due to an increase of k larger than the increase of remanent magnetization.

(d) The theoretical Koenigsberger ratio, when ARM is used instead of NRM, produces a smaller range of values and recognize the maximum potential for induced magnetization.

(e) The point of inflexion of the ARM-k graph in granites is attributed to the magnetic interaction between magnetite grains.

(f) The ARM intensity shows two proportional relations with the bulk susceptibility and this variation of relations are probably due to a different quantity a ferromagnetic minerals (magnetite in the case of studied granitic rocks) in the specimen.

IV.5. Data of Wabigoon belt (44 sites).

samples	K in SI	NRM (A/m)	Q	ARM (A/m)	Q_{th}
ATUP01A	0.015964	0.098	0.1		
ATUP01B	0.015759	0.093	0.1	0.376	0.3
ATUP02A	0.018516	0.128	0.1		
ATUP02B	0.024148	0.164	0.1	0.357	0.2
ATUP03A	0.002397	0.018	0.1		
ATUP03B	0.001256	0.010	0.1	0.091	0.9
ATUP04A	0.005824	0.170	0.4		
ATUP04B	0.00428	0.283	0.8	0.185	0.5
ATUP05A	0.005662	0.044	0.1		
ATUP05B	0.005509	0.047	0.1	0.106	0.2
ATUP05C	0.009434	0.069	0.1		
ATUP06A	0.002189	0.026	0.1		
ATUP06B	0.00158	0.019	0.1	0.052	0.4
ATUP06C	0.001464	0.022	0.2		
ATUP07B	0.017422	0.065	0.0	0.290	0.2
ATUP07C	0.014327	0.099	0.1		
ATUP08A	0.007748	0.074	0.1		
ATUP08B	0.015381	0.203	0.2	0.328	0.3
ATUP09A	0.015517	0.084	0.1		
ATUP09B	0.017260	0.133	0.1	0.178	0.1
ATUP10A	0.019134	0.103	0.1		
ATUP10B	0.015830	0.079	0.1	0.245	0.2
ATUP11A	0.000210	0.006	0.4		
ATUP11B	0.000693	0.012	0.2	0.127	2.3
ATUP11C	0.000554	0.010	0.2		
ATUP11D	0.000263	0.005	0.2		
ATUP12A	0.001048	0.011	0.1		
ATUP12B	0.000835	0.009	0.1	0.143	2.1
ATUP12C	0.001283	0.010	0.1		
ATUP13A	0.012595	0.056	0.1		
ATUP13B	0.010106	0.066	0.1	0.238	0.3
ATUP14A	0.009979	0.042	0.1		
ATUP14B	0.018707	0.080	0.1	0.237	0.2
ATUP15A	0.001882	0.012	0.1		
ATUP15B	0.001633	0.011	0.1	0.071	0.5
ATUP16A	0.00107	0.010	0.1		
ATUP16B	0.000844	0.009	0.1	0.124	1.8
ATUP17A	0.006883	0.021	0.0		
ATUP17B	0.006883	0.025	0.0	0.049	0.1
ATUP18A	0.007972	0.021	0.0		
ATUP18B	0.008754	0.032	0.0	0.151	0.2
ATUP19A	0.013144	0.035	0.0		

samples	K in SI	NRM (A/m)	Q	ARM (A/m)	Q_{th}
ATUP19B	0.012111	0.029	0.0	0.111	0.1
ATUP20A	0.001373	0.011	0.1		
ATUP20B	0.001331	0.049	0.5	0.181	1.7
ATUP21B	0.005558	0.038	0.1	0.245	0.6
ATUP22A	0.01048	0.043	0.1		
ATUP22B	0.008157	0.025	0.0	0.165	0.3
ATUP23A	0.007204	0.034	0.1		
ATUP23B	0.005906	0.026	0.1	0.118	0.3
ATUP24A	0.003841	0.016	0.1		
ATUP24B	0.002914	0.011	0.0	0.089	0.4
ATUP25A	0.002145	0.012	0.1		
ATUP25B	0.001557	0.003	0.0	0.160	1.3
ATUP26A	0.001919	0.008	0.1		
ATUP26B	0.014821	0.101	0.1	0.162	0.1
ATUP27A	0.002117	0.010	0.1		
ATUP27B	0.001872	0.016	0.1	0.108	0.7
ATUP28A	0.000876	0.003	0.0		
ATUP28B	0.000463	0.004	0.1	0.095	2.6
ATUP28C	0.000382	0.002	0.1		
ATUP28D	0.000897	0.004	0.1		
ATUP29A	0.000312	0.003	0.1		
ATUP29B	0.000286	0.003	0.1	0.047	2.1
ATUP30B	0.000118	0.002	0.3	0.059	6.3
ATUP30C	9.85E-05	0.001	0.2		
ATUP30D	0.000102	0.001	0.2		
ATUP31A	0.000794	0.001	0.0		
ATUP32A	0.000465	0.003	0.1		
ATUP32B	0.00055	0.003	0.1	0.105	2.4
ATUP32C	0.000302	0.002	0.1		
ATUP33A	0.000365	0.001	0.0		
ATUP33B	0.000759	0.005	0.1	0.060	1.0
ATUP34A	0.000113	0.000	0.1		
ATUP34B	0.000109	0.001	0.1	0.028	3.2
ATUP35A	0.007614	0.023	0.0		
ATUP35B	0.006070	0.012	0.0	0.113	0.2
ATUP35C	0.013535	0.037	0.0		
ATUP36A	0.003209	0.010	0.0		
ATUP36B	0.002369	0.013	0.1	0.097	0.5
ATUP36C	0.002777	0.011	0.0		
ATUP37A	0.017280	0.047	0.0		
ATUP37B	0.013264	0.055	0.1	0.259	0.2
ATUP37C	0.009594	0.041	0.1		
ATUP38A	0.009025	0.010	0.0		
ATUP38B	0.009085	0.027	0.0	0.136	0.2
ATUP39A	0.003828	0.012	0.0		
ATUP39B	0.004382	0.060	0.2	0.180	0.5

Samples	K in SI	NRM (A/m)	Q	ARM (A/m)	Q_{th}
ATUP40A	0.001139	0.006	0.1		
ATUP40B	0.001343	0.010	0.1	0.069	0.6
ATUP40C	0.002465	0.011	0.1		
ATUP41A	0.002719	0.010	0.0		
ATUP41B	0.002198	0.008	0.0	0.085	0.5
ATUP42A	0.023066	0.268	0.1		
ATUP42B	0.028115	0.502	0.2	1.708	0.8
ATUP42C	0.021981	0.494	0.3		
ATUP42D	0.025595	0.573	0.3		
ATUP43B	0.019043			0.694	0.5
ATUP44A	0.001434	0.007	0.1		
ATUP44B	0.006119	0.030	0.1	0.115	0.2

IV.6 Data of Minto block (130 samples).

Samples	k in SI	NRM (A/m)	Q	ARM (A/m)	Q_{th}
C9114	0.029998	0.231	0.1	1.003	0.4
PB89105	0.034740	0.287	0.1		
PB89107B	0.020123	0.117	0.1		
PB89109	0.022051	0.056	0.0	0.220	0.1
PB89112	0.000566	0.008	0.2		
PB89114	0.047593	0.340	0.1		
PB89124	0.013941	0.078	0.1		
PB89126	0.000900	0.003	0.0		
PB89138	0.005680	0.011	0.0	0.136	0.3
PB8917A	0.090649	0.706	0.1	2.898	0.4
PB8922	0.075783	0.300	0.0	1.653	0.3
PB8927	0.025354	0.119	0.1		
PB8932	0.064302	0.403	0.1	2.632	0.5
PB8936	0.031118	0.474	0.2	1.238	0.5
PBAC8939	0.021433	0.220	0.1		
PB8944	0.011868	0.205	0.2	2.669	2.8
PB8954	0.000168	0.001	0.1		
PB8957	0.006981	0.034	0.1		
PB8969	0.010234	0.070	0.1		
PB8973	0.023731	0.093	0.0		
PB8978	0.023034	0.125	0.1	0.642	0.4
PB8982B	0.009494	0.842	1.1		
PBC8987	0.020935	0.333	0.2	0.636	0.4
PB8993	0.006296	0.052	0.1		
PB90102	0.000184	0.001	0.1		
PB90107	0.025019	0.087	0.0		
PB90111	0.112002	0.763	0.1		
PB9012	0.016595	0.079	0.1	0.236	0.2
PB90120	0.000279	0.003	0.1		
PB90130B	0.026830	0.293	0.1		
PB90131	0.015492	0.184	0.1		
PB90144	0.009688	0.032	0.0		
PB90146	0.040655	19.229	5.9	2.248	0.7
PB9016	0.010403	0.022	0.0	0.223	0.3
PB90161	0.009579	0.024	0.0		
PB901641	0.022501	0.035	0.0		
PBC90166	0.060299	0.262	0.1		
PB90170	0.023591	0.329	0.2		
PB90173A	0.000964	0.002	0.0	0.016	0.2
PB9018	0.000262	0.000	0.0		
PB9028	0.000202	0.011	0.7		
PB9035	0.043424	7.271	2.1	1.556	0.5
PB9043	0.023597	0.091	0.0		
PB9046	0.006528	0.067	0.1	0.238	0.5

samples	k in SI	NRM (A/m)	Q	ARM (A/m)	Q_{th}
PB90150	0.000672	0.000	0.0	0.002	0.0
PB9051	0.045814	0.407	0.1		
PB9057	0.000316	0.005	0.2	0.007	0.3
PB9058	0.049209	0.496	0.1		
PB9067	0.010489	0.180	0.2		
PB9074	0.016528	0.071	0.1		
PB908	0.031946	0.199	0.1	0.847	0.3
PB9084	0.048038	0.248	0.1		
PB9087	0.008740	0.114	0.2		
PB9110B	0.023366	0.204	0.1		
PB91140B	0.023763	0.344	0.2		
PB91146A	0.020747	0.073	0.0		
PB91164	0.002181	0.031	0.2		
PB91168	0.000696	0.001	0.0		
PB91172	0.026617	0.015	0.0	0.531	0.3
PB91173	0.002094	0.158	0.9	0.176	1.1
PB91174	0.007896	0.055	0.1	0.149	0.2
PB91175	0.003368	0.422	1.6		
PB91176	0.065333	0.769	0.1	3.898	0.7
PB91180	0.033172	0.098	0.0	0.346	0.1
PB91183	0.068365	5.440	1.0		
PB9121	0.027821	0.056	0.0	0.819	0.4
PB91211	0.057045	0.298	0.1		
PB9123	0.091254	1.428	0.2		
PB9125	0.011861	0.142	0.2		
PBC9128	0.046701	0.302	0.1		
PB9132A	0.017619	0.376	0.3		
PB9132B	0.066578	0.083	0.0	1.550	0.3
PB9134	0.050854	0.567	0.1	1.592	0.4
PB9142	0.003240	0.020	0.1	0.080	0.3
PB9144B	0.000412	0.000	0.0		
PB9146A	0.000021	0.000	0.3		
PB9146B	0.027523	0.075	0.0		
PB9152	0.000402	0.000	0.0		
PB9175	0.001807	0.124	0.9		
PB9176A	0.008656	0.094	0.1		
PB9178	0.031957	0.296	0.1		
PB9190	0.006317	2.378	4.7	1.094	2.2
PBB9012B	0.056437	0.237	0.1	1.777	0.4
PBB9022	0.045638	0.719	0.2	1.803	0.5
PBB9060	0.045723	0.304	0.1		
PBB9066	0.008463	0.278	0.4	1.442	2.1
PBC89100	0.000413	0.006	0.2	0.013	0.4
PBC8917	0.015711	0.129	0.1	0.280	0.2
PBC8919	0.000552	0.000	0.0	0.001	0.0
PBC8939	0.079340	0.220	0.0	2.362	0.4

samples	k in SI	NRM (A/m)	Q	ARM (A/m)	Q_{th}
PBC8942	0.230318	6.555	0.4	6.354	0.3
PBC8950	0.025452	0.071	0.0	0.353	0.2
PBC8970	0.008795	0.034	0.0	0.267	0.4
PBC8978	0.033553	0.138	0.1	0.423	0.2
PBC8983	0.046959	0.243	0.1	2.169	0.6
PBC8987	0.020935	0.426	0.3	0.501	0.3
PBC8989	0.026282	0.623	0.3		
PBC8992	0.008813	0.033	0.0		
PBC8993	0.018541	0.113	0.1		
PBC8994	0.000899	0.299	4.2		
PBC8997	0.031421	0.116	0.0		
PBC901	0.071544	0.545	0.1	1.357	0.2
PBC9012B	0.008467	0.270	0.4		
PBC9016	0.000059	0.001	0.1	0.003	0.7
PBC9020	0.001576	0.055	0.4		
PBC9021	0.014824	0.490	0.4	0.881	0.7
PBC9063	0.037334	0.181	0.1	0.592	0.2
PBC9071	0.205767	2.413	0.1	35.710	2.2
PBC9074	0.065549	1.049	0.2	4.509	0.9
PBC9087	0.062698	0.285	0.1		
PBC91115	0.041880	0.161	0.0		
PBC91125	0.001452	0.011	0.1		
PBC91126	0.034704	0.929	0.3	0.749	0.3
PBC91128	0.024592	2.920	1.5	1.020	0.5
PBC9113	0.064593	0.653	0.1		
PBC91136	0.001013	0.726	9.0		
PBC9117	0.047696	0.324	0.1	1.091	0.3
PBC9119	0.000650	0.017	0.3	0.027	0.5
PBC9120	0.007996	0.259	0.4	0.199	0.3
PBC91127	0.106164	0.679	0.1	0.813	0.1
PBC9140	0.016774	0.346	0.3		
PBC9148	0.000156	0.002	0.1	0.006	0.5
PBC9154A	0.000907	0.002	0.0	0.007	0.1
PBC9158	0.003927	0.015	0.0	0.033	0.1
PBC9165	0.004924	0.047	0.1	0.178	0.5
PBC9166	0.081259	0.412	0.1		
PBC9170	0.000027	0.001	0.3	0.003	1.2
PBC9180	0.013951	0.029	0.0		
PBC9183A	0.000425	0.002	0.1	0.005	0.2
PBC90201	0.001743	0.002	0.0		

IV.7. Data of McKenzie granite (69 sites).

Samples	K in SI	NRM (A/m)	Q	ARM (A/m)	Q_{th}
LC001A	0.017735	0.048	0.0		
LC001B	0.016604	0.103	0.1	0.312	0.2
LC002A	0.004189	0.795	2.4		
LC002B	0.011779	1.480	1.6	0.238	0.3
LC002C	0.007921	0.800	1.3		
LC003A	0.017411	0.055	0.0		
LC003B	0.023053	0.080	0.0	0.293	0.2
LC004A	0.000230	0.002	0.1		
LC004B	0.000260	0.002	0.1	0.017	0.8
LC005A	0.000268	0.006	0.3		
LC005B	0.000210	0.008	0.5	0.044	2.6
LC006A	0.000311	0.001	0.1		
LC006B	0.000340	0.001	0.0	0.038	1.4
LC007A	0.000342	0.003	0.1		
LC007B	0.000256	0.002	0.1	0.041	2.0
LC007C	0.000259	0.002	0.1		
LC008A	0.005401	0.038	0.1		
LC008B	0.000458	0.005	0.1	0.059	1.6
LC008C	0.004962	0.033	0.1		
LC009A	0.000312	0.002	0.1		
LC009B	0.000325	0.002	0.1	0.018	0.7
LC009C	0.000294	0.002	0.1		
LC010A	0.013154	0.025	0.0		
LC010B	0.016070			0.133	0.1
LC010C	0.016070	0.040	0.0		
LC011A	0.014266	0.041	0.0		
LC011B	0.016845	0.055	0.0	0.174	0.1
LC011D	0.014924	0.064	0.1		
LC012A	0.000207	0.002	0.1		
LC012B	0.000178	0.002	0.1	0.029	2.0
LC013B	0.000507	0.000	0.0	0.010	0.3
LC014A	0.000057	0.002	0.5		
LC014B	0.000048	0.003	0.7	0.013	3.4
LC015A	0.009234	0.024	0.0		
LC015B	0.001579	0.010	0.1	0.042	0.3
LC016A	0.001015	0.000	0.0		
LC016B	0.000782	0.001	0.0	0.033	0.5
LC016C	0.000836	0.001	0.0		
LC016D	0.000870	0.001	0.0		
LC017A	0.000295	0.003	0.1		
LC017B	0.000262	0.003	0.2	0.011	0.5
LC017C	0.000308	0.007	0.3		
LC018A	0.001168	0.002	0.0		
LC018B	0.001545	0.001	0.0	0.003	0.0

Samples	K in SI	NRM (A/m)	Q	ARM (A/m)	Q_{th}
LC018C	0.001340	0.002	0.0		
LC019A	0.001660	0.013	0.1		
LC019B	0.001886	0.007	0.0	0.009	0.1
LC020A	0.000317	0.001	0.1		
LC020B	0.000561	0.001	0.0	0.085	3.0
LC020C	0.000356	0.002	0.1		
LC021A	0.003441	0.012	0.0		
LC021B	0.002617	0.007	0.0	0.067	0.3
LC021C	0.001016	0.002	0.0		
LC022A	0.000268	0.001	0.0		
LC022B	0.000233	0.007	0.4	0.020	1.1
LC022C	0.000262	0.002	0.1		
LC022D	0.000260	0.001	0.0		
LC024A	0.000197	0.001	0.1		
LC024B	0.000176	0.001	0.1	0.016	1.1
LC024C	0.000198	0.001	0.0		
LC024D	0.000203	0.001	0.0		
LC025B	0.015774	0.036	0.0	0.226	0.2
LC026A	0.014735	0.031	0.0		
LC026B	0.013647	0.015	0.0	1.733	1.6
LC026C	0.020577	0.035	0.0		
LC026D	0.017897	0.028	0.0		
LC027A	0.000183	0.001	0.1		
LC027B	0.000182	0.001	0.1	0.020	1.4
LC028A	0.000392	0.064	2.1		
LC028B	0.009350	0.035	0.0	0.176	0.2
LC028C	0.000346	0.038	1.4		
LC029A	0.007760	0.039	0.1	0.144	0.2
LC030A	0.013741	0.037	0.0		
LC030B	0.012251	0.019	0.0	0.098	0.1
LC031A	0.011311	0.032	0.0		
LC031B	0.013361	0.008	0.0	0.109	0.1
LC031C	0.014541	0.026	0.0		
LC031D	0.012913	0.031	0.0		
LC032A	0.000972	0.002	0.0		
LC032B	0.000700	0.003	0.1	0.043	0.8
LC033A	0.000252	0.003	0.1		
LC033B	0.000259	0.003	0.1	0.031	1.5
LC034A	0.003056	0.011	0.0		
LC034B	0.002951	0.006	0.0	0.054	0.2
LC034D	0.003242	0.007	0.0		
LC036A	0.001756	0.014	0.1		
LC036B	0.000703	0.086	1.5	0.170	3.0
LC037A	0.001503	0.031	0.3		
LC037B	0.002028	0.027	0.2	0.146	0.9
LC038A	0.003237	0.013	0.0		

samples	K in SI	NRM (A/m)	Q	ARM (A/m)	Q_{th}
LC038B	0.003135	0.006	0.0	0.063	0.3
LC038C	0.002389	0.023	0.1		
LC039A	0.001005	0.003	0.0		
LC039B	0.001583	0.004	0.0	0.068	0.5
LC039C	0.002139	0.003	0.0		
LC040A	0.000295	0.008	0.3		
LC040B	0.000291	0.006	0.3	0.051	2.2
LC041A	0.001121	0.004	0.1		
LC041B	0.000910	0.005	0.1	0.032	0.4
LC041C	0.001233	0.005	0.1		
LC041D	0.000956	0.006	0.1		
LC042A	0.010534	0.010	0.0		
LC042B	0.009632	0.004	0.0	0.115	0.2
LC043A	0.008560	0.016	0.0		
LC043B	0.002712	0.012	0.1	0.700	3.2
LC043C	0.012897	0.025	0.0		
LC044A	0.015355	0.035	0.0		
LC044B	0.014543	0.027	0.0	0.982	0.8
LC045A	0.015954	0.034	0.0		
LC045B	0.011890	0.027	0.0	0.136	0.1
LC045C	0.012221	0.032	0.0		
LC045D	0.010363	0.024	0.0		
LC046A	0.002410	0.068	0.4		
LC046B	0.002078	0.097	0.6	0.046	0.3
LC047A	0.010642	0.028	0.0		
LC047B	0.012665	0.036	0.0	0.121	0.1
LC047C	0.012833	0.038	0.0		
LC047D	0.011551	0.038	0.0		
LC048A	0.017215	0.071	0.1		
LC048B	0.017792	0.069	0.0	0.218	0.2
LC049A	0.000187	0.004	0.2		
LC049B	0.000156	0.002	0.2	0.078	6.3
LC049C	0.000183	0.004	0.2		
LC050A	0.012413	0.005	0.0		
LC050B	0.012767	0.038	0.0	0.139	0.1
LC051A	0.008975	0.036	0.1		
LC051B	0.008301	0.041	0.1	0.110	0.2
LC051C	0.007496	0.037	0.1		
LC052A	0.000426	0.009	0.3		
LC052B	0.000671	0.003	0.1	0.026	0.5
LC054A	0.003285	0.003	0.0		
LC054B	0.003713	0.005	0.0	0.272	0.9
LC054C	0.002876	0.005	0.0		
LC054D	0.003711	0.004	0.0		
LC055A	0.006935	0.037	0.1		
LC055B	0.003164	0.008	0.0	0.086	0.3

samples	K in SI	NRM (A/m)	Q	ARM (A/m)	Q_{th}
LC056A	0.014212	0.067	0.1		
LC056B	0.015885	0.032	0.0	0.211	0.2
LC056C	0.016267	0.075	0.1		
LC056D	0.015524	0.024	0.0		
LC057A	0.016197	0.046	0.0		
LC057B	0.007141	0.022	0.0	0.138	0.2
LC057C	0.011175	0.026	0.0		
LC058A	0.010630	0.023	0.0		
LC058B	0.013441	0.040	0.0	0.152	0.1
LC059A	0.017421	0.017	0.0		
LC059B	0.012923	0.011	0.0	0.003	0.0
LC060A	0.011049	0.030	0.0		
LC060B	0.008842	0.029	0.0	0.152	0.2
LC061A	0.000104	0.003	0.4		
LC061B	0.000083	0.002	0.3	0.005	0.7
LC062A	0.006064	0.037	0.1		
LC062B	0.003345	0.012	0.0	0.051	0.2
LC062C	0.004022	0.019	0.1		
LC062D	0.006301	0.023	0.0		
LC063B	0.010952	0.045	0.1	0.195	0.2
LC064A	0.012788	0.028	0.0		
LC064B	0.012186	0.023	0.0	0.173	0.2
LC065A	0.000174	0.004	0.3		
LC065B	0.000143	0.004	0.3	0.045	4.0
LC065C	0.000129	0.003	0.3		
LC065D	0.000237	0.006	0.3		
LC066A	0.013245	0.058	0.1		
LC066B	0.014108	0.068	0.1	0.334	0.3
LC066C	0.013952	0.068	0.1		
LC067A	0.008526	0.039	0.1		
LC067B	0.008293	0.045	0.1	0.212	0.3
LC068A	0.003097	0.026	0.1		
LC068B	0.004582	0.036	0.1	0.322	0.9
LC069A	0.014607	0.171	0.1		
LC069B	0.016081	0.127	0.1	3.157	2.5

IV.8. Data of Barnum lake granite (31 samples)

samples	K in SI	NRM (A/m)	Q	ARM (A/m)	Q_{th}
bl9402a	0.029491	0.096	0.0	0.213	0.1
bl9402b	0.047016	0.127	0.0	0.271	0.1
bl9403b	0.027712	0.098	0.0	0.177	0.1
bl9403c	0.031641	0.168	0.1	0.201	0.1
bl9404a	0.028161	0.038	0.0	0.159	0.1
bl9404b	0.031211	0.032	0.0	0.152	0.1
bl9405b	0.021273	0.071	0.0	0.108	0.1
bl9406a	0.027686	0.051	0.0	0.115	0.1
bl9406b	0.026704	0.049	0.0	0.102	0.0
bl9407a	0.045718	0.099	0.0	0.184	0.1
bl9408a	0.024420	0.075	0.0	0.158	0.1
bl9408b	0.028083	0.186	0.1	0.173	0.1
bl9409a	0.027820			0.121	0.1
bl9409b	0.026428	0.076	0.0		
bl9409c	0.028424	0.105	0.0	0.123	0.1
bl9410a	0.036481	0.247	0.1	0.243	0.1
bl9411a	0.029120	0.056	0.0	0.154	0.1
bl9412a	0.033704	0.081	0.0	0.164	0.1
bl9412b	0.027617	0.056	0.0	0.150	0.1
bl9413	0.001626	0.012	0.1	0.116	0.9
bl9414a	0.031303	0.067	0.0	0.162	0.1
bl9414b	0.036570	0.078	0.0	0.185	0.1
bl9415a	0.022533	0.089	0.0	0.148	0.1
bl9416a	0.001501	0.019	0.2	0.121	1.0
bl9416b	0.030484	0.141	0.1		
bl9417a	0.025702	0.044	0.0	0.102	0.1
bl9418a	0.035201	0.158	0.1	0.182	0.1
bl9418b	0.025977	0.227	0.1	0.131	0.1
bl9419a	0.031632	0.181	0.1	0.192	0.1
bl9420a	0.003943	0.004	0.0	0.023	0.1
bl9420b	0.019981	0.078	0.0	0.088	0.1

IV.9. Data of Trout lake granite (53 samples)

samples	K in SI	NRM (A/m)	Q	ARM (A/m)	Q_{th}
tl7604a	0.020911	0.104	0.1		
tl7604b	0.023683	0.074	0.0	0.103	0.1
tl7604c	0.024785	0.103	0.1		
tl76102a	0.019118	1.722	1.1	0.090	0.1
tl76115a	0.019640	2.675	1.7	0.679	0.4
tl76115b	0.020368	3.390	2.1		
tl7613a	0.002016	0.010	0.1	0.011	0.1
tl7613b	0.001295	0.009	0.1	0.009	0.1
tl7618a	0.006234	0.083	0.2	0.072	0.1
tl7618c	0.005594	0.093	0.2		
tl7629a	0.024175	0.083	0.0	0.138	0.1
tl7629c	0.017923	0.070	0.0		
tl7633a	0.018023	0.074	0.1	0.120	0.1
tl7633c	0.019594	0.072	0.0	0.114	0.1
tl7634a	0.000679	0.021	0.4	0.033	0.6
tl7634b	0.000362			0.114	3.9
tl7637a	0.019542	0.021	0.0		
tl7637b	0.019436	0.008	0.0		
tl7638d	0.016094	0.036	0.0		
tl7638e	0.017729	0.054	0.0	0.091	0.1
tl7638f	0.018313	0.013	0.0		
tl7638g	0.051508	0.241	0.1		
tl7638e	0.017729			0.037	0.1
tl7651g	0.008845	0.012	0.0		
tl7651h	0.005568	0.011	0.0		
tl7654a	0.024321	0.073	0.0	0.097	0.1
tl7654c	0.025825	0.096	0.0		
tl7657b	0.000708	0.019	0.3	0.069	1.2
tl7657c	0.000612	0.010	0.2		
tl7661a	0.016332	0.044	0.0		
tl7661c	0.019678	0.021	0.0	0.115	0.1
tl7661d	0.016195	0.028	0.0	0.098	0.1
tl7663a	0.004700	0.032	0.1		
tl7663b	0.007132	0.041	0.1	0.064	0.1
tl7664a	0.000187	0.004	0.3	0.008	0.5
tl7677b	0.000103	0.006	0.7	0.037	4.4
tl7692a	0.009717	0.011	0.0	0.062	0.1
tl7692b	0.011693	0.056	0.1		
tl7693a	0.025835	0.028	0.0	0.110	0.1
tl7694a	0.021906	0.049	0.0	0.082	0.0
tl7694c	0.025690	0.113	0.1		
tl7696a	0.029545	0.065	0.0	0.218	0.1
tl7696b	0.021487	0.135	0.1	0.170	0.1
tl7696d	0.029107	0.094	0.0		

samples	k in SI	NRM (A/m)	Q	ARM (A/m)	Q_{th}
tl7696e	0.021343	0.126	0.1		
tl9401a	0.019330	0.171	0.1	0.138	0.1
tl9401d	0.024235	0.234	0.1	0.161	0.1
tl9402a	0.018264	0.020	0.0	0.082	0.1
tl9402c	0.016453	0.023	0.0		
tl9402d	0.018061	0.022	0.0		
tl9403a	0.000847	0.012	0.2		
tl9403b	0.001863	0.013	0.1	0.021	0.1
tl9404b	0.000588	0.028	0.6	0.016	0.3

IV.10. Data of Sawbill dome (53 samples)

samples	k in SI	NRM (A/m)	Q	ARM (A/m)	Q_{th}
GBR008A	0.000191	0.006	0.4		
GBR008B	0.000242	0.006	0.3		
GBR008C	0.000174			0.021	1.5
GBR009A	0.000390	0.006	0.2		
GBR009B	0.000857	0.017	0.3		
GBR009C	0.000783			0.019	0.3
GBR0010A	0.000063	0.000	0.0		
GBR0010B	0.000051	0.000	0.0		
GBR0010C	0.000071			0.006	1.1
GRB0011A	0.008355	0.115	0.2		
GBR0011B	0.003501	0.024	0.1		
GBR0011C	0.003165			0.030	0.1
GBR0012A	0.000055	0.004	0.8		
GBR0012B	0.000242	0.010	0.5		
GBR0012C	0.000074			0.008	1.4
GBR0013A	0.000158	0.001	0.1		
GBR0013B	0.000175	0.001	0.1		
GBR0013C	0.000132			0.013	1.2
GBR0014A	0.000570	0.024	0.5		
GBR0014B	0.002544	0.029	0.1		
GBR0014C	0.001437			0.056	0.5
GBR0015A	0.004541	0.280	0.8		
GBR0015B	0.003655	0.264	0.9		
GBR0015C	0.001510			0.060	0.5
GBR0016A	0.000977	0.006	0.1		
GBR0016B	0.001931	0.008	0.1		
GBR0016C	0.002122			0.038	0.2
GBR0017A	0.000187	0.004	0.2		
GBR0017B	0.000038	0.001	0.3		
GBR0017C	0.000335			0.007	0.3
GBR0017D	0.000230	0.004	0.2		
GBR0018A	0.000888	0.004	0.1		
GBR0018B	0.001158	0.003	0		
GBR0018C	0.000935			0.010	0.1
GBR0019A	0.002156	0.024	0.1		
GBR0019B	0.003220	0.033	0.1		
GBR0019C	0.003234			0.052	0.2
GBR0019D	0.001111	0.084	0.9		

samples	k in SI	NRM (A/m)	Q	ARM (A/m)	Q_{th}
GBR0020A	0.000423	0.014	0.4		
GBR0020B	0.000937	0.006	0.1		
GBR0020C	0.004755			0.015	0.0
GBR0021A	0.003037	0.017	0.1		
GBR0021B	0.003435	0.017	0.1		
GBR0021C	0.004255			0.035	0.1
GBR0022A	0.000030	0.000	0.1		
GBR0022B	0.000027	0.008	3.9		
GBR0022C	0.000034			0.003	1.0
GBR0022D	0.000026	0.000	0.0		
GBR0023A	0.005110	0.025	0.1		
GBR0023B	0.007394	0.027	0.0		
GBR0023C	0.007444			0.029	0.0
GBR0024C	0.000029			0.003	1.2
GBR0025C	0.000018			0.000	0.3

V- The Mackenzie granite

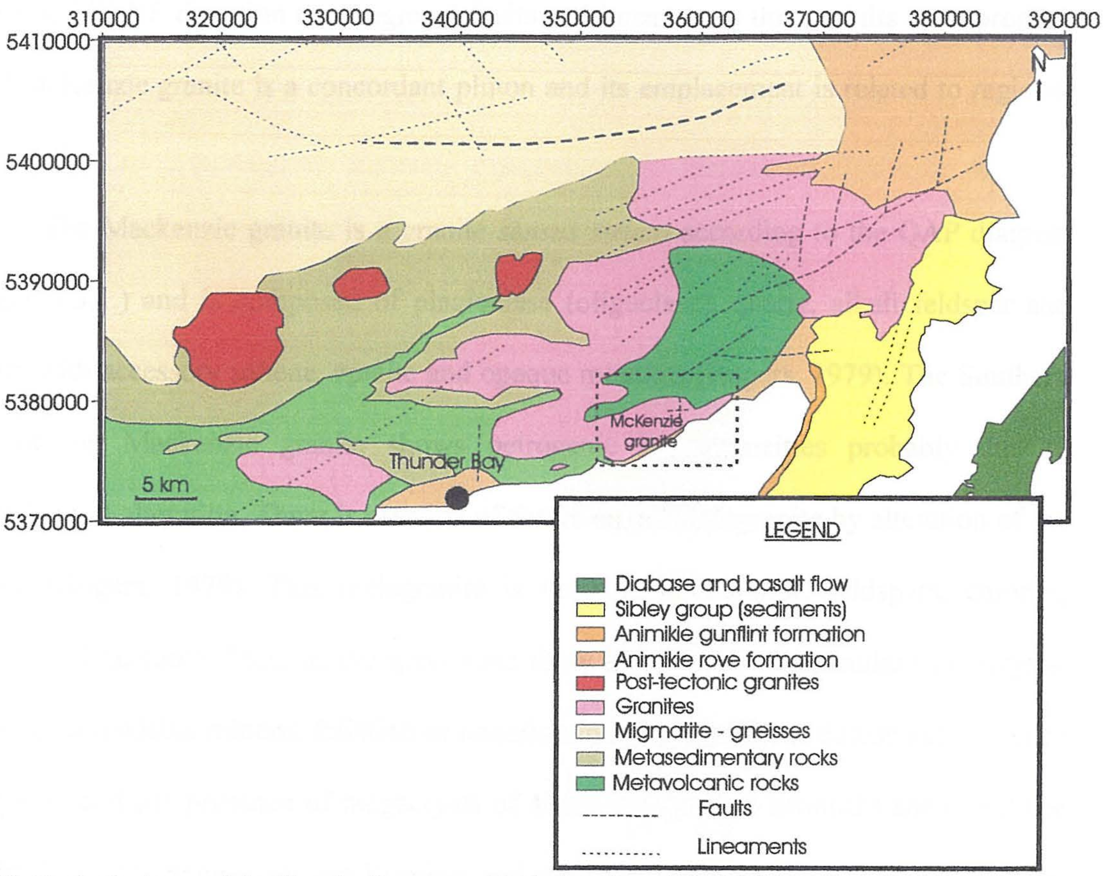

Figure V.1. Geological map of the Thunder Bay area with the location of the McKenzie granite.

The Mackenzie granite is located to the NE of Thunder Bay on the edge of Lake Superior (figure V.1). Highway 11-17 crosses the granite along its length. This intrusion is located in the Wawa subprovince. The Mackenzie granite is emplaced in metavolcanic rocks (2.5 to 2.9 Ga) to the North, consisting of massive mafic flows and intermediate to felsic volcanoclastic deposits. On the western side of the granite, the same rocks appear and the Macgregor granite extends into the Mackenzie granite. In the South, Proterozoic sedimentary rocks of the Animikie group (1.5 to 2.5 Ga) overlay the granite. The MacKenzie granite emplacement (2.4 to 2.75 Ga) is older than the Animikie group. These sedimentary rocks comprise shales, wackes and iron formation and are intruded by diabase dykes and sills (1 to 1.6 Ga). The shape of the McKenzie granite is elongated in the same SW-NE direction than regional faults and lineaments: this permits us to propose that MacKenzie granite is a concordant pluton and its emplacement is related to regional deformation.

The Mackenzie granite is a granite *sensus stricto* according to the QAP diagram (figure II.3.1.) and is composed of plagioclase (oligoclase), quartz, alkali feldspar and biotite with accessory sphene, apatite and opaque minerals (Rogers, 1979). The Southern part of the Mackenzie granite shows petrogenic heterogeneities probably due to hydrothermal alteration. There is creation of the so-called melagranite by alteration of the granite (Rogers, 1979). This melagranite is composed of quartz, feldspars, chlorite, sericite and hematite. Most of the specimens show imbricated equigranular microcrysts. There is no readable mineral foliation or lineation in the field. The undulose extinction of the quartz and the presence of megacrysts of alkali feldspars in xenoliths show that the granite has undergone a recrystallization and a metamorphic tectonic process (Rogers, 1979).

V.1. Fabrics study

197 cores from 81 stations have been collected; the anisotropy of magnetic susceptibility (AMS) of the 197 specimens and anisotropy of anhysteritic remanent magnetism (AARM) of 81 specimens (one from each station) have been measured. The magnetic susceptibility k_{MEAN} shows a wide variation of intensities (from 48 to 23053 μSI). The Mackenzie granite has a multimodal frequency-distribution of k_{MEAN} (figure V.2.). Borradaile and Henry (1997) have suggested that multimodal frequency-distribution is typical of granitoids with susceptibilities ≥ 1000 μSI: this is the case for the Mackenzie

granite where average susceptibility (mean susceptibility of all specimens) is 6280 ± 442 μSI. The frequency-distribution is divided in two groups of specimens (≤ 6000 μSI and > 6000 μSI; figure V.2. They may be related to either two different ages, two different textures of the ferromagnetic minerals (magnetite), or the presence of two different ferromagnetic minerals with different proportions in the specimens.

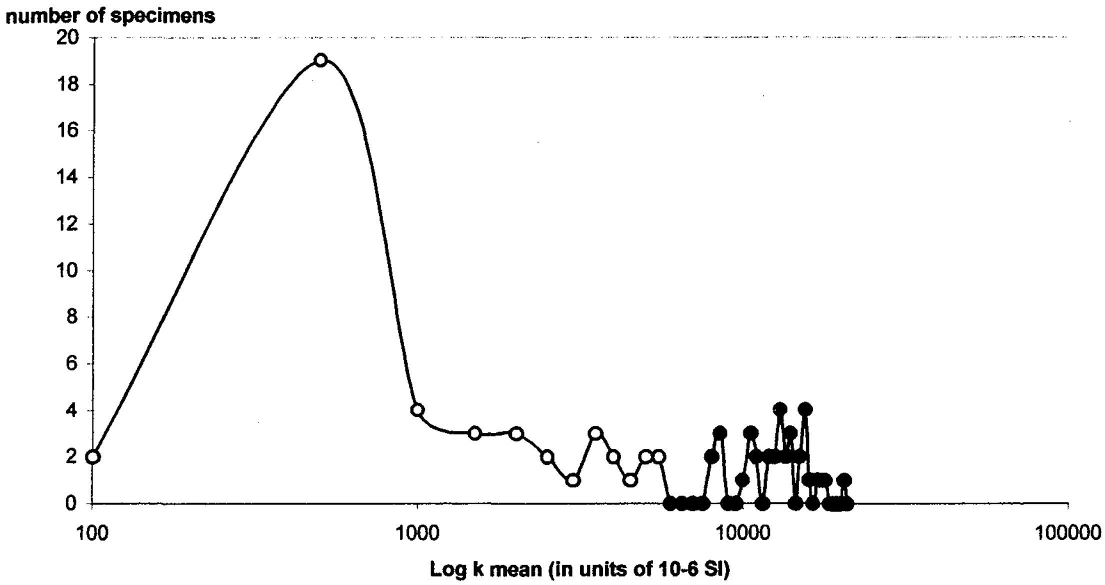

Figure V.2. Frequency-distributions of mean (or "bulk") susceptibility of the Mackenzie granite. The first discriminated group is represented by the gray dots (k ≤ 6000 μSI) and the second group by black dots (k > 6000 μSI) (n = 81).

The relation of the ARM (mA/m) versus the k_{MEAN} provides information about the relation between ferromagnetic minerals and the matrix (diamagnetic and paramagnetic minerals) (King *et al*, 1982). In figure V.3., two lines can be distinguished. The black dots (n = 47) fitted by the second line suggest that the remanent intensity (mA/m) results from a single ferromagnetic mineral.

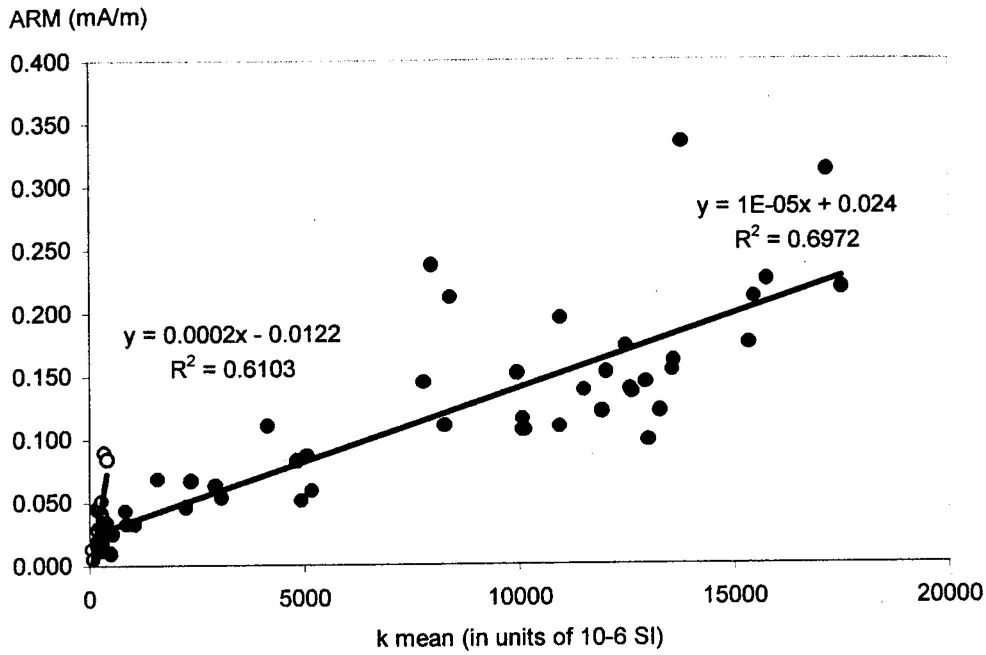

Figure V.3. Relation between the remanent intensity (mA/m) (calculated using the average of remanent intensities of maximum, intermediate and minimum axes of AARM ellipsoids of one specimen from one location) related to ferromagnetic content of the specimens and the mean susceptibility (mean susceptibility is the sum of bulk susceptibility (($k_{max}+k_{int}+k_{min}$*)/3) of specimens from the same location divided by their numbers) related to diamagnetic, paramagnetic and ferromagnetic content of the specimens of the MacKenzie granite. Two groups of specimens (white dots with 15 locations and black dots with 47 locations) are differentiated and are aligned along two lines.*

The theoretical intersection of this line with the x-axis is equal to - 2400 but the possible susceptibility values of minerals cannot be less than – 14 μSI (diamagnetic minerals). The intercept shown is a meaningless artefact of poorly distributed points on the graph. The predicted matrix susceptibility of the line of black dots specimens cannot consequently be known using this relation (figure V.3).

The white dots having very low susceptibilities (≤ 500 μSI) follow also a line of regression (n = 15). The predicted matrix susceptibility is equal to 59 μSI (paramagnetic matrix with a very low susceptibility) for these rocks. The specimens of this group do not show the same behavior than the other group. This differentiation of these two groups of rocks (one with specimens' susceptibilities ≤ 500 μSI and another with susceptibilities ≤ 24000 μSI) could not have been found by looking at the frequency of the mean susceptibility of the specimens because of the too low susceptibilities of the rocks of the group with bulk k ≤ 500 μSI. In figure V.4., the frequency-distributions of the group of bulk k ≤ 500 μSI have been differentiated and describe a Gaussian distribution.

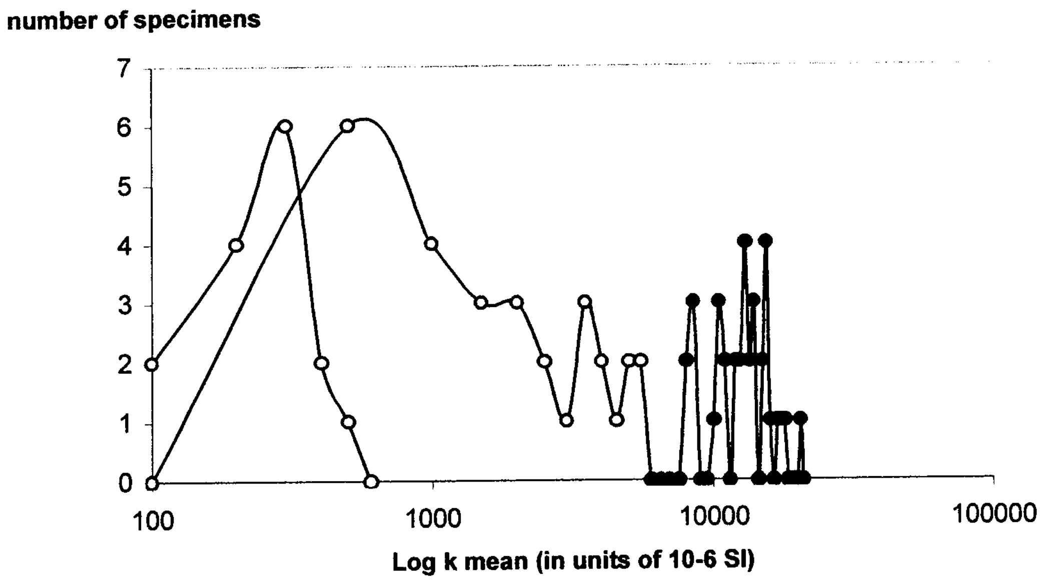

Figure V.4. Multimodal-frequency distribution of mean susceptibility of the Mackenzie granite with three differentiated groups: the first group with k mean ≤ 6000 μSI is represented by gray dots, the second group with k mean > 6000 μSI is represented by black dots and the third group (k ≤ 500 μSI) is represented by white dots (n = 15) and has been discriminated thanks to figure V.3..

According to figures V.3.and V.2., three groups have been distinguished: a first group of data with susceptibilities ≤ 500 μSI (white dots), a second group of data with susceptibilities ≤ 6000 μSI (gray dots) and a last one with susceptibilities > 6000 μSI (black dots) (figure V.4).

The relationships (Henry, 1983) between k_{MEAN} and the k_{max}, k_{int} and k_{min} susceptibilities of each specimen (figure V.5.) show a linear correlation. These lines prove that the magnetic susceptibility can be divided into two components: a paramagnetic component (the matrix) with susceptibility equal to 267 ± 442 μSI and a ferromagnetic component having only one high susceptibility phase mineral (Borradaile and Lagroix, 2000). Thus, because there is only one ferromagnetic mineral, the multimodal-distribution frequency can only be due to a change of structures of this ferromagnetic mineral, which can consequently be only magnetite. The susceptibility of the matrix is found using the average of the points of intersection of the lines between one another: the intersection point of the relation between k_{max} and k_{int} with the bulk k is equal to 480 μSI; the intersection point between k_{max} and k_{min} with the bulk k is equal to 289 μSI and the intersection point between k_{min} and k_{int} with bulk k is equal to32 μSI. The three lines do not cross one another exactly in one point but their intersection's points values are included in the margin of error (± 442 μSI) and this proves the linearity of the directions of the axes of the ferromagnetic minerals with the directions of the axes of the matrix minerals (Borradaile and Lagroix, 2001).

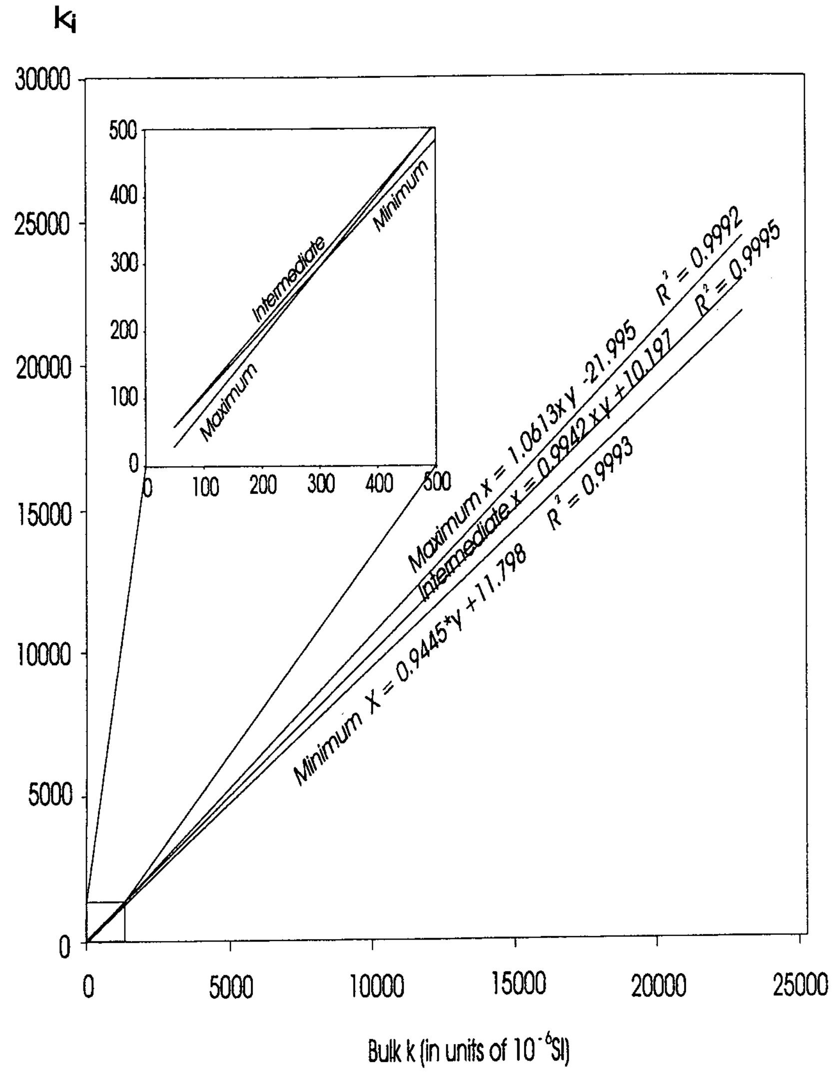

Figure V.5. Relationships between k_{MEAN} and k_i (i = max, int or min) of each specimen (Henry, 1983) (n = 197) of the MacKenzie granite.

Figure V.6. shows the relation between the intensity of anisotropy of the magnetic ellipsoid (P_j) and the shape of the ellipsoid (T_j). The latter parameter (T_j) ranges from + 1, which represents an oblate shape (S-fabric), to – 1 which represents a prolate shape (L-fabric). In figure V.6., the susceptibility contours corresponding to the population of points (n = 197) and the remanent susceptibility (n = 81) have been represented as contours. The MS contours show a symmetry around the axis of P_j (T_j mean = + 0.001 ±

0.032) and P_j is less than 1.3 (P_j mean = 1.105 ± 0.007) (except for 7 specimens). This may be due to crystallographic alignments fully developed and this is a common feature in igneous rocks (Borradaile and Lagroix, 2000).

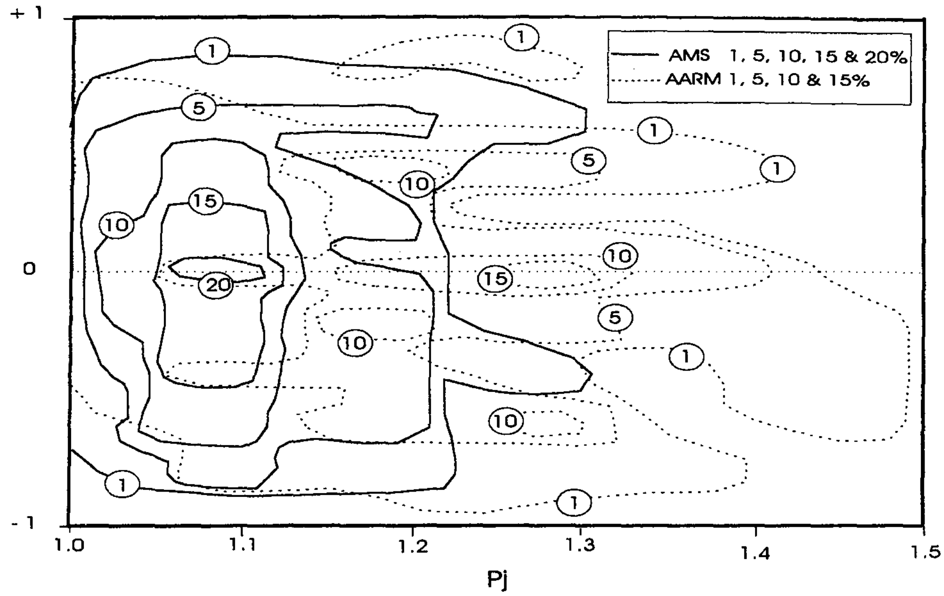

Figure V.6. Diagram of the relation between Pj (intensity of the ellipsoid) and Tj (shape of the ellipsoid) (n = 197 for AMS and n = 81 for AARM) of the MacKenzie granite.

The AARM T_j and P_j are more dispersed than for AMS with higher intensities of P_j (Pj mean = 1.22 ± 0.01). AARM has a P_j maximum smaller than 1.5 (except 8 specimens whose P_j > 1.5). Even though $T_{j\ mean}$ very close to 0 (- 0.035 ± 0.047), it seems that its dispersion is large in the prolate side ($0 \leq T_j \leq -1$) than in the oblate side. Four points of concentrations are differentiated: a first one around Tj ≈ 0.5, a second one more important with $T_j \approx 0$ and a third and a fourth one in the prolate domain ($T_j \approx$ - 0.2 and $T_j \approx$ - 0.5).

The relation of P_j versus log bulk k for each specimen (figure V.7.) shows overall increase of Pj with increasing.

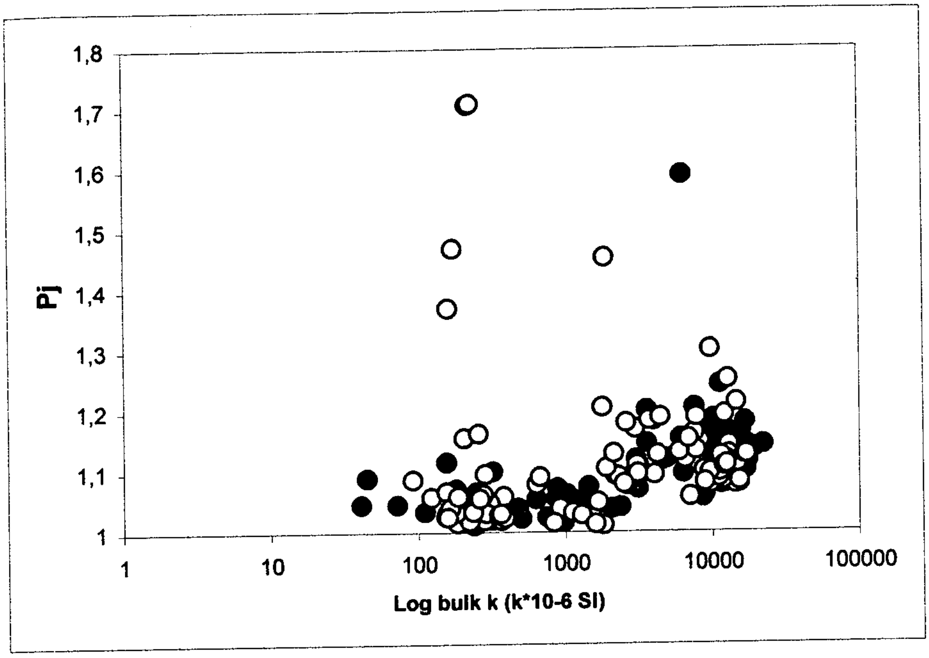

Figure V.7. Relation between the intensity of anisotropy of the magnetic ellipsoid (Pj) of AMS and the logarithm of the bulk susceptibility (($k_{max} + k_{int} + k_{min}$*)/3 for each specimen). Black dots represent prolate shape (Tj<0) and oblate shape (Tj>0) is represented by white dots (n = 197) of the AMS ellipsoid of the MacKenzie granite.*

There is no evident obvious relationship between the shape parameter (Tj) and both Pj and k: oblate and prolate fabrics are both present whatever the values of Pj and k are. This property is typical of granitoids having a susceptibities larger than 1000 μSI, i.e. mainly controlled by their ferromagnetic minerals (Borradaile and Henry, 1997; Bouchez, 1997) and is due to the interaction of magnetites' grains with one another (Gregoire *et al*, 1995).

In figure V.8., showing the relation between the Tj and log k , three groups can be distinguished: a first one has low susceptibilities (k < 500 μSI), a second one is transitional with susceptibilities ranging between 500 to 6000 μSI and a last one, whose susceptibility is greater than 6000 μSI. These differentiations fit quite well with the groups distinguished previously in figures V.3. and V.4..

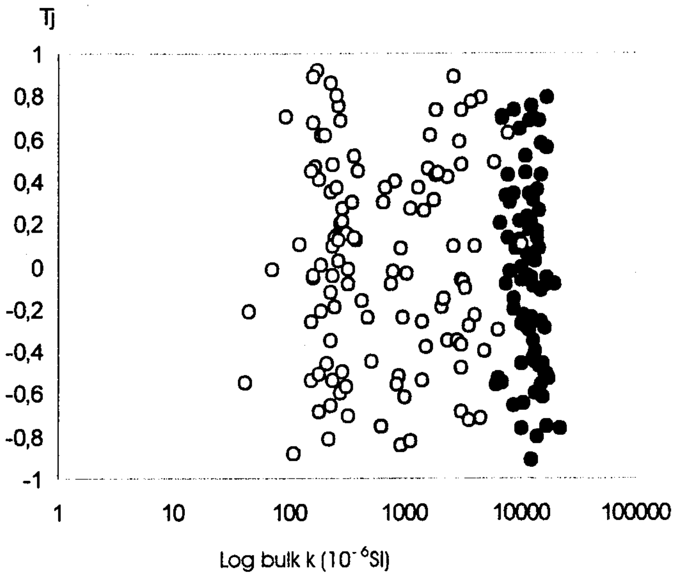

Figure V.8. Relation of the Tj with log bulk k of each specimen of the MacKenzie granite (n = 197) . The first group with k mean ≤ 6000 μSI is represented by gray dots, the second group with k mean > 6000 μSI is represented by black dots and the third group (k ≤ 500 μSI) is represented by white dots

The group k <500 μSI (n = 38) distinguished in figure V.3. has low susceptibilities and the contribution of ferromagnetic minerals is not important. Their fabrics are controlled by paramagnetic minerals. Most of the specimens of this group are located in the southern part of the granite (see figure V.9.). Most of the specimens with k ≤ 6000 μSI are located in the NE part of the granite and are controlled by magnetite behavior whereas the specimens with k > 6000 μSI are found in the western, the southern and the eastern part of the granite and are also controlled by the magnetite behavior.

The Tj mean of the three groups are similar and the Pj mean of the groups with susceptibilities ≤ 6000 μSI and 500 μSI are also very close. The Pj mean of specimens' k ≥ 6000 μSI is greater (see table V.1.).

Table V.1.

	k	Pj	Tj
$k_{mean} \geq 6000$ μSI	12163 ± 349 μSI	1.14 ± 0.01	-0.03 ± 0.05
6000 μSI > $k_{mean} \geq 500$ μSI	1902 ± 216 μSI	1.08 ± 0.01	0.05 ± 0.05
$k_{mean} < 500$ μSI	214 ± 15 μSI	1.10 ± 0.03	- 0.03 ± 0.09

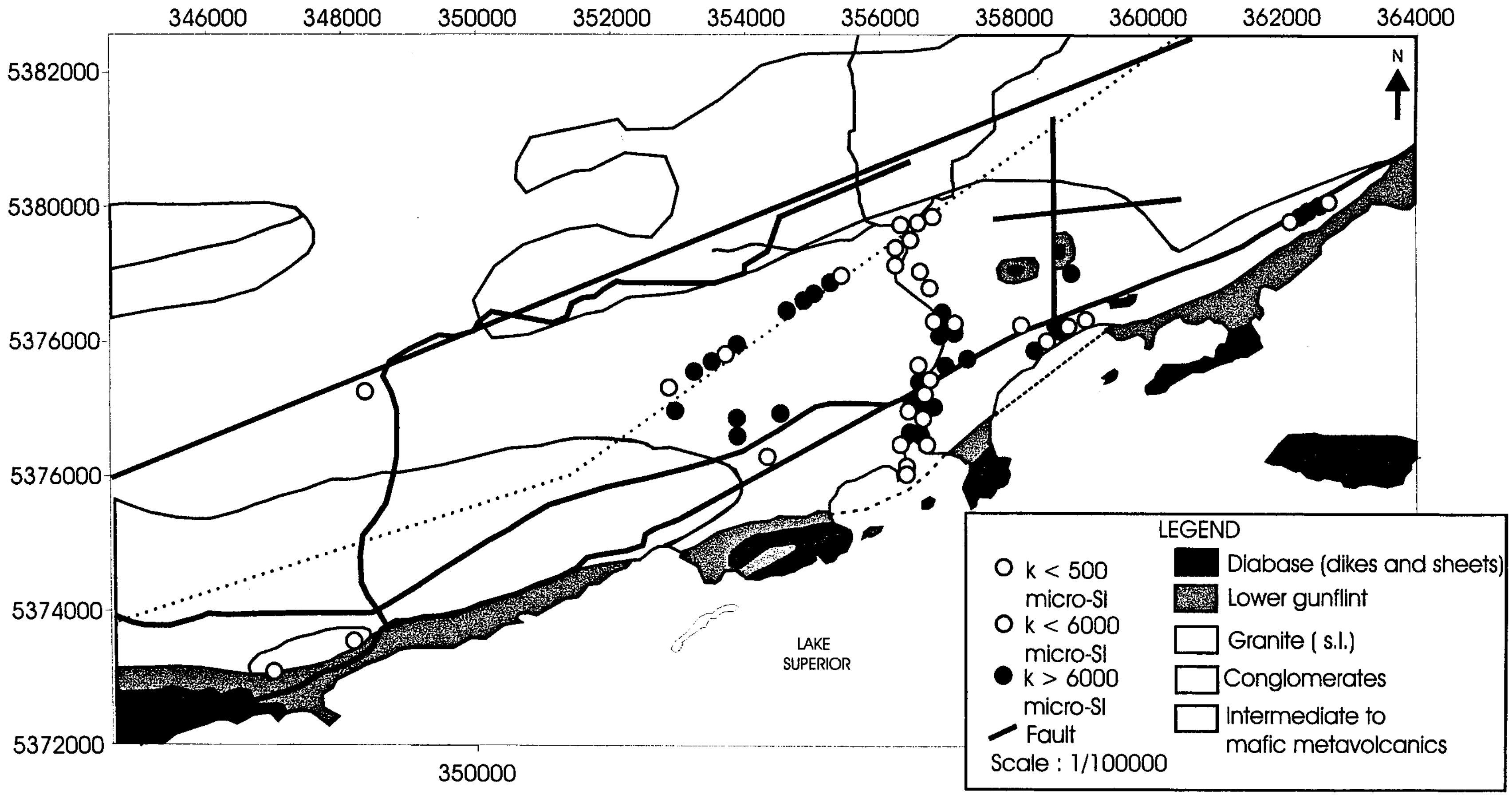

Figure V.9. Location of the collected specimens (81) of the MacKenzie granite. The groups have been discriminated by their bulk susceptibilities. Some specimens locations are too close from one another to be differentiated on the map.

V.2. Orientation-distribution of fabrics

V.2.1. *Stereonets*

In figure V.10., stereonets of the direction of k_{max}, k_{int} and k_{min} of AMS and AARM are shown. A good correlation between maximum directions, intermediate directions and minimum directions of AMS and AARM can be seen: ferromagnetic minerals contribution controls the susceptibility. The directions of k_i of AMS seem less dispersed than the principals directions of AARM: the magnetic silicates contribution is consequently less dispersed and its proportion sufficiently important to affect the AMS. A group of specimens maximum orientations is concentrated in the eastern part of the stereonet but the AARM maximum orientations directions do not show the same concentration: this suggest that this group is more controlled by paramagnetic minerals in the specimens (perhaps some specimens of the group < 500 μSI and ≤ 6000 μSI). The directions of axes of AMS define an $L > S$ ellipsoid: the plane formed by intermediate axes directions seems similar to the plane formed by minimum axes directions. The intersections of the planes drawn in figure V.10. for the maximum and minimum directions of AMS give the values of the eigenvectors. The directions of maximum axes are concentrated around the 283/01 direction whereas directions of intermediate and minimum axes lie along a N-S plane: this is coherent with the geology of the area, subprovinces show a N-S shortening and geological complexes show an E-W elongation (figure V.1.).

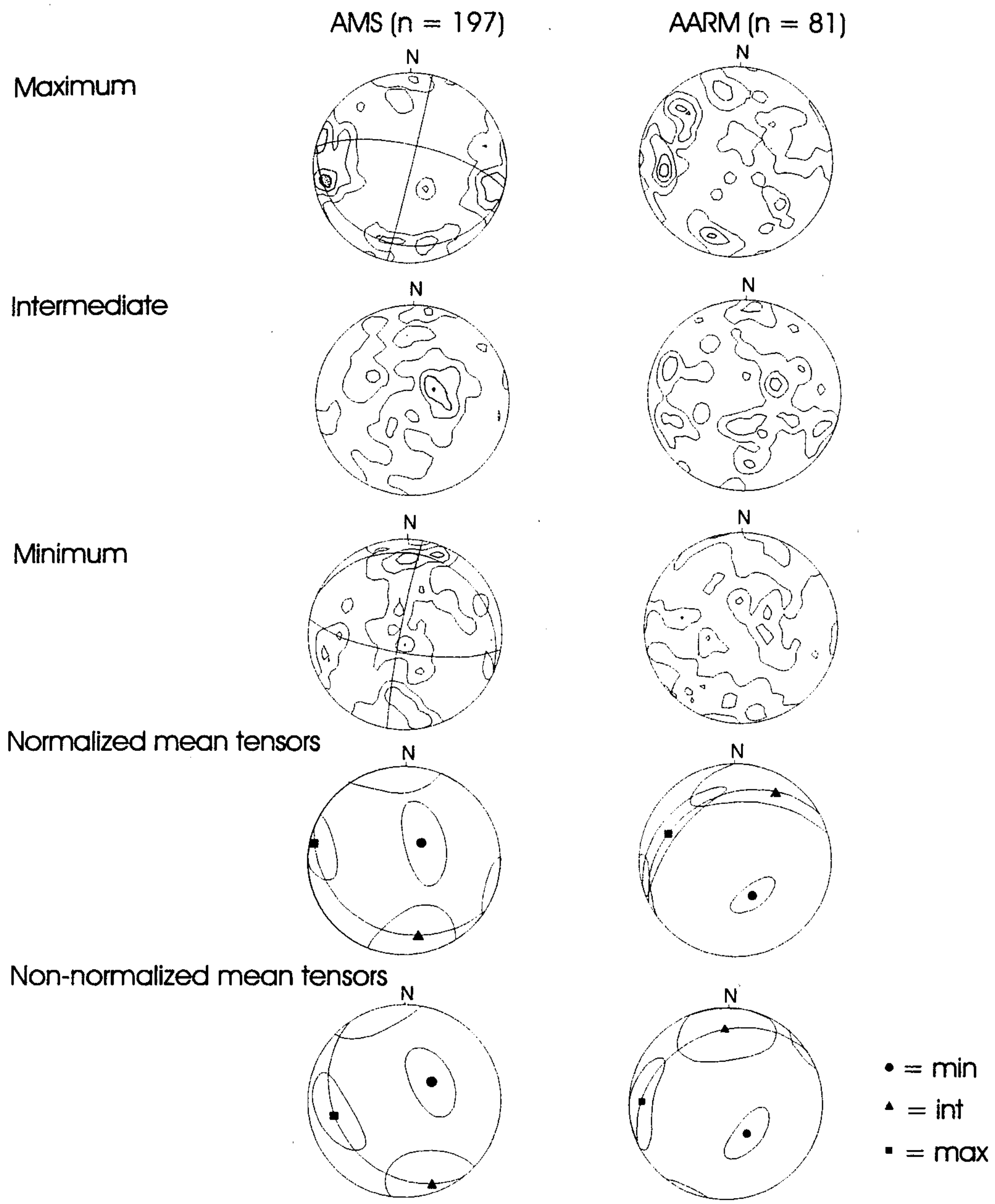

Figure V.10. Stereonets of the orientations of the susceptibility axes (n = 197) and of the anhysteretic remanent axes (n = 81) of the MacKenzie granite and their normalized and non-normalized tensors. The contours are multiple of the uniform density.

The directions of axes of AARM are more complicated to analyze because they are more dispersed especially the orientation of the minimum axes. The orientation of intermediate axes defines two planes: one is oriented N-S like the AMS minimum axes orientations and another group of points is oriented horizontally toward the East. It seems consequently there are two fabrics imbricated with one another: the first one corresponds to the AMS fabric and is an L > S ellipsoid with the maximum axes in an horizontal plane and oriented toward the East and a second one with vertical minimum axes directions and the maximum and intermediate axes in an horizontal plane (L < S ellipsoid). This interpretation is corroborated by the study of tensors orientations. The normalized tensor of AMS is affected equally by all the specimens whatever are their susceptibilities intensities: the tensor of intermediate axes orientations is aligned with the tensor of minimum axes orientations and therefore the tensors show an L > S fabric like the AMS stereonets. Thus the tensors ellipses do not show a perfect orthorhombic symmetry. Borradaile (2000) has suggested that this proves the non-coaxiality of the fabrics' orientations. The non-normalized tensors (figure V.10.) are more affected by high suscetibilities intensities and therefore by ferromagnetic minerals such as magnetite in the case of the MacKenzie granite. The intermediate axes orientations ellipses are aligned with the maximum axes orientations ellipse and therefore, in the case of non-normalized tensors, the ellipses describe an L < S orientation-distribution and a magnetic foliation. Thus, the ellipses are not perfectly aligned with the plane of magnetic foliation and therefore the orientation-distribution is non-coaxial. In both cases, the ellipse of minimum axes distribution is steep and the intermediate and maximum axes ellipses are more or less in the horizontal plane. The magnetic foliation of AMS normalized and non-normalized tensors is changed but the locations of the ellipses stay more or less in the same area. The AARM normalized and non-normalized tensors have their ellipses of orientations of maximum and intermediate axes well aligned along the magnetic foliation

(L < S fabric) and the orientation of the magnetic foliation has the same direction. The ellipses of non-normalized AARM tensor are bigger and consequently the orientations of maximum, intermediate and minimum axes are more dispersed. Although the direction of minimum AARM axes is the same in normalized and non-normalized tensors, the orientation of the ellipse is changed and the ellipses of AARM normalized tensor are more non-coaxial than the non-normalized ones. The variation of orientation of the magnetic foliation and fabric in AMS tensors is explained by the AARM tensor: the AMS non-normalized tensor is more affected by ferromagnetic minerals, which have higher susceptibilities and consequently will tend to be closer to AARM tensors. The study of the tensors proves that there is a difference of fabric between the ferromagnetic minerals, which have an oblate distribution and the paramagnetic and diamagnetic minerals, which have a prolate distribution. The intermediate and maximum axes in every tensors are always subhorizontal and the minimum axes subvertical.

V.2.2. *Maps*

The Maps of the MacKenzie granite have been drawn using Sigmaplot software for the bulk k ((k max. + k int + k min)/3), the Pj (intensity of the ellipsoid) and the Tj (shape of the ellipsoid) of the AMS and the AARM and Spheristat software for the maximum orientations and the minimum axes orientations. The spatial averaging in both softwares have been chosen to fill entirely the granite and to lose the less possible information. The points have been weighted by inverse distance to the stations.

V.2.2.1. <u>Maps using AMS ellipsoid.</u>

The arrows representing the orientations of maximum and minimum AMS axes in the figures V.11 and V.12 their length proportional to their inclination: the more the arrows are elongated and the more the inclination is subhorizontal. As said previously in chapter V.2.1., most of the maximum AMS directions of the MacKenzie granite are subhorizontal and are oriented toward the East or the West except in four areas: in the left and right side of the granite in figure V.11., the maximum orientations are more vertical; in the central area and in the Northeastern area, the maximum orientation directions are random. Consequently, fabrics' orientations cannot be used as kinematic indicators: this is probably due to the non-coaxial emplacement of the granite and a secondary metamorphic fabric, which have overprinted a primary magmatic one.

The minimum AMS directions of the MacKenzie granite are oriented toward the North or the South in the left and the right side of the granite (figure V.12.). In the central part of the granite, the directions are more random: they are more vertical in the Southern part of the granite with a random orientation and they are more horizontal and oriented toward the North or the South. In the Northeastern part of the granite, the minimum orientations are vertical and oriented toward the SE.

The map of bulk k of the MacKenzie granite (figure V.13.) shows a greater susceptibility in the Northwestern part of the granite and in the central part of the granite. The bulk k tends to decrease in the Southern and Northeastern areas. The map of AMS Pj (intensity of the ellipsoids) (figure V.14.) is very similar to the map of bulk k with greater Pj values in the Northwestern part of the granite, which tend to decrease in the central and Eastern part of the granite. This result is consistent with what have been said previously with the Pj related to the ferromagnetic content of the specimens.

Three areas where fabrics are oblate can be distinguished in the map of AMS Tj (shape of the ellipsoid) of the MacKenzie granite (figure V.15): one in the extreme western part of the granite, a second one in the central part of the granite and a third one in the extreme eastern part of the granite. Except in these areas, the granite shows a prolate fabric.

There is a relation between "oblate" fabrics areas and horizontal northern or southern directions of minimum axes and vertical or random orientations of maximum axes. "Prolate" fabrics areas are related to vertical directions of minimum axes and horizontal eastern or western orientations of maximum axes. No relation can be found between these areas and the AMS Pj and bulk k.

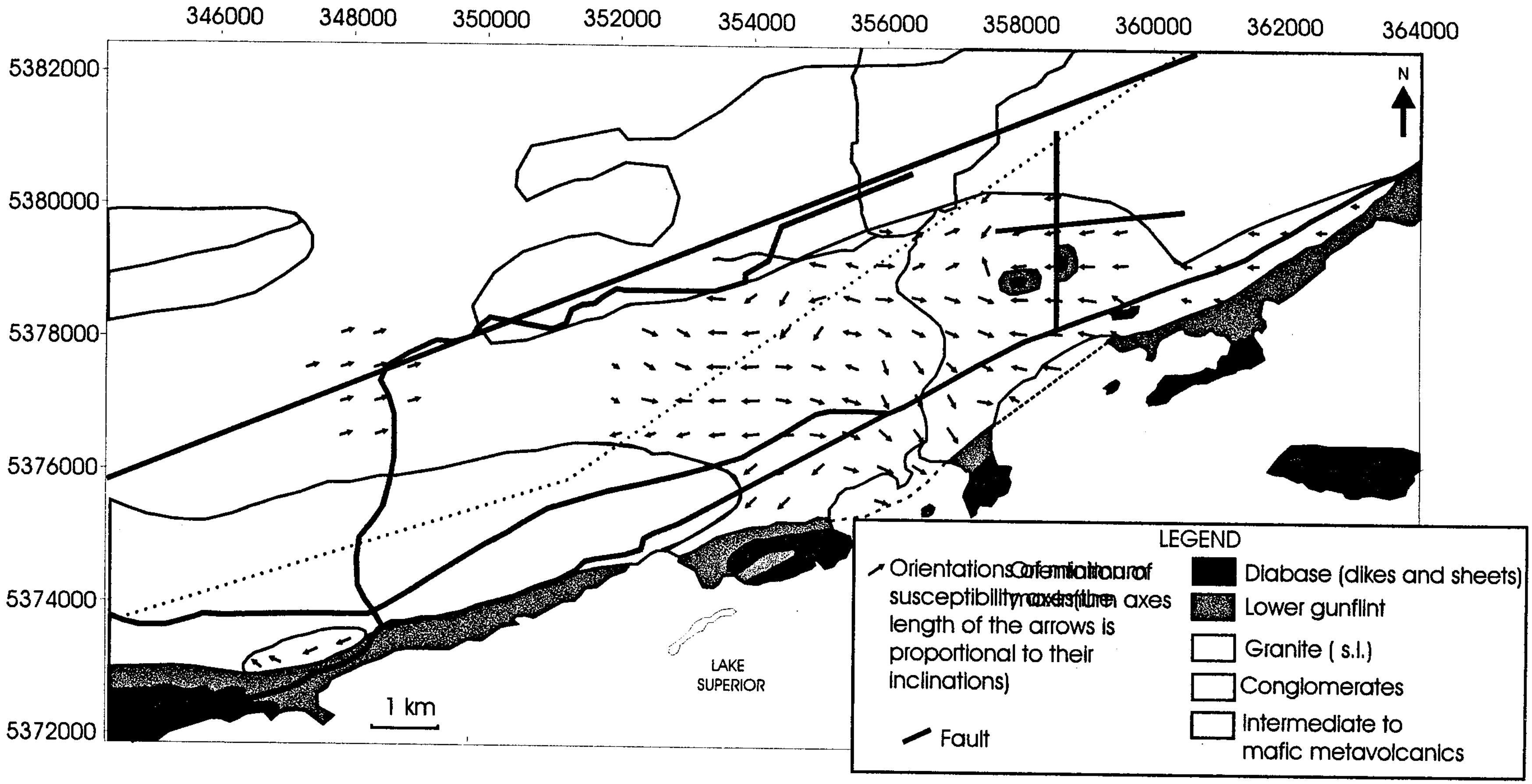

V.11. Map of orientations of maximum susceptibility axes of the MacKenzie granite

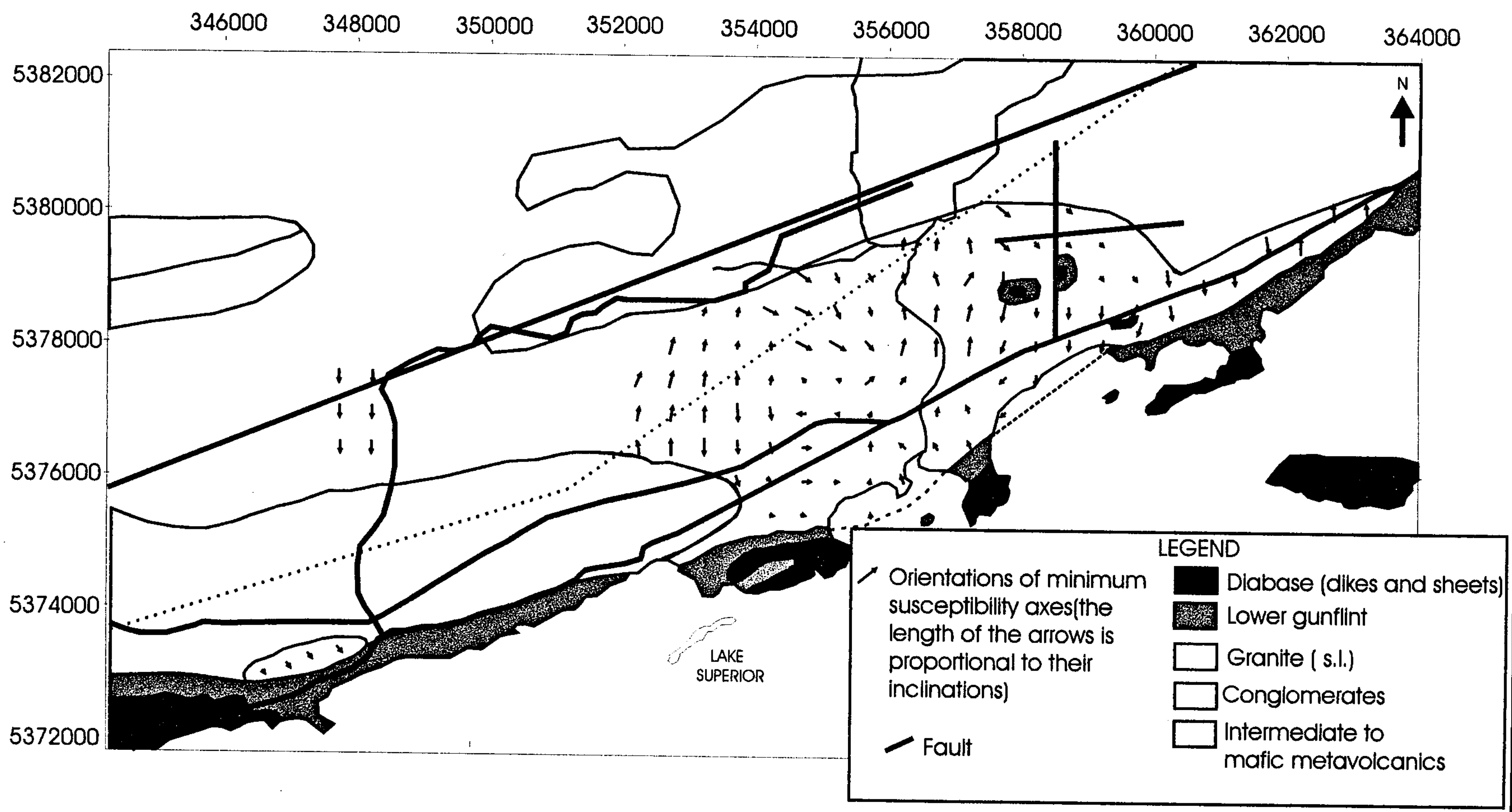

V.12. Map of orientations of minimum susceptibility axes of the MacKenzie granite

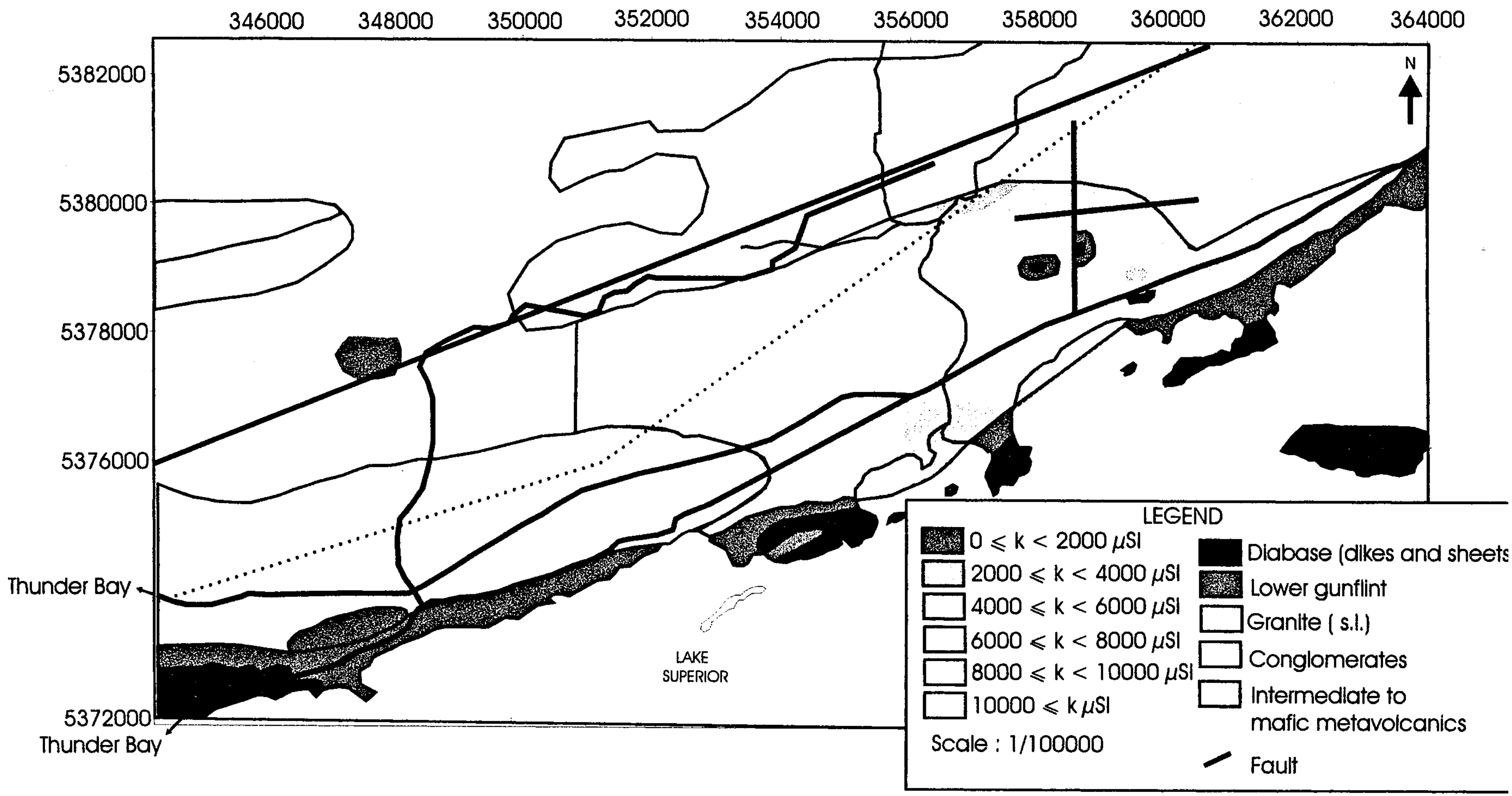

Figure V.13 Map of bulk k ((k max+ k int + k min)/3) of MacKenzie granite.

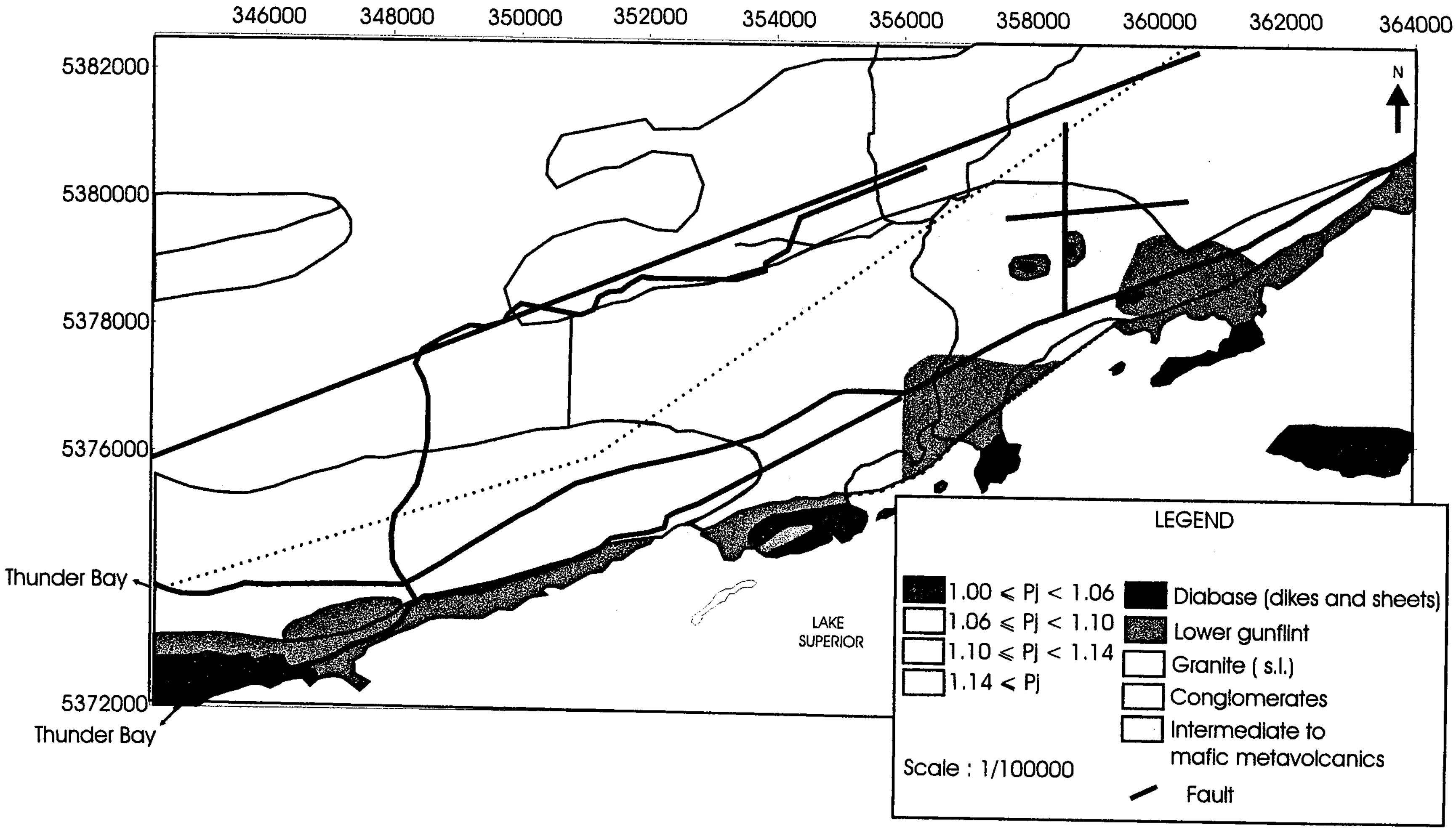

Figure V.14. Map of Pj (intensity of anisotropy of the magnetic ellipsoid) of the susceptibility of the MacKenzie granite.

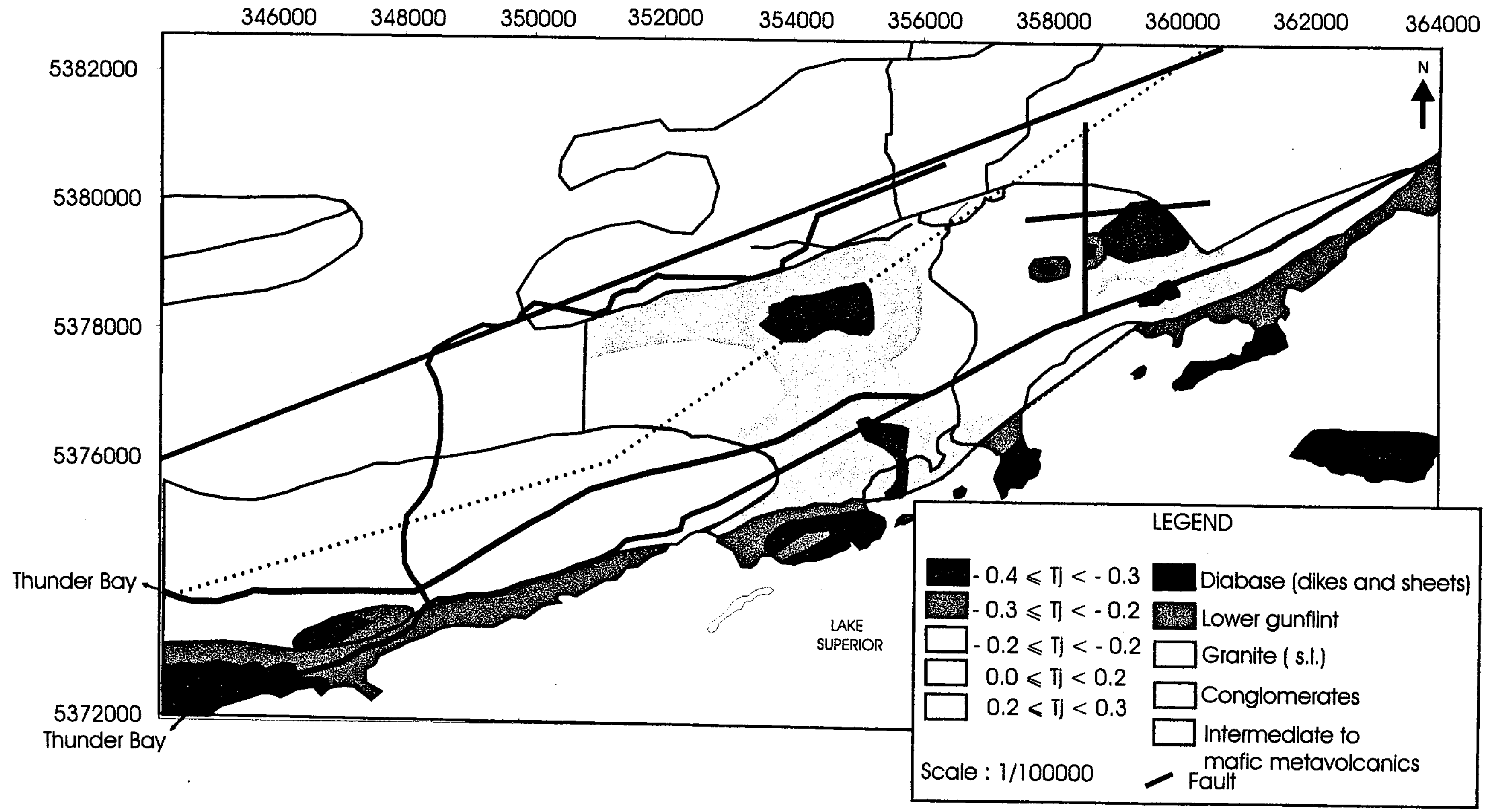

V.15. Map of Tj (shape parameter of the ellipsoid) of the susceptibility of the MacKenzie granite

V.2.2.2.2. Maps using AARM ellipsoid.

The arrows representing the orientations of maximum and minimum AARM axes in the figures V.16 and V.17 have their azimuths and their length will be proportional to their inclination: the more the arrows are elongated and the more the inclination is subhorizontal. The maximum orientations of AARM of the MacKenzie granite (figure V.16.) correspond to ferromagnetic minerals maximum remanent orientations and consequently magnetites maximum axes. The western part of MacKenzie granite has horizontal northern maximum orientations and its eastern part has also horizontal maximum orientations but oriented toward the South. In the central part of the granite, the maximum orientations are steeper with random directions.

The minimum orientations of AARM of the MacKenzie granite (figure V.17.) are very difficult to analyze, orientations of minimum axes seems to compete with one another: in the western part of the granite, minimum directions tend to be aligned toward the East; in the eastern part of the granite, minimum directions tend to be aligned toward the West; in the southern part of the granite, minimum directions tend to be aligned toward the North and in the northern part of the granite, minimum directions tend to be aligned toward the South. The minimum orientations of AARM are totally different from the minimum orientations of AMS.

The ARM map (remanent intensity in mA/m is the average of minimum, intermediate and maximum axes values) of the MacKenzie granite shows one area with very high remanent intensity in the western part of the granite (figure V.18.). This area corresponds to the highest susceptibility area in the map of k mean and to the area of maximum Pj of AMS and AARM. The rest of the granite remanent intensity is quite homogenous with two lower remanent susceptibilities areas: one in the south of the granite and a second in the center part of the granite. The southern part of the granite is the region where the specimens of the group with susceptibility ≤ 500 μSI are the more important and therefore it is logical that the remanent intensity is lower in this area.

Two areas of AARM Pj ≥ 1.3 can be distinguished in the MacKenzie granite: a first one corresponding to highest remanent intensity values (in western part of the granite) and a second one in the middle part of the granite. The second area might correspond to maximum directions toward the West competing with vertical maximum directions of fabrics (figure V.19.). Low Pj values occur in the southern part of the granite where the remanent intensity is the lowest.

The MacKenzie granite is divided in two parts: a western part where the AARM Tj < 0 (prolate fabrics) and the eastern part where the Tj > 0 (oblate fabrics). This division fits very well with the orientations of maximum remanent axes map: the eastern area corresponds to maximum directions toward the West whereas the western area corresponds to variable maximum directions (from the northern to the southern directions). No relations can be found with the minimum axes directions (figure V.20.).

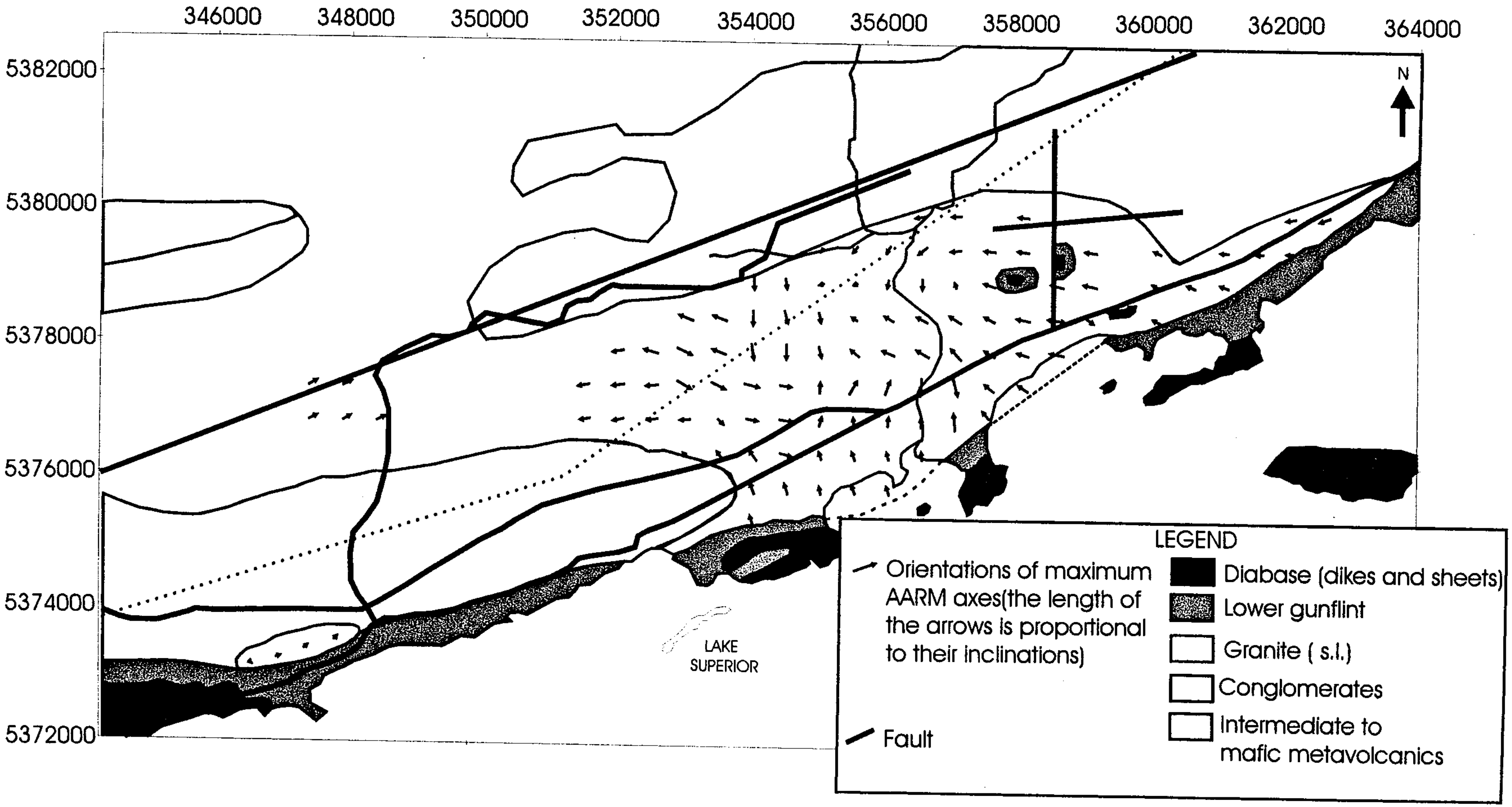

Figure V.16. Map of orientations of the maximum remanent axes (AARM max.) of the MacKenzie granite

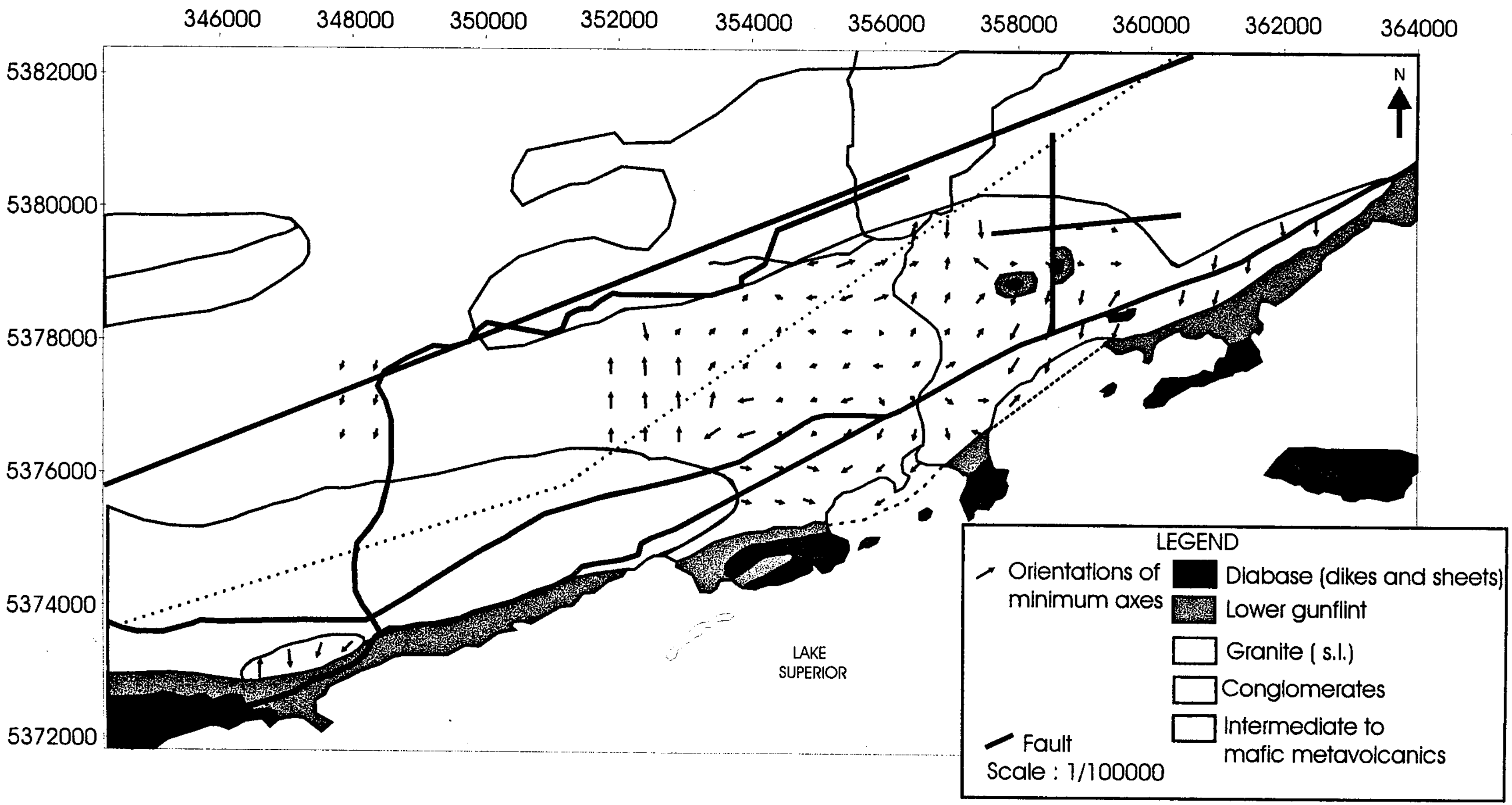

Figure V.17. Map of orientations of minimum remanent axes (AARM min.) of the MacKenzie granite

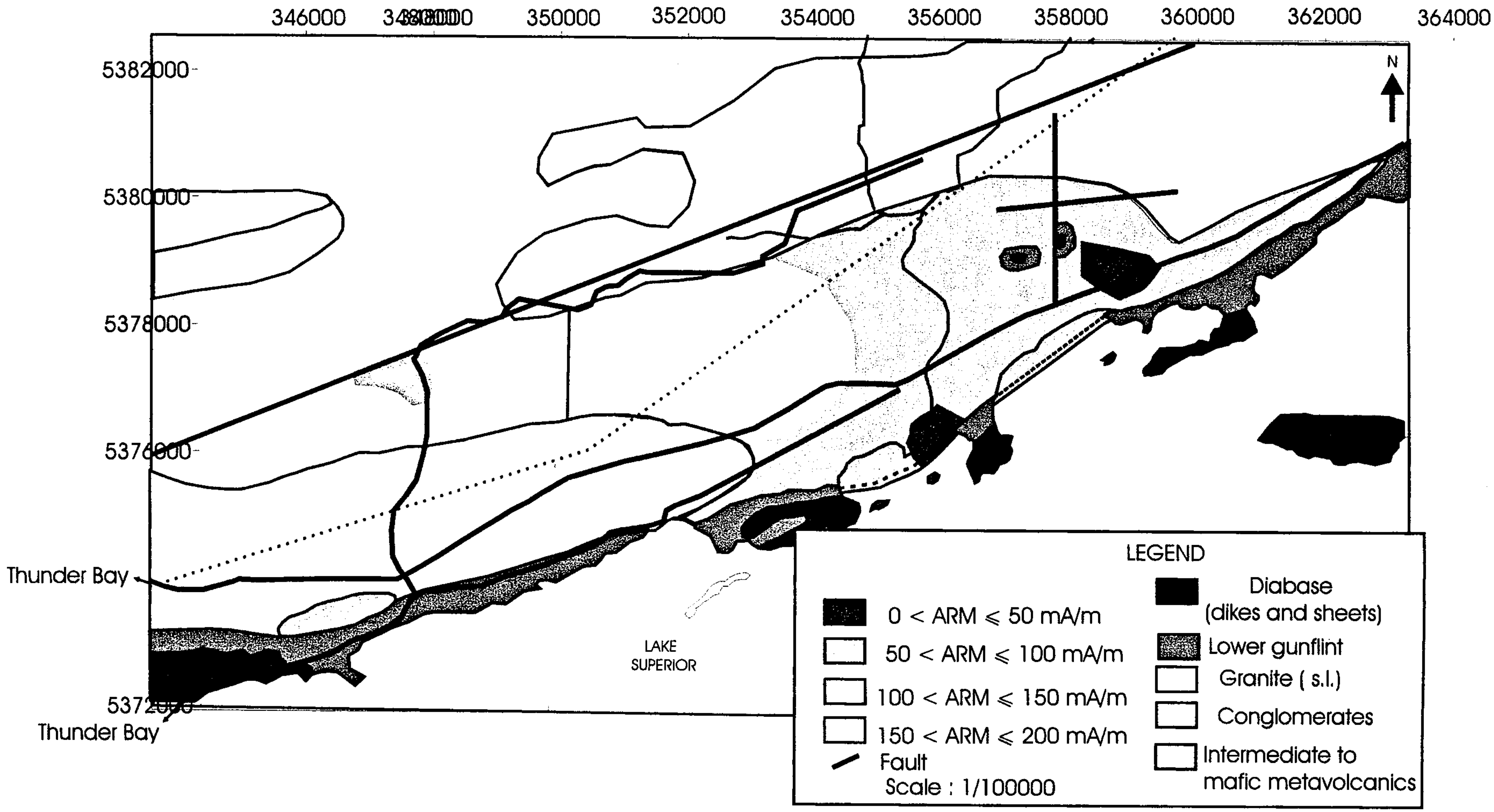

Figure V.18. Map of bulk ARM (bulk remanent intensity (mA/m)) of the MacKenzie granite

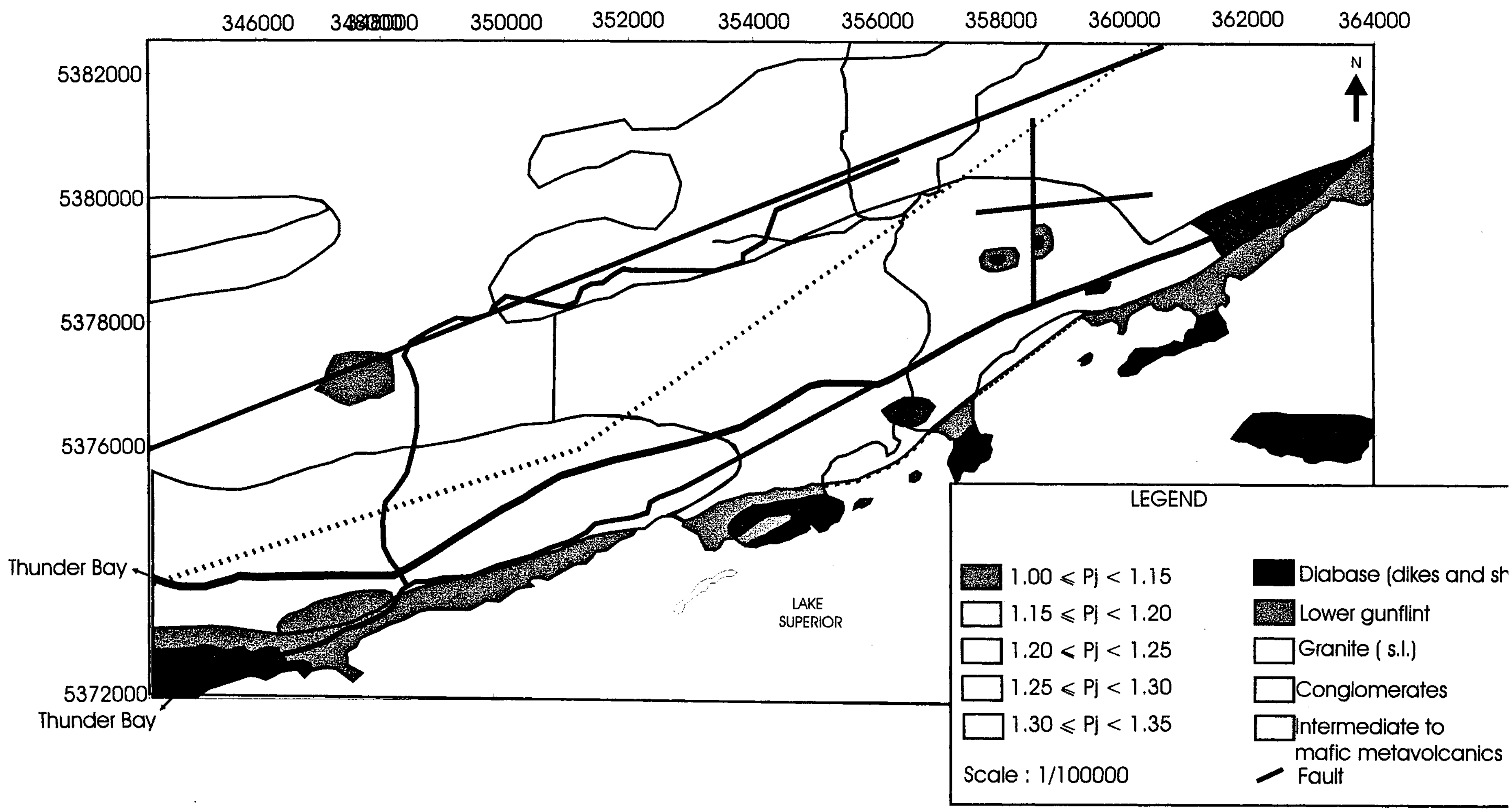

Figure V.19. Map of Pj (intensity of the magnetic ellipsoid) of AARM of the MacKenzie granite

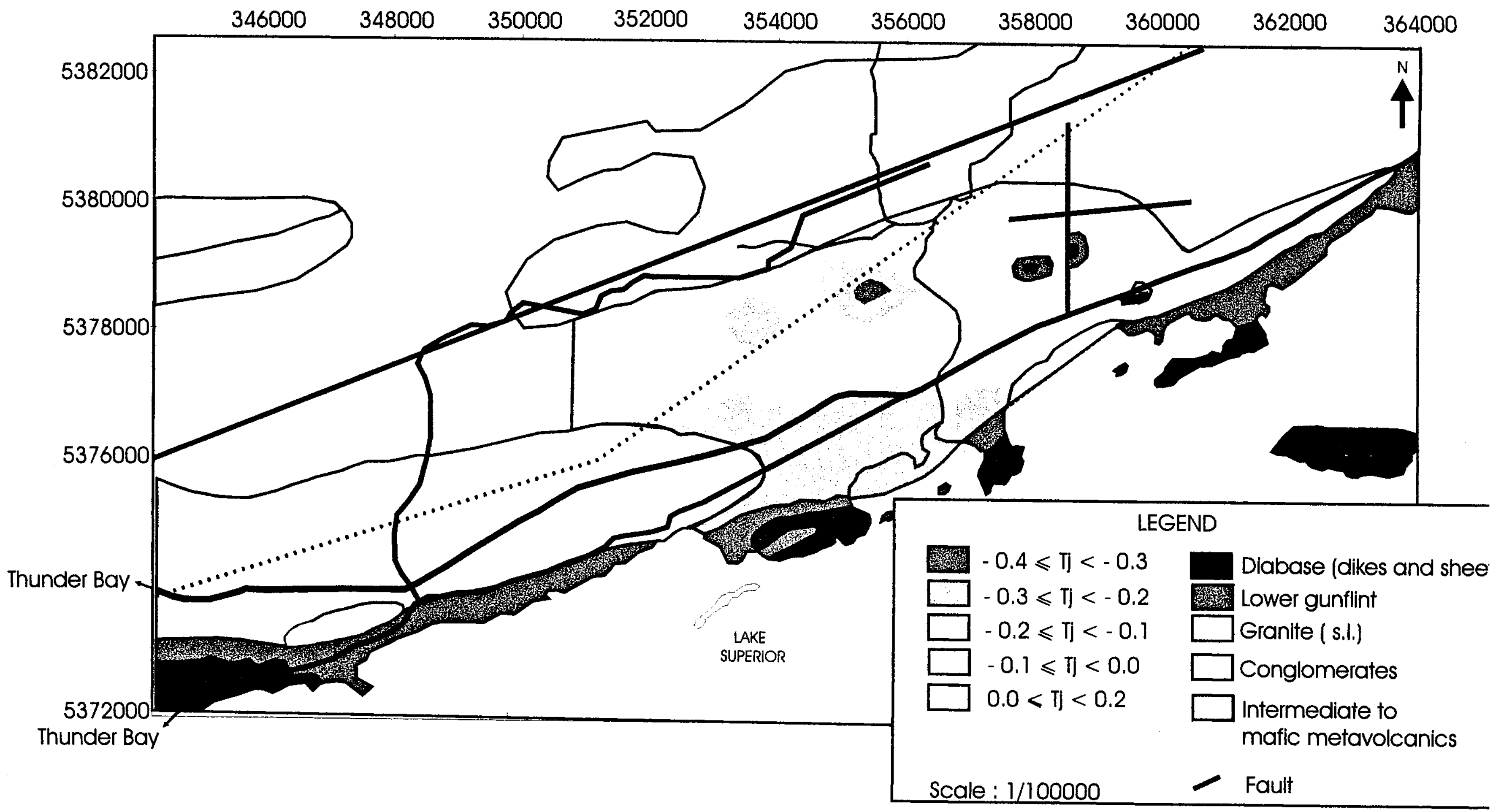

Figure V..20. Map of Tj (shape parameter of the magnetic ellipsoid) of AARM of the MacKenzie granite

V.3. Conclusion

The Mackenzie granite is a granite *sensus stricto.* It is a concordant pluton and its emplacement is related to regional faults directions (emplacement in transcurrent context). It has high susceptibilities values and has a multimodal frequency-distribution typical of granites having a mean susceptibility ≥ 1000 μSI. The susceptibilities of the specimens are controlled by their ferromagnetic content (magnetite). The Pj, the bulk k and the remanent intensity (mA/m) has the same behaviors due to magnetite in the granite. Three groups of specimens have been discriminated: a first one whose susceptibilities are ≤ 500 μSI, a second one whose susceptibilities are ≤ 6000 μSI and a third one whose susceptibilities are > 6000 μSI.

Stereonets and tensors show two orientation-distributions of the fabrics: a first one (L > S) including the majority of orientations of the specimens related to areas where the plunge of minimum axes of AMS is steeper and related to paramagnetic and diamagnetic minerals and a second one (L < S) related to areas where the plunge of minimum axes of AMS is more or less horizontal (on the map) and vertical in the stereonets and related to ferromagnetic minerals. AMS and AARM maximum and intermediate axes orientations are variable. Thus, the tensors ellipses show that the orientations-distribution of the fabrics is non-coaxial.

These two remarks explain why the orientation-distribution of fabrics cannot be used as kinematic indicators: the fabrics' orientations distribution is non-coaxial and a primary magmatic fabric has been overprinted by a second metamorphic one (the metamorphic and alteration processes are visible on the field).

V.4. Data of the McKenzie granite

samples	dec.	inc.	k. min. (μSI)	dec.	inc.	k. int. (μSI)	dec.	inc.	k. max (μSI)	bulk k. (μSI)	Pj	Tj
LC001A	283	5	16734	177	72	17400	14	17	19071	17735	1.14	-0.05
LC001B	216	16	15530	338	61	16447	119	23	17833	16604	1.15	-0.29
LC002A	167	9	3897	42	74	4121	259	13	4550	4189	1.18	-0.23
LC002B	178	33	10649	15	56	11491	273	8	13196	11779	1.24	-0.29
LC002C	170	14	7291	39	70	7771	264	15	8702	7921	1.21	-0.09
LC003A	266	69	16228	13	7	16935	106	20	19072	17411	1.18	-0.75
LC003B	301	66	21614	200	5	22796	108	23	24750	23053	1.14	-0.76
LC004A	158	56	225	1	32	227	264	11	238	230	1.71	-0.82
LC004B	22	6	255	167	82	257	291	4	269	260	1.05	-0.35
LC005A	49	51	265	164	19	268	266	33	272	268	1.01	-0.54
LC005B	103	4	202	203	68	212	12	22	215	210	1.02	0.00
LC006A	352	58	305	191	31	310	96	9	318	311	1.06	-0.59
LC006B	55	72	331	205	16	342	297	9	346	340	1.03	-0.57
LC007A	215	0	329	307	87	347	125	3	350	342	1.05	0.16
LC007B	230	75	253	49	15	254	139	0	260	256	1.03	-0.04
LC007C	10	64	257	240	18	258	144	19	262	259	1.01	-0.12
LC008A	177	2	5191	276	77	5272	87	13	5741	5401	1.12	-0.40
LC008B	153	64	452	323	26	459	55	4	462	458	1.03	-0.16
LC008C	334	32	4721	200	49	4875	80	24	5289	4962	1.12	-0.72
LC009A	123	64	305	276	23	313	11	11	316	312	1.02	0.20
LC009B	4	13	318	246	63	325	99	23	332	325	1.03	0.27
LC009C	223	58	289	19	30	296	116	11	298	294	1.02	0.14
LC010A	244	0	12611	336	81	12889	154	9	13962	13154	1.10	0.19
LC010C	90	47	15319	282	42	15752	186	6	17140	16070	1.12	-0.50
LC011A	146	53	13402	353	34	14368	254	14	15028	14266	1.13	0.06
LC011B	348	84	16147	81	0	16367	171	6	18021	16845	1.11	0.43
LC011D	164	52	14104	348	38	15099	257	2	15570	14924	1.11	0.36
LC012A	340	1	204	72	68	207	250	22	209	207	1.47	0.93
LC012B	113	68	174	265	20	178	359	10	181	178	1.03	-0.53
LC013B	344	53	499	166	37	504	75	1	518	507	1.04	-0.24
LC014A	158	53	56	330	36	57	63	4	58	57	1.09	-0.21
LC014B	130	37	46	10	33	47	252	35	51	48	1.05	-0.55
LC015A	351	45	9020	173	45	9172	82	1	9509	9234	1.06	-0.65
LC015B	357	22	1549	157	67	1573	264	7	1615	1579	1.04	-0.54
LC016A	40	59	1008	185	26	1014	283	15	1023	1015	1.02	-0.62
LC016B	85	29	775	218	51	783	341	24	789	782	1.03	-0.09
LC016C	64	9	828	160	33	835	321	55	844	836	1.02	-0.02
LC016D	5	23	866	123	48	868	258	33	877	870	1.02	0.40
LC017A	166	59	286	57	11	299	321	28	301	295	1.06	0.68

samples	dec.	inc.	k. min. (µSI)	dec.	inc.	k. int. (µSI)	dec.	inc.	k. max (µSI)	bulk k. (µSI)	Pj	Tj
LC017B	194	43	254	32	46	265	293	9	267	262	1.06	0.76
LC017C	165	68	294	51	9	314	318	20	316	308	1.10	0.21
LC018A	173	34	1146	286	31	1172	47	41	1187	1168	1.03	0.27
LC018B	221	51	1524	336	19	1539	78	33	1573	1545	1.03	0.26
LC018C	197	34	1323	312	33	1339	74	39	1359	1340	1.03	0.37
LC019A	173	26	1647	303	53	1663	70	24	1671	1660	1.01	0.45
LC019B	164	79	1864	358	10	1892	268	3	1901	1886	1.01	0.43
LC020A	353	73	311	203	15	316	111	8	323	317	1.03	-0.49
LC020B	268	61	552	11	7	561	105	28	571	561	1.02	-0.45
LC020C	233	8	335	122	70	362	326	19	371	356	1.10	-0.02
LC021A	265	36	3316	101	53	3449	1	7	3558	3441	1.07	-0.48
LC021B	263	14	2589	73	76	2603	172	2	2659	2617	1.04	-0.35
LC021C	270	20	993	121	67	1014	4	11	1040	1016	1.04	0.08
LC022A	174	50	263	315	33	266	59	20	275	268	1.03	0.48
LC022B	264	70	223	165	3	232	73	20	243	233	1.16	0.62
LC022C	126	77	256	320	13	262	229	3	268	262	1.04	0.09
LC022D	337	69	252	214	12	260	120	17	267	260	1.03	-0.65
LC024A	53	74	190	221	16	200	312	3	202	197	1.03	0.41
LC024B	87	73	174	250	16	175	341	5	178	176	1.03	-0.05
LC024C	226	34	165	69	54	210	323	11	220	198	1.07	-0.51
LC024D	148	85	200	256	2	204	347	4	206	203	1.02	-0.22
LC025B	333	67	15030	91	11	15339	185	20	16954	15774	1.14	-0.47
LC026A	161	79	14176	354	11	14474	263	2	15554	14735	1.10	-0.55
LC026B	194	82	13055	10	8	13432	100	1	14452	13647	1.10	-0.60
LC026C	168	77	19305	353	13	20456	262	1	21970	20577	1.14	-0.09
LC026D	194	81	17045	10	9	17411	101	1	19236	17897	1.13	-0.51
LC027A	333	74	179	237	2	183	147	16	186	183	1.03	0.68
LC027B	289	59	178	27	5	183	120	31	187	182	1.37	0.89
LC028A	300	11	384	71	73	392	208	13	398	392	1.03	0.51
LC028B	64	19	8897	331	9	9528	217	69	9624	9350	1.08	0.73
LC028C	268	17	339	115	71	348	0	8	351	346	1.03	-0.08
LC029A	72	21	7511	306	57	7831	172	24	7939	7760	1.06	0.71
LC030A	351	33	12912	93	18	14083	207	51	14227	13741	1.11	0.75
LC030B	346	31	11557	81	9	12529	185	58	12668	12251	1.10	0.52
LC031A	61	45	10817	274	41	11323	169	17	11793	11311	1.09	0.06
LC031B	50	47	12824	269	36	13291	163	21	13969	13361	1.09	-0.06
LC031C	58	41	13809	280	41	14558	169	22	15258	14541	1.11	0.14
LC031D	48	37	12425	268	46	12876	155	21	13439	12913	1.08	0.34
LC032A	73	40	940	294	42	963	182	22	1013	972	1.07	-0.52
LC032B	71	45	678	299	34	698	189	26	722	700	1.05	-0.75
LC033A	183	25	245	44	59	254	282	18	258	252	1.05	0.37
LC033B	200	9	252	95	59	260	295	29	265	259	1.71	0.87
LC034A	185	60	2880	319	22	3103	58	20	3186	3056	1.11	0.48

samples	dec.	inc.	k. min. (µSI)	dec.	inc.	k. int. (µSI)	dec.	inc.	k. max (µSI)	bulk k. (µSI)	Pj	Tj
LC034B	5	24	2841	203	65	2911	98	7	3101	2951	1.09	-0.35
LC034D	351	52	3107	196	35	3220	98	12	3398	3242	1.09	-0.68
LC036A	341	19	1712	173	71	1764	73	4	1794	1756	1.05	0.61
LC036B	331	85	672	208	3	705	118	4	733	703	1.09	0.37
LC037A	330	31	1461	226	21	1487	108	51	1563	1503	1.08	-0.27
LC037B	311	34	1970	208	19	2012	94	50	2100	2028	1.45	0.74
LC038A	47	39	3116	302	18	3214	192	46	3381	3237	1.10	0.74
LC038B	45	20	3029	300	36	3118	158	47	3260	3135	1.07	-0.06
LC038C	50	23	2292	308	26	2386	175	55	2489	2389	1.09	0.42
LC039A	148	38	989	34	27	1001	279	40	1024	1005	1.04	-0.25
LC039B	13	33	1542	148	47	1595	266	24	1612	1583	1.05	-0.38
LC039C	51	51	2097	174	24	2139	278	29	2181	2139	1.04	-0.19
LC040A	336	19	291	92	52	295	234	32	301	295	1.16	0.80
LC040B	101	34	282	310	52	292	201	14	297	291	1.03	0.12
LC041A	335	33	1091	207	44	1118	86	28	1154	1121	1.06	-0.04
LC041B	347	0	893	257	64	896	77	26	940	910	1.06	-0.84
LC041C	202	35	1214	321	34	1217	81	37	1269	1233	1.05	-0.82
LC041D	273	55	938	6	2	952	97	35	979	956	1.06	-0.56
LC042A	296	35	9980	83	50	10545	194	17	11077	10534	1.10	0.11
LC042B	298	31	9152	51	34	9664	176	41	10081	9632	1.10	0.34
LC043A	270	33	8029	50	50	8673	166	20	8978	8560	1.13	0.43
LC043B	275	37	2475	75	51	2798	177	10	2863	2712	1.18	0.89
LC043C	256	35	12129	28	45	13050	146	26	13513	12897	1.12	0.20
LC044A	349	21	14691	256	6	15197	151	68	16178	15355	1.10	0.16
LC044B	14	17	14007	279	17	14271	147	66	15352	14543	1.10	0.02
LC045A	353	28	15024	225	49	16094	99	27	16743	15954	1.11	0.08
LC045B	349	22	11138	232	48	12103	95	34	12428	11890	1.13	0.22
LC045C	354	24	11468	240	42	12357	105	38	12839	12221	1.12	0.18
LC045D	349	31	9709	222	46	10422	98	29	10957	10363	1.30	0.21
LC046A	175	28	2289	346	62	2437	83	4	2504	2410	1.09	-0.16
LC046B	178	21	1956	296	51	2120	75	31	2159	2078	1.11	0.44
LC047A	351	65	10298	192	23	10430	98	8	11199	10642	1.09	-0.46
LC047B	9	22	12199	220	64	12544	104	12	13253	12665	1.09	0.23
LC047C	22	8	12444	263	75	12547	114	13	13507	12833	1.09	0.18
LC047D	7	13	11120	224	74	11307	99	10	12227	11551	1.10	-0.25
LC048A	198	14	16143	33	76	17239	289	3	18264	17215	1.13	0,56
LC048B	206	12	16664	0	77	17933	115	6	18778	17792	1.13	0.79
LC049A	153	78	181	4	10	189	273	6	191	187	1.06	0.61
LC049B	152	40	148	255	14	155	0	46	166	156	1.12	-0.26
LC049C	71	19	177	258	71	183	162	2	189	183	1.04	0.47
LC050A	167	14	11982	30	71	12264	261	12	12993	12413	1.08	-0.05
LC050B	171	1	12125	77	75	12557	261	15	13619	12767	1.13	-0.30
LC051A	259	16	8320	140	59	9088	357	25	9517	8975	1,15	0.30

samples	dec.	inc.	k. min. (μSI)	dec.	inc.	k. int. (μSI)	dec.	inc.	k. max (μSI)	bulk k. (μSI)	Pj	Tj
LC051B	253	17	7686	143	47	8354	357	38	8861	8301	1.16	0.33
LC051C	93	15	6919	201	49	7640	351	37	7928	7496	1.15	0.70
LC052A	16	21	414	283	7	431	177	68	432	426	1.06	0.12
LC052B	31	16	644	125	13	681	254	70	688	671	1.08	0.30
LC054A	320	15	3113	209	54	3287	60	32	3454	3285	1.11	-0.07
LC054B	107	34	3529	290	56	3578	198	2	4033	3713	1.15	-0.73
LC054C	295	35	2742	120	55	2897	27	2	2989	2876	1.08	0.10
LC054D	116	5	3366	252	84	3641	26	4	4125	3711	1.20	-0.28
LC055A	243	11	5588	335	14	6361	116	73	8856	6935	1.59	-0.53
LC055B	236	2	3046	327	28	3074	143	62	3374	3164	1.12	-0.37
LC056A	190	44	13613	328	38	14147	77	22	14875	14212	1.10	-0.81
LC056B	283	56	15315	78	32	15695	175	12	16644	15885	1.08	-0.46
LC056C	217	45	15437	351	35	16275	99	24	17089	16267	1.11	-0.12
LC056D	264	30	14825	59	57	15479	168	12	16269	15524	1.11	-0.27
LC057A	113	9	14995	5	61	16053	208	27	17543	16197	1.17	-0.62
LC057B	298	1	6675	30	67	7110	208	23	7638	7141	1.14	-0.55
LC057C	103	16	10537	337	64	11096	199	20	11893	11175	1.13	-0.76
LC058A	202	15	9820	81	63	10477	298	23	11594	10630	1.19	-0.01
LC058B	247	24	12614	109	60	13174	345	18	14536	13441	1.16	-0.35
LC059A	345	4	16654	208	84	17082	75	4	18527	17421	1.12	-0.52
LC059B	352	5	12058	202	84	12926	83	3	13786	12923	1.14	0.04
LC060A	80	35	10297	305	45	10957	188	24	11894	11049	1.15	-0.06
LC060B	105	21	8222	314	67	8757	199	10	9547	8842	1.16	-0.16
LC061A	226	56	100	12	30	105	112	16	107	104	1.09	0.70
LC061B	230	64	81	26	24	84	120	9	85	83	1.05	-0.02
LC062A	135	62	5726	31	7	5902	297	27	6565	6064	1.15	-0.56
LC062B	165	19	3196	61	34	3332	279	50	3508	3345	1.10	-0.10
LC062C	183	4	3837	90	38	4031	279	51	4198	4022	1.09	0.10
LC062D	129	54	6046	24	11	6240	287	34	6618	6301	1.10	-0.30
LC063B	2	23	10467	219	62	10807	99	15	11582	10952	1.12	-0.27
LC064A	18	51	12259	174	37	12796	273	12	13308	12788	1.10	-0.23
LC064B	21	49	11682	187	40	12183	283	7	12694	12186	1.08	-0.92
LC065A	160	12	169	42	67	175	254	20	178	174	1.07	0.45
LC065B	356	72	140	169	18	142	259	2	145	143	1.06	0.10
LC065C	23	52	124	116	2	129	207	39	134	129	1.03	-0.88
LC065D	120	21	233	343	62	236	217	17	243	237	1.04	-0.46
LC066A	5	36	12173	260	20	13144	147	47	14420	13245	1.19	0.06
LC066B	21	48	13226	259	26	13951	152	31	15146	14108	1.16	-0.43
LC066C	351	40	13226	253	9	13609	153	48	15022	13952	1.15	-0.10
LC067A	186	17	7935	46	68	8553	281	13	9091	8526	1.14	0.14
LC067B	196	23	7646	34	67	8205	289	6	9030	8293	1.17	-0.03
LC068A	21	14	2831	272	53	3181	121	34	3279	3097	1.17	0.59
LC068B	23	11	4201	286	34	4659	128	54	4887	4582	1.19	0.79

samples	dec.	inc.	k. min. (µSI)	dec.	inc.	k. int. (µSI)	dec.	inc.	k. max (µSI)	bulk k. (µSI)	Pj	Tj
LC069A	165	2	13042	70	70	15173	255	20	15607	14607	1.21	0.69
LC069B	359	17	14325	104	41	16776	251	44	17144	16081	1.25	0.69
LC070A	221	71	363	103	9	367	10	17	370	367	1.02	0.14
LC070B	294	14	315	201	9	316	79	73	321	317	1.02	-0.70
LC071A	186	36	11259	51	44	12205	295	25	12393	11952	1.11	0.68
LC071B	195	36	14564	35	52	15467	292	10	15719	15250	1.08	0.58
LC072A	183	30	16102	38	55	16840	283	16	17757	16900	1.10	-0.08
LC072B	182	24	9257	63	49	9657	288	32	9983	9632	1.08	0.12
LC073A	289	71	12871	187	4	13155	96	18	13927	13318	1.08	-0.45
LC073B	196	45	8365	352	42	8548	93	13	8834	8582	1.06	-0.21
LC074A	273	7	240	181	18	246	23	70	256	247	1.07	-0.19
LC074B	185	11	246	70	65	251	279	22	255	251	1.03	0.13
LC074C	189	38	259	21	52	262	283	6	265	262	1.02	0.02
LC075A	142	53	12743	1	30	13117	260	19	14042	13301	1.10	-0.40
LC075B	135	67	11942	355	18	12443	260	14	13305	12563	1.12	-0.24
LC076A	28	14	177	282	49	178	129	38	185	180	1.05	-0.69
LC076B	192	38	222	57	42	225	303	25	226	225	1.02	0.35
LC077A	175	23	1606	69	33	1813	293	48	1932	1784	1.21	0.31
LC077B	168	13	6133	52	62	6562	264	24	6860	6518	1.12	0.21
LC078A	317	13	349	63	51	355	217	36	358	354	1.03	0.31
LC078B	334	28	386	161	62	392	66	3	394	391	1.02	0.45
LC079A	208	3	10547	110	67	11190	299	23	11454	11064	1.09	0.44
LC079B	199	2	8694	106	58	9103	290	32	9466	9088	1.09	0.08
LC080A	205	9	13734	103	54	14402	301	35	14805	14314	1.08	0.27
LC080B	173	10	12153	74	42	12947	274	47	13387	12829	1.10	0.31
LC081A	359	16	10330	110	52	10485	258	34	11238	10684	1.09	-0.65
LC081B	178	6	9107	75	65	9795	270	24	9948	9617	1.10	0.65
LC083A	354	5	3356	88	35	3851	257	54	3918	3708	1.18	0.78
LC083B	341	1	5517	75	74	6027	250	16	6212	5919	1.13	0.49

samples	dec.	inc.	min. ARM (mA/m)	dec.	inc.	int. ARM (mA/m)	dec.	inc.	max ARM (mA/m)	remanent int. (mA/m)	Pj	Tj
LC002B	103	2	185	12	15	219	198	75	310	237	1.69	-0.36
LC003B	253	62	261	3	10	301	97	25	315	292	1.22	0.53
LC004B	49	22	15	189	63	18	312	16	19	17	1.29	0.18
LC005B	286	14	40	184	40	45	31	47	47	44	1.18	0.47
LC006B	237	27	36	122	39	36	351	39	43	38	1.23	-0.79
LC007B	198	37	40	73	38	41	315	31	43	41	1.06	0.10
LC008B	276	25	55	152	50	58	21	29	63	58	1.16	-0.27
LC009B	207	7	17	115	16	18	319	72	19	17	1.10	-0.63
LC010B	98	60	122	248	27	132	345	13	146	133	1.20	-0.06
LC011B	140	56	156	325	34	179	234	2	187	174	1.21	0.53
LC012B	105	40	28	230	34	29	344	32	30	28	1.09	-0.23
LC013B	161	36	10	303	48	10	56	19	11	10	1.09	-0.09
LC014B	334	1	12	243	48	13	65	42	14	13	1.15	0.03
LC015B	174	9	41	67	61	43	268	28	44	42	1.08	0.29
LC016B	12	11	31	277	21	33	129	66	35	32	1.14	0.08
LC017B	224	14	10	131	9	12	11	73	12	11	1.17	0.56
LC018B	232	36	2	328	9	3	70	52	3	2	1.33	0.07
LC019B	189	26	8	292	23	9	57	54	9	8	1.13	0.42
LC020B	176	31	82	61	36	84	295	39	88	84	1.08	-0.35
LC021B	360	30	50	181	60	55	90	0	96	67	2.04	-0.76
LC022B	210	27	20	74	55	20	311	21	21	20	1.09	-0.40
LC024B	132	43	15	249	27	16	0	35	18	16	1.26	-0.41
LC026B	126	53	1601	219	2	1656	311	37	1941	1732	1.23	-0.65
LC027B	165	15	18	260	16	20	34	68	22	19	1.23	-0.12
LC028B	315	9	150	210	59	164	50	29	216	176	1.46	-0.52
LC029A	86	77	120	253	13	149	344	3	163	144	1.37	0.42
LC030B	337	41	96	155	49	98	246	1	100	98	1.04	0.06
LC031B	65	66	100	291	17	111	196	16	116	108	1.17	0.33
LC032B	47	49	41	171	26	44	277	29	44	42	1.07	0.78
LC033B	235	52	29	104	27	29	1	25	36	31	1.29	-0.82
LC034B	217	67	51	351	16	54	86	16	56	53	1.09	0.06
LC035B	51	3	67	148	69	74	320	21	82	74	1.23	-0.05
LC036B	125	38	153	18	21	167	266	45	189	169	1.24	-0.19
LC037B	12	32	133	107	8	149	210	57	155	145	1.17	0.46
LC039B	110	19	64	355	50	68	214	33	74	63	1.20	-0.39
LC039B	125	22	61	332	65	67	219	10	75	68	1.16	-0.19
LC040B	173	2	38	80	64	56	264	26	58	50	1.62	0.80
LC041B	211	30	26	327	37	32	94	39	38	32	1.44	-0.01
LC042B	74	46	108	290	38	112	185	19	125	115	1.17	-0.46
LC043B	90	2	213	181	29	897	357	61	990	699	5.97	0.87
LC044B	2	81	606	186	9	876	96	1	1466	982	2.46	-0.17
LC045B	2	43	39	245	26	60	134	36	308	135	11.08	-0.59
LC046B	342	3	40	79	68	47	251	21	52	46	1.29	0.11
LC047B	20	27	104	162	57	121	281	17	138	121	1.32	0.07

samples	dec.	inc.	min. ARM (mA/m)	dec.	inc.	int. ARM (mA/m)	dec.	inc.	max ARM (mA/m)	remanent int. (mA/m)	Pj	Tj
LC048B	50	29	194	209	59	220	314	9	240	218	1.24	0.19
LC049B	62	63	75	294	18	80	197	20	80	78	1.08	0.75
LC050B	167	6	117	64	66	133	259	24	167	139	1.44	-0.28
LC051B	254	5	98	151	68	111	346	22	121	110	1.23	0.13
LC052B	327	4	24	237	9	26	82	80	27	25	1.13	-0.13
LC054B	95	74	234	281	16	270	190	2	312	271	1.33	-0.01
LC055B	275	38	82	6	1	85	97	52	92	86	1.13	-0.29
LC056B	348	65	192	86	21	203	180	12	239	210	1.25	-0.50
LC057B	355	70	128	109	8	132	202	18	153	137	1.21	-0.67
LC058B	254	16	137	132	62	142	350	22	178	152	1.33	-0.72
LC059B	287	51	1	36	15	2	137	35	7	3	11.57	0.01
LC060B	255	60	139	114	20	151	213	21	166	152	1.20	-0.04
LC061B	248	19	4	352	34	5	135	50	6	4	1.28	-0.45
LC062B	65	35	46	176	27	51	295	43	56	50	1.21	0.08
LC063B	26	31	180	186	58	191	291	9	214	194	1.19	-0.34
LC064B	118	64	147	356	14	173	261	21	197	172	1.34	0.11
LC065B	38	33	42	252	52	46	140	17	48	45	1.14	0.23
LC066B	5	63	301	252	11	321	157	24	381	334	1.28	-0.46
LC067B	163	35	195	6	53	206	261	12	235	211	1.21	-0.42
LC068B	357	10	284	107	62	323	262	26	359	321	1.26	0.10
LC069B	1	23	2681	126	54	3171	259	26	3619	3157	1.35	0.12
LC070B	219	21	87	123	16	88	358	63	93	89	1.07	-0.50
LC071B	45	17	143	187	69	165	311	13	175	161	1.23	0.43
LC072B	190	17	113	63	63	120	287	20	133	121	1.18	-0.23
LC073B	196	45	100	65	34	111	316	26	116	108	1.16	0.37
LC074B	180	16	0	3	74	2	270	1	65	13	1.27	0.40
LC075B	111	66	128	9	5	145	277	23	159	144	1.24	0.10
LC076B	38	8	5	297	53	5	133	36	25	11	7.64	-0.90
LC077B	194	14	102	85	53	110	293	34	121	110	1.19	-0.14
LC078B	319	47	32	121	42	33	219	9	37	33	1.15	-0.50
LC079B	210	5	97	115	41	106	306	49	117	106	1.21	-0.08
LC080B	188	29	137	31	59	160	284	10	162	153	1.20	0.84
LC081B	168	20	96	49	53	106	271	30	117	106	1.22	0.02
LC083B	152	18	77	41	48	83	255	37	89	83	1.16	0.07

VI. The Rice Bay dome

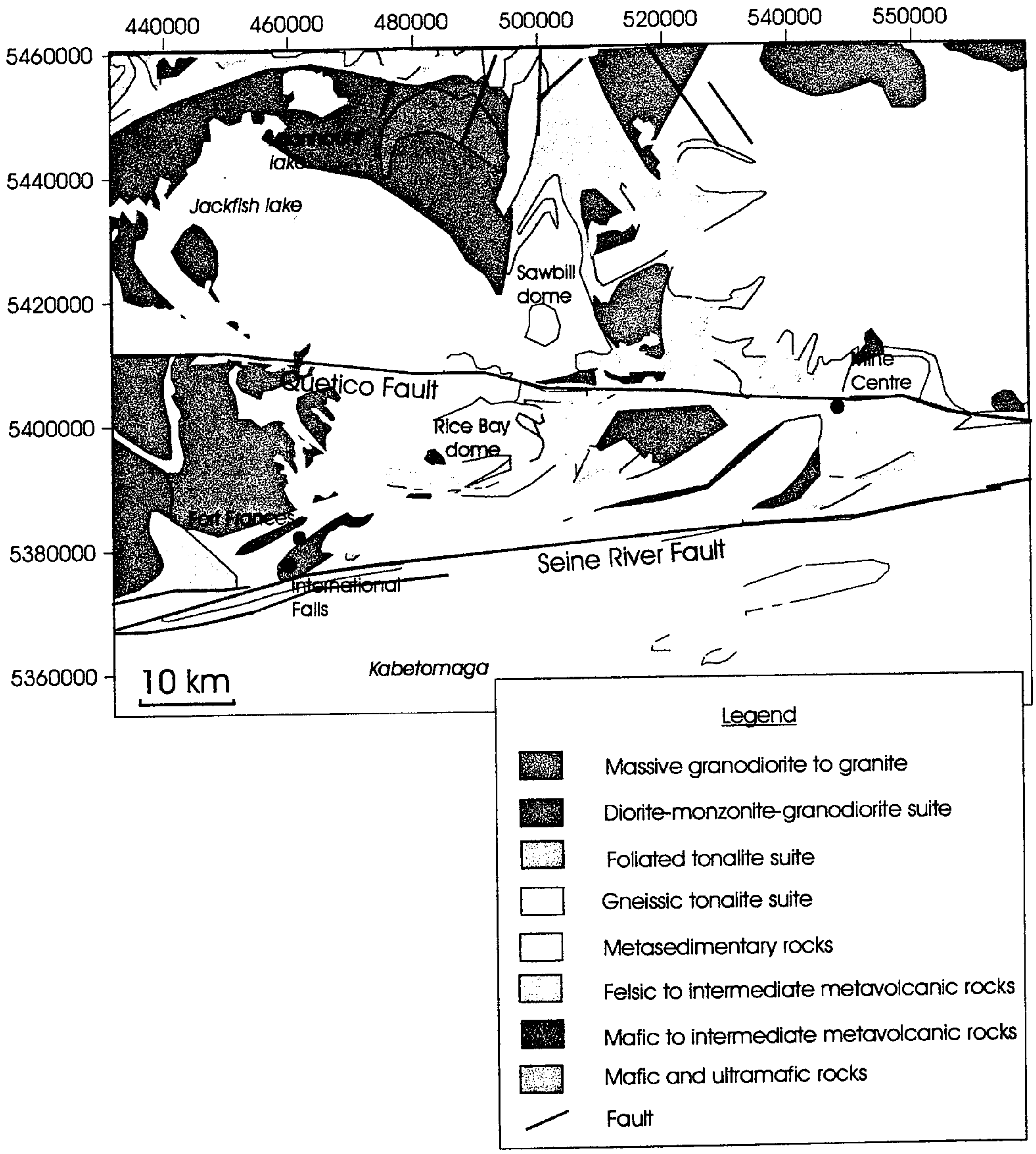

Figure VI.1. Geological map of the area between Fort Frances and Mine Centre with the location of the Sawbill dome and the Rice Bay dome.

The Rice Bay dome is located around 20 kms in the East of Fort Frances and crossed by the highway 11 going from Fort Frances to Atikokan. The eastern limit of the granite coincides with the junction between the highway 11 and the highway 612 going to Dryden.

The RiceBay dome is surrounded by felsic to intermediate intrusive rocks (2737 ± 42 Ma using $^{143}Nd/^{144}Nd$ versus $^{147}Sm/^{144}Nd$ isochron method (Shirey and Hanson, 1986)) (figure VI.1.). The sequence of sediments overlying the dome is overturned (Poulsen *et al*, 1980). Rice Bay dome is composed of tonalites (quartz, plagioclases and biotite) and has been emplaced in a basin delimited by the Quetico fault in the North and the Seine River fault in the South. The dome is elongated from the SW to the NE and its shape is ellipsoidal. It has taken place under ductile conditions and therefore the dome rose by diapirism. The basin is transpressive. The studied area is the apex of the dome (Figure VI.8).

VI.1. Fabrics' study

40 cores from 14 stations have been collected and their susceptibilities have been measured. k_{bulk} ((k max + k int + k min)/3) vary from 7 to 18041 μSI. The k_{mean} (sum of bulk susceptibility of all the specimens divided by their numbers) is equal to 3156 ± 924 μSI. Rice Bay dome has a multimodal frequency distribution of k_{bulk} of each station with two groups: a first group with very low k_{bulk} ($<=$ 100 μSI) and a second one whose k_{bulk} $>$ 2000 μSI (figure VI.2.). These variations of k explain the value of the standard error (± 924 μSI). The group of k_{bulk} $>$ 2000 μSI is controlled by their ferromagnetic content whereas the group of k_{bulk} $\leq$ 100 μSI is influenced by their diamagnetic and paramagnetic content.

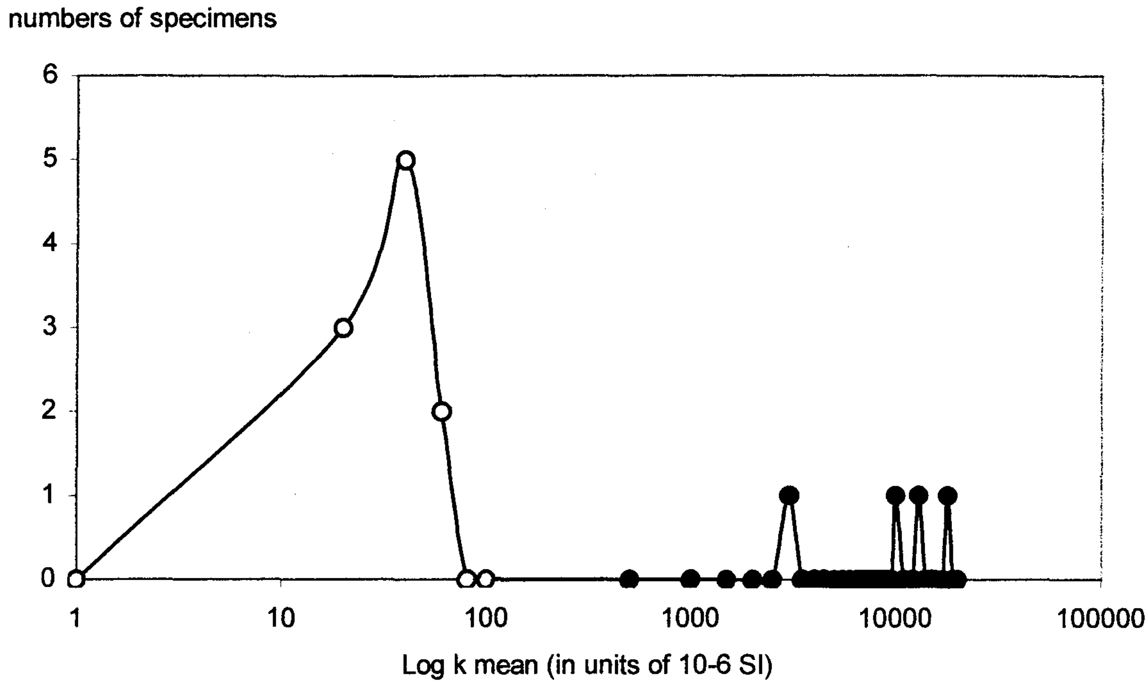

Figure VI.2. Frequency distribution of k mean of specimens (the mean susceptibility is the sum of the bulk susceptibilities of specimens from one location divided by their numbers) of the Rice Bay dome: two groups are differentiated. The gray dots represent the group with susceptibilities smaller than 100 μSI. The black dots are the group with susceptibilities greater than 2000 μSI (n = 14).

The relationship between each axis susceptibilities (k max, k int and k min) and the k_{bulk} of each specimen is linear for the three relations (Figure VI.3.). Therefore, the susceptibility of the specimens is due to a matrix (paramagnetic + diamagnetic minerals) and one ferromagnetic mineral. The calculated matrix susceptibility is equal to 71 ± 924 μSI and its value is due to paramagnetic minerals content of the tonalite (biotite). Therefore the points of intersections of two linear relations, which equal to 118 μSI (k max. and k int. related to the bulk k of specimens), 81 μSI (k max. and k min. related to the bulk k of specimens) and 12 μSI (k min. and k int. related to the bulk k of specimens) are included in the range of susceptibilities given by the standard error.

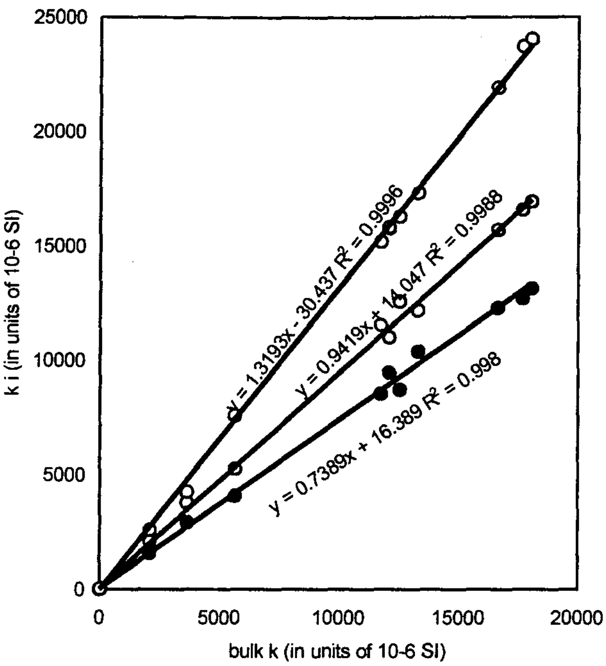

Figure VI.3. Relationship between axes susceptibilities and the bulk susceptibility of each specimen (Henry, 1983) of the Rice Bay dome. The black dots represent the relation between the k min. and the bulk susceptibility. The gray dots represent the relation between the k int. and the bulk susceptibility. The white dots represent the relation between the k max. and the bulk susceptibility (n = 40).

Some specimens have a smaller susceptibility than the calculated matrix: therefore their matrix susceptibility is smaller than the calculated one. These specimens (bulk k ≤ 100 μSI) have been differentiated and the relation between their axes susceptibilities (k max, k int and k min) and bulk susceptibility is shown in figure VI. 4.

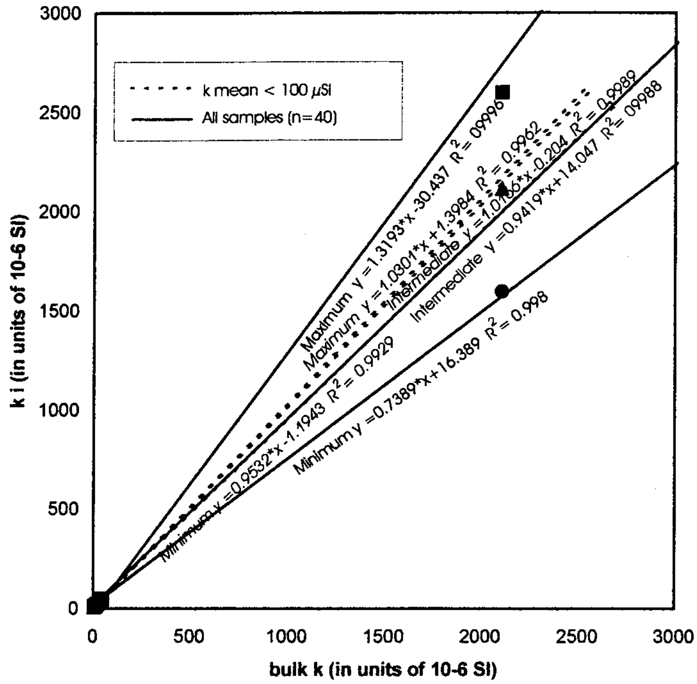

Figure VI.4. Relationship between the axes susceptibilities (k max, k int and k min) and the bulk susceptibility of each specimen of the Rice Bay dome. The lines represent the relations of all the specimens (n = 40) and the dashed lines with italic equations are the relations of the specimens whose susceptibilities are smaller than 100 μSI (n = 29). 10 points are out of range.

The relations of axes susceptibilities (k max, k int and k min) with the bulk susceptibility of the group with susceptibilities ≤ 100 μSI are linear with also a very high coefficient of regression. These lines slopes do not correspond to lines slopes defined for all the specimens: this suggests that specimens of the first group do not have the same behavior as the specimens of $k_{bulk} > 2000$ μSI. The high coefficients of regression can be explained by the concentration of points with low k_{bulk}, which affect less significantly the lines slopes than the high ones because of their concentrations and their proximity to the points of intersections of the lines.

In figure VI.5. showing the relation between the Tj_{AMS} and the Pj_{AMS} two groups of fabrics are clearly differentiated. The two groups have both prolate and oblate fabrics and are differentiated thanks to the Pj. The first group has Pj < 1.4: it shows symmetry around the Pj axis with 5 areas where the density of fabrics is greater than 10 % but these areas are dispersed. The fabrics of this group have a Pj_{mean} equal (sum of Pj of the group with bulk k ≤ 100 μSI) to 1.29 ± 0.04 and a Tj_{mean} (sum of Tj of the group with bulk k ≤ 100 μSI) equal to 0.09 ± 0.03: the fabrics are consequently slightly oblate (S ≥ L). Some of the specimens of this group have a Pj > 1.4 but no specimens from the group whose bulk k > 2000 μSI have a Pj smaller than 1.4. The k mean of this group (bulk k ≤ 100 μSI) is equal to 23 ± 2 μSI and the number of specimens is 29.

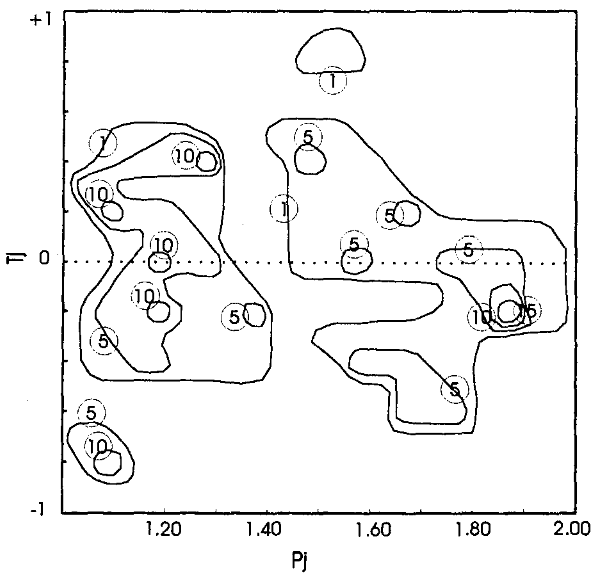

Figure VI.5. Diagram of Pj versus Tj of the Rice Bay dome. The contours correspond to the limit of the percentage of specimens (1, 5, 10 and 15 %) (n = 40).

The second group contours (1 % and 5 %) are more dispersed and located in the prolate area (0 > Tj > -1). The specimens Tj are concentrated around – 0.1 (contour equal to 15 %). Specimens have a bigger Pj (from 1.4 to 2) with Pj mean = 1.75 ± 0.04 and the Tj mean = – 0.10 ± 0.08. The group with bulk k > 2000 μSI has a k mean = 11415 ± 1641μSI.

The relation of Pj with the logarithm of bulk k ((k max + k int + k min)/3) (figure VI.6.) shows also two different groups with both prolate and oblate fabrics. The group with k ≤ 100 µSI have Pj < 1.4. The specimens with highest k (> 50 µSI) have oblate shapes and susceptibilities ≤ 50 µSI have prolate ones.

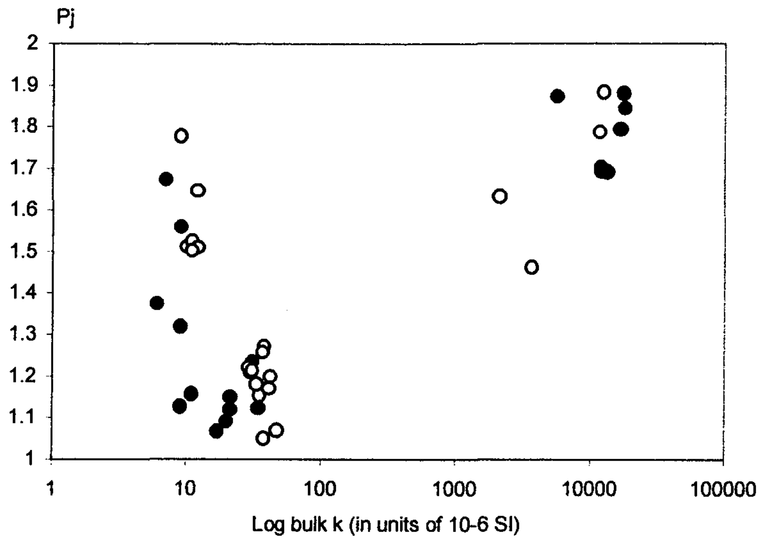

Figure VI.6. Relationship between the log bulk k of the Rice Bay dome with the Pj. Black circles correspond to prolate (Tj < 0) fabrics and white circles are oblate fabrics (Tj > 0) (n = 40).

A second group with k ≤ 100 µSI can be differentiated. The specimens have AMS Pj < 1.5. 2 specimens have prolate fabrics and 6 have oblate ones. The lowest susceptibilities specimens are prolate and the "highest" susceptibilities are oblate like for the previous group.

A third group previously described can be seen in the figure VI.6.: its k values are > 2000 µSI and its Pj is > 1.4. Fabrics are in majority prolate.

No linear relation between the Pj and the logarithm of the bulk susceptibility exists.

The relation between the Tj and log bulk k (figure VI.7.) shows two groups of specimens differentiated with log bulk k. As shown previously, a first group with k ≤ 100 μSI whose fabrics are more concentrated in the oblate side (Tj > 0) and a second group with k > 2000 μSI whose fabrics are more concentrated in the prolate side (Tj < 0) are differentiated.

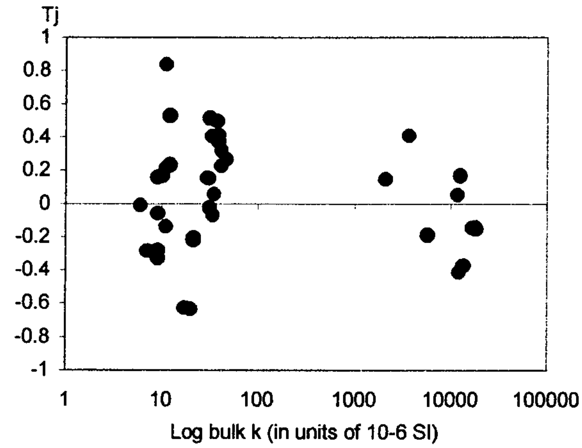

Figure VI.7. Relationship between log bulk k and Tj (n = 40) of the Rice Bay dome.

The specimens from the group with k > 2000 μSI are located in the middle of the dome (see figure VI.8.).

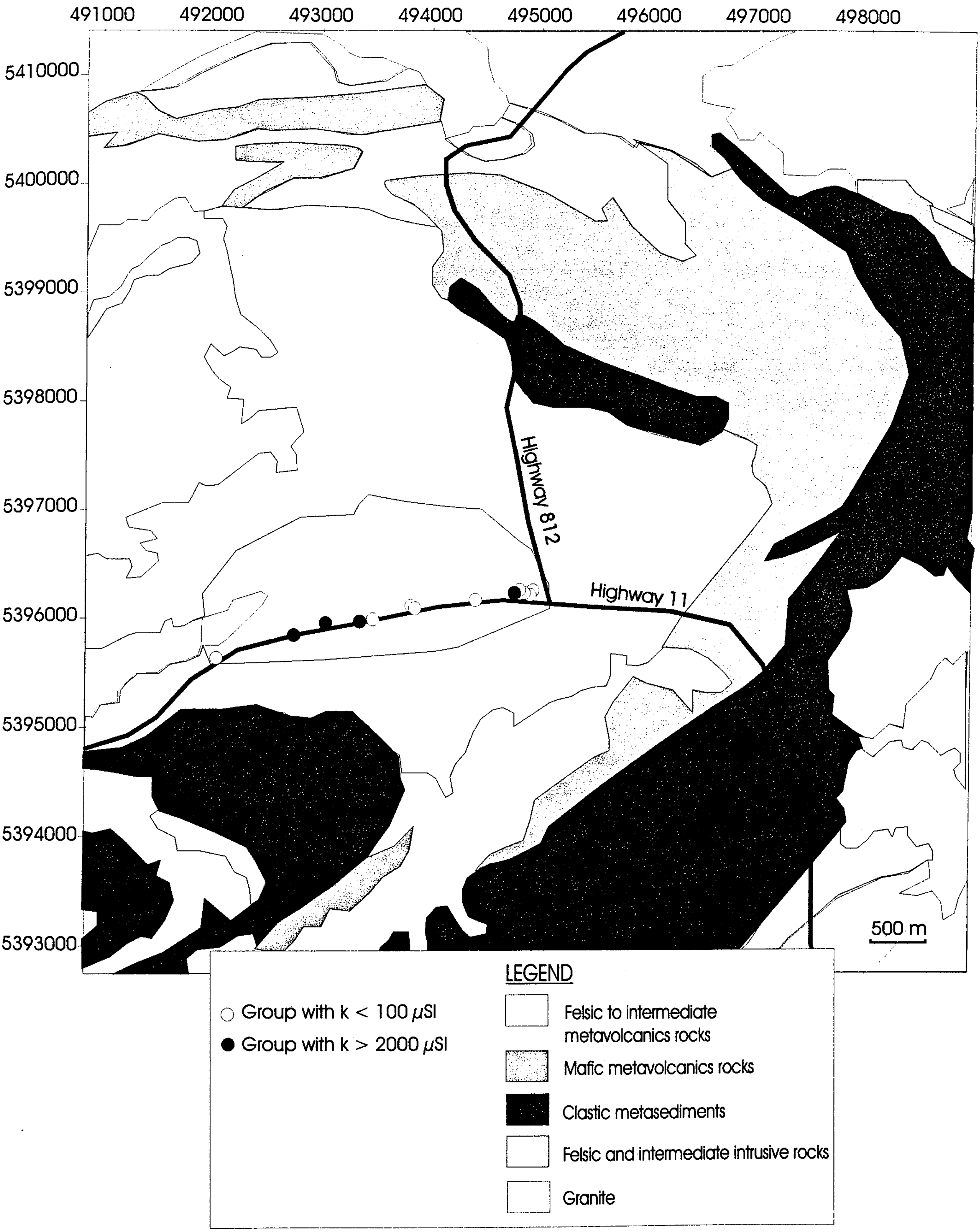
491000
492000
493000
494000
495000
496000
497000
498000
5410000
5400000
5399000
5398000
5397000
5396000
5395000
5394000
5393000
Highway 812
Highway 11
500 m
LEGEND
Group with k < 100 μSI
Group with k > 2000 μSI
Felsic to intermediate metavolcanics rocks
Mafic metavolcanics rocks
Clastic metasediments
Felsic and intermediate intrusive rocks
Granite

VI.2. Orientation distribution of fabrics.

VI.2.1. **Stereonets**

The stereonets of orientations of maximum, intermediate and minimum axes of AMS and the normalized and non-normalized tensors are drawn in figure VI.9. It is difficult to define the orientation-distribution of AMS axes using the stereonets of orientations of AMS axes because of the disparity of orientations of the minimum axes. Although, the maximum orientations plane is clearly perpendicular to intermediate axes and therefore this suggest that the orientation-distribution would be more prolate (L > S fabric).

The orientations of maximum susceptibility axes are included in the horizontal plane. Four groups of orientations are clearly differentiated: one group of orientations is located in the East, one in the North, one in the West and one in the South. The most important group is concentrated in the East.

The orientations of intermediate susceptibility axes lie along a vertical plane. Their inclinations vary from horizontal to vertical. The vertical plane has a North-South direction. No denser area along this plane can be distinguished.

The orientations of the minimum susceptibility axes are more difficult to describe. They seem to be concentrated along two planes: one oriented East-West and the other oriented North-South and they both seem subvertical. No denser group can be distinguished.

The directions of maximum susceptibility axes have an eigenvector value equal to 80/8. The orientations of maximum susceptibility axes oriented toward the East correspond to the mineral lineation visible on the field: this suggests that the magnetic fabrics are coaxial with the mineral fabrics and they reflect the movement and emplacement of the gneiss.

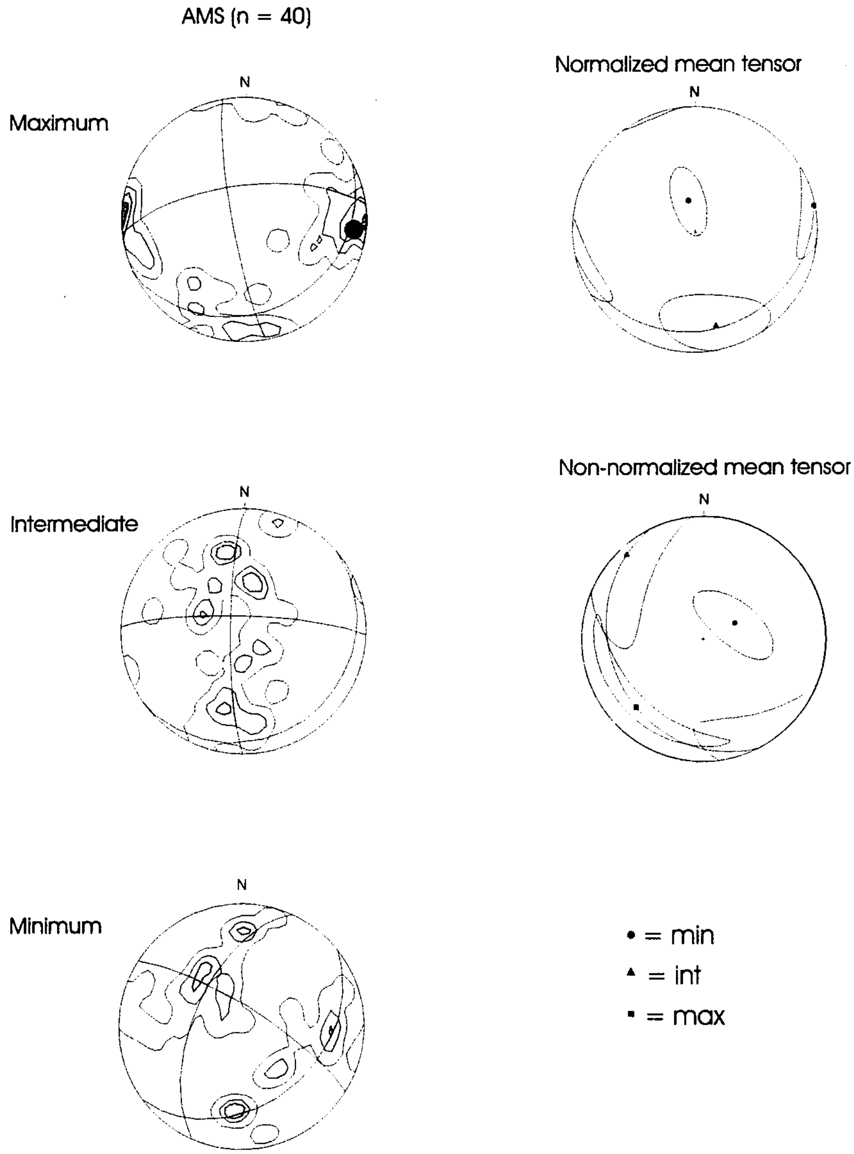

Figure VI.9. Stereonets of directions of specimens of the Rice Bay dome (n = 40). Contours are multiple of the uniform density. The black circle in the stereonet of orientations of AMS maximum axes is the mineral lineation measured on the field.

The ellipses of maximum and intermediate axes in the mean tensors stereonets are aligned and define a magnetic foliation. The normalized mean tensors' ellipses are smaller than non-normalized mean tensors' ones. The group of bulk susceptibility greater than 2000 μSI, which affects more the non-normalized mean tensor has consequently a bigger variation of orientations than the group of bulk susceptibilities smaller than 100 μSI. In the normalized tensor stereonet, the ellipse of orientations of intermediate susceptibility axes is included in the horizontal plane and oriented toward the SSE; the ellipse of orientations of maximum axes is also included in the horizontal plane and its direction is ENE and WSW; the ellipse of orientations of minimum axes has a direction equal to 331/66 on the stereonet. The orientation-distribution is consequently oblate. The ellipses do not show an orthorhombic symmetry and therefore, the strain fossilized by magnetic minerals was non-coaxial. The ellipses of the non-normalized tensors do not have the same directions than ellipses of normalized tensors: the ellipse of orientations of maximum axes has a direction of 225/23, the ellipse of orientations of intermediate axes has a direction of 318/7 and the ellipse of orientations of minimum axes has a direction of 64/66. The orientations-distribution is also non-coaxial and is described by an oblate ellipsoid. These ellipsoids shapes are consistent with the regional tectonic (transpressive context).

VI.2.2.2. **Maps**

The arrows representing the orientations of maximum and minimum AMS axes in the figures VI.10 and VI.11 have their length proportional to their inclination: the more the arrows are elongated and the more the inclination is subhorizontal. The orientations of the maximum susceptibility axes of the Rice Bay dome are more or less horizontal and oriented toward the West or the East except in the western border of the dome. Although the studied area is the center and the apex of the dome, no vertical susceptibility maximum axes have been found. Despite the non-coaxiality context, lineations are very well defined and their orientations are consistent in all the studied area. The magnetic lineations cross the border of the dome and do not show any concentric forms: the dome is consequently concordant with the country rocks. This syntectonism is also proved by the parallelism of the orientations of magnetic lineations (maximum susceptibility axes) (except in the western border of the dome) with the axis of elongation of the dome (Figure VI.10.).

The orientations of the minimum susceptibility axes of the Rice Bay dome cannot be used as kinematic indicators. Generally, the orientations are very steep. The eastern part of the dome has consistent orientations of minimum susceptibility axes oriented in the SW-NE direction. In the western part of the dome, the orientations of the minimum susceptibility axes are not coherent (Figure VI.11.).

The group of specimens having susceptibilities > 2000 μSI has been taken out to produce maps of Pj, Tj and k mean. Because of the extreme contrast of susceptibilities between the two groups, the group of specimens with susceptibilities ≤ 100 μSI would have been masked by the other group (with bulk k > 2000 μSI). Therefore the next interpretations are strictly for specimens having susceptibilities ≤ 100 μSI.

The bulk susceptibility ((k max + k int + k min)/3) of the Rice Bay dome varies from 0 to 100 μSI. The smallest susceptibilities are located in the middle of the dome and increases toward the NE in the eastern border of the dome and toward the SW in the western border of the dome. These variations are symmetrical but are not concentric and are related to the anticline axis and parallel to the elongation of the dome (Figure VI.12.).

The AMS Pj (intensity of anisotropy of AMS ellipsoid) map of the Rice Bay dome (Figure VI.13.) shows a concentric variation. The Pj tend to increase from the borders to the center. The Pj minimum value is equal to 1.2 and increases to be greater than 1.5. The areas are elongated in the E-W direction. These directions of elongation of the sections of Pj correspond very well with the azimuth of the orientations of maximum susceptibility axes.

The map of AMS Tj (shape parameter of the AMS ellipsoid) of the Rice Bay dome (Figure VI.14.) shows also a symmetrical variation. The Tj is negative (prolate fabric) in the center of the dome and increase toward the borders to become positive (oblate fabric). The map of Tj is very similar to the map of k mean with no concentric variations of Tj. The Tj becomes positive in the NE and SW areas of the dome and its variations along the axis of elongation of the dome. The Tj varies very rapidly in a very small area. These variations of Tj and k mean are related to the plunge directions of the maximum susceptibility axes.

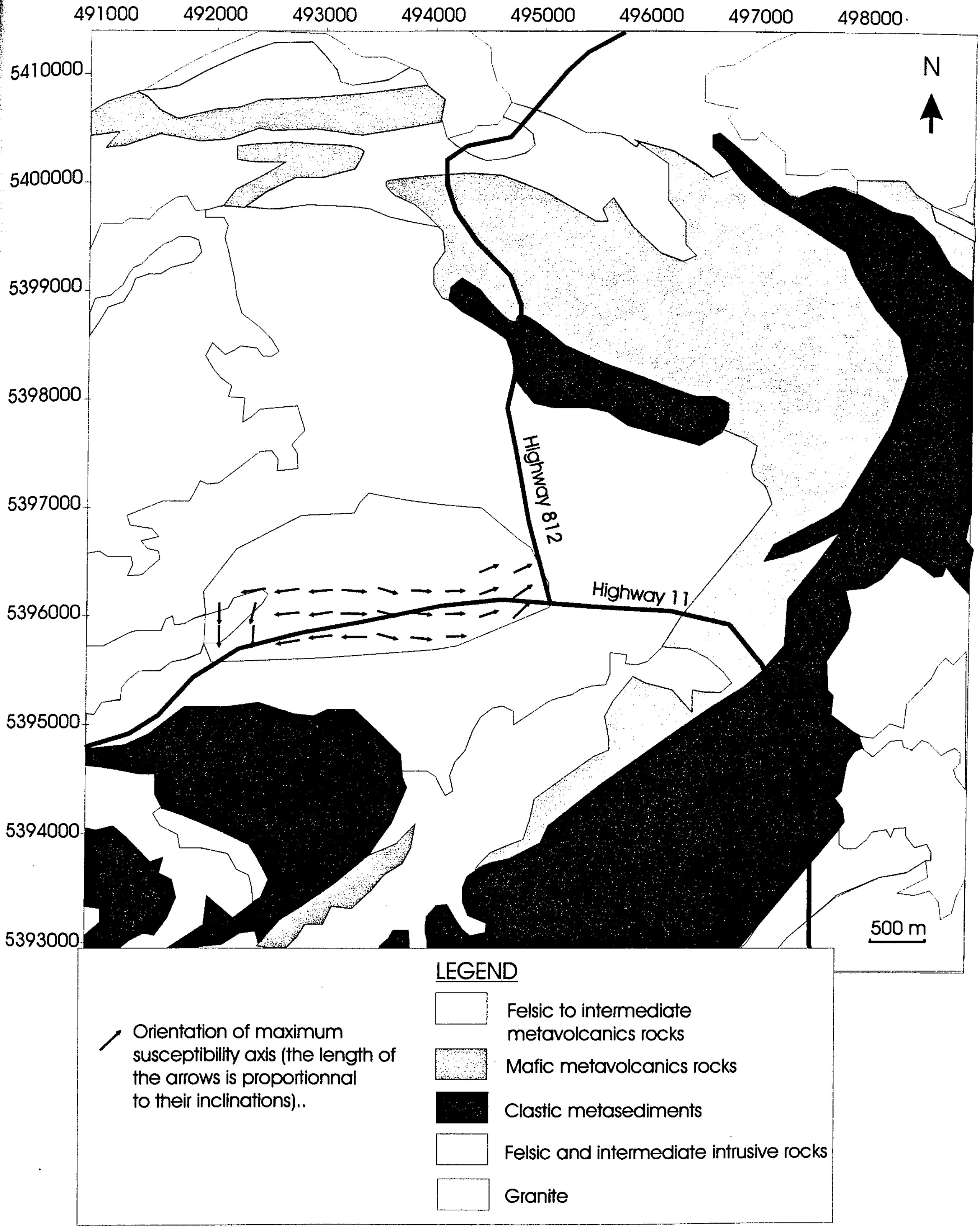

Figure VI.10. Map of orientations of maximum susceptibility axes of the Rice Bay dome.

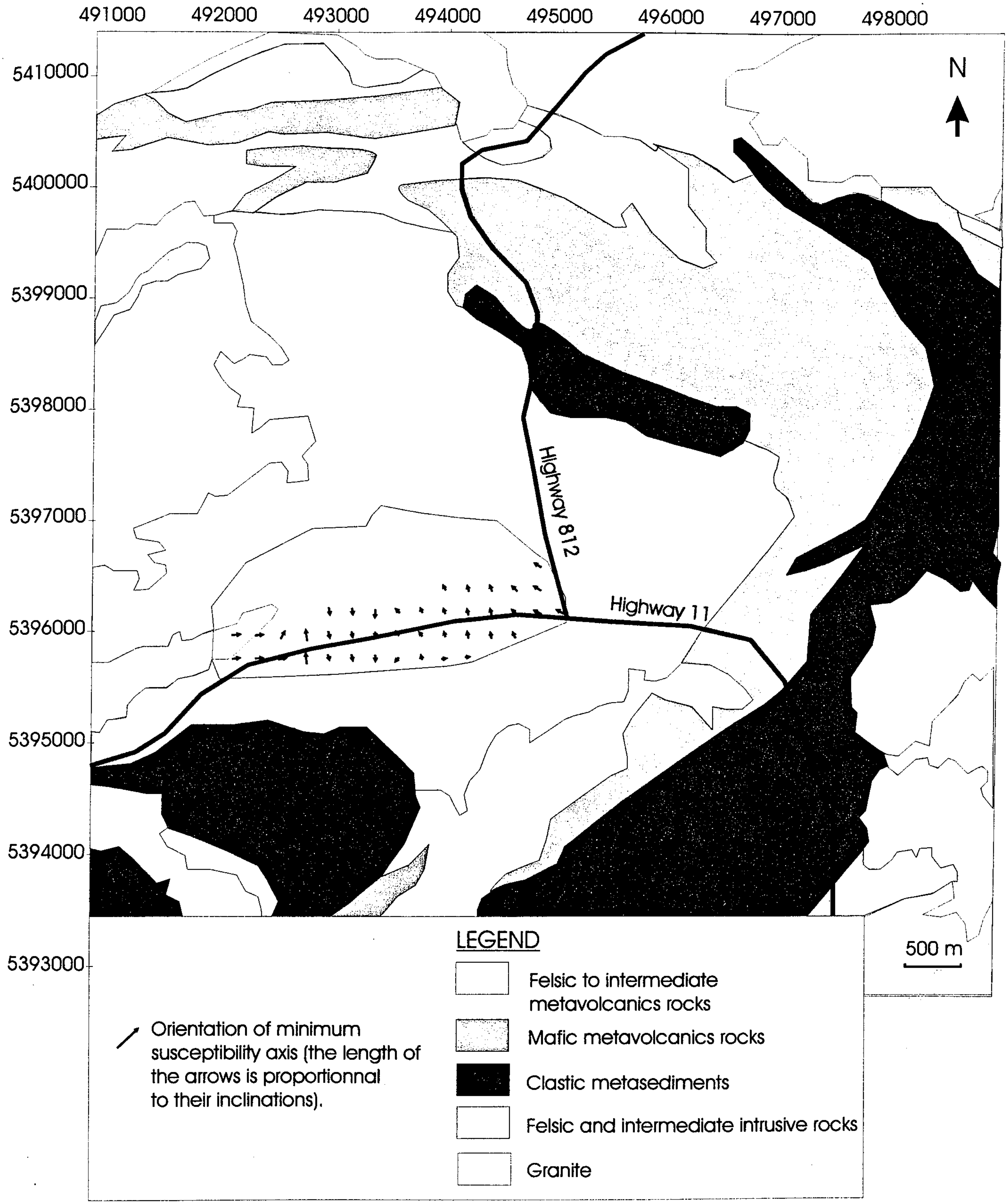

Figure VI.11. Map of orientations of minimum susceptibility axes of the Rice Bay dome.

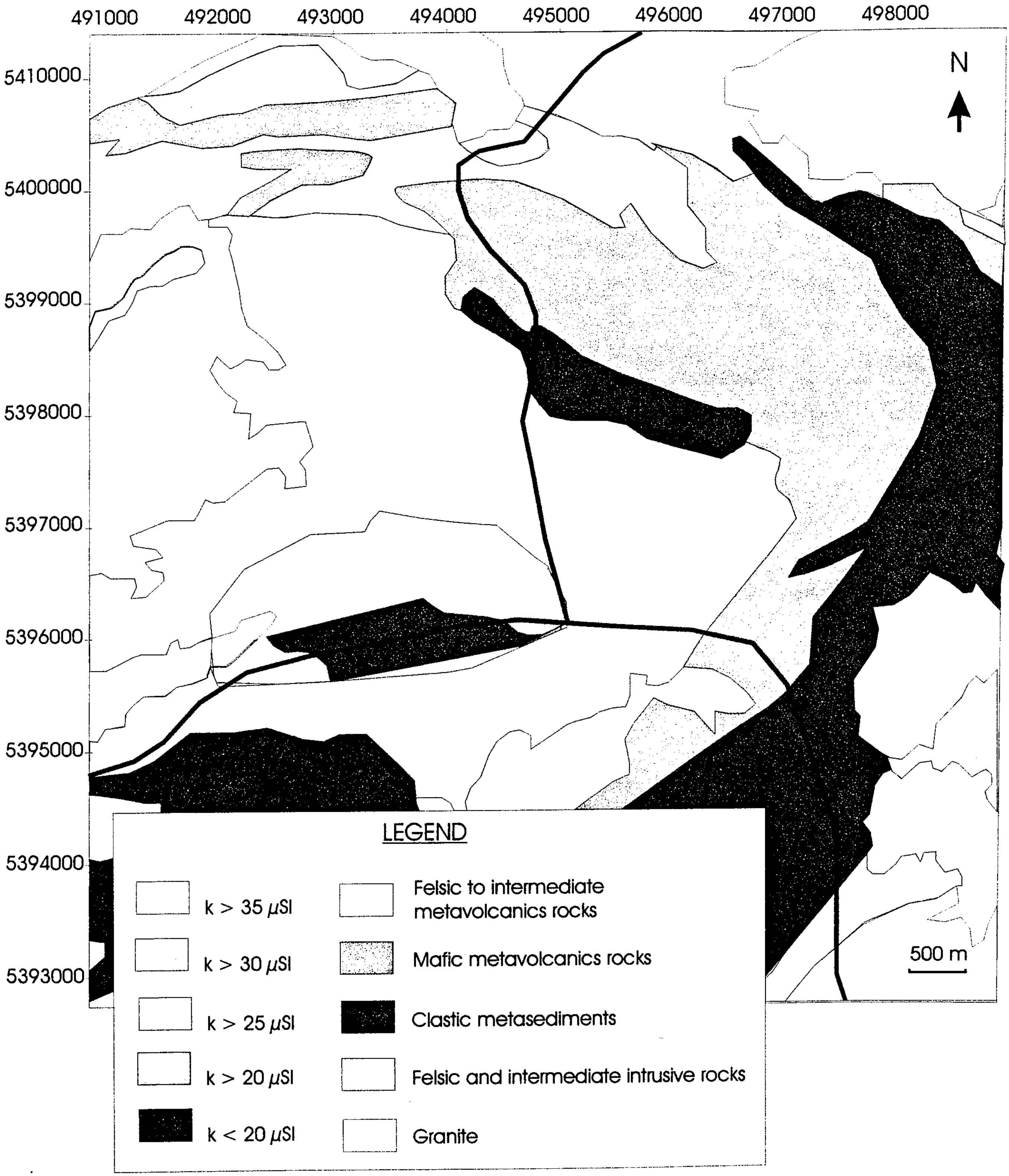

Figure VI.12. Map of bulk susceptibility ((k max + k int + k min)/3) of the Rice Bay dome.

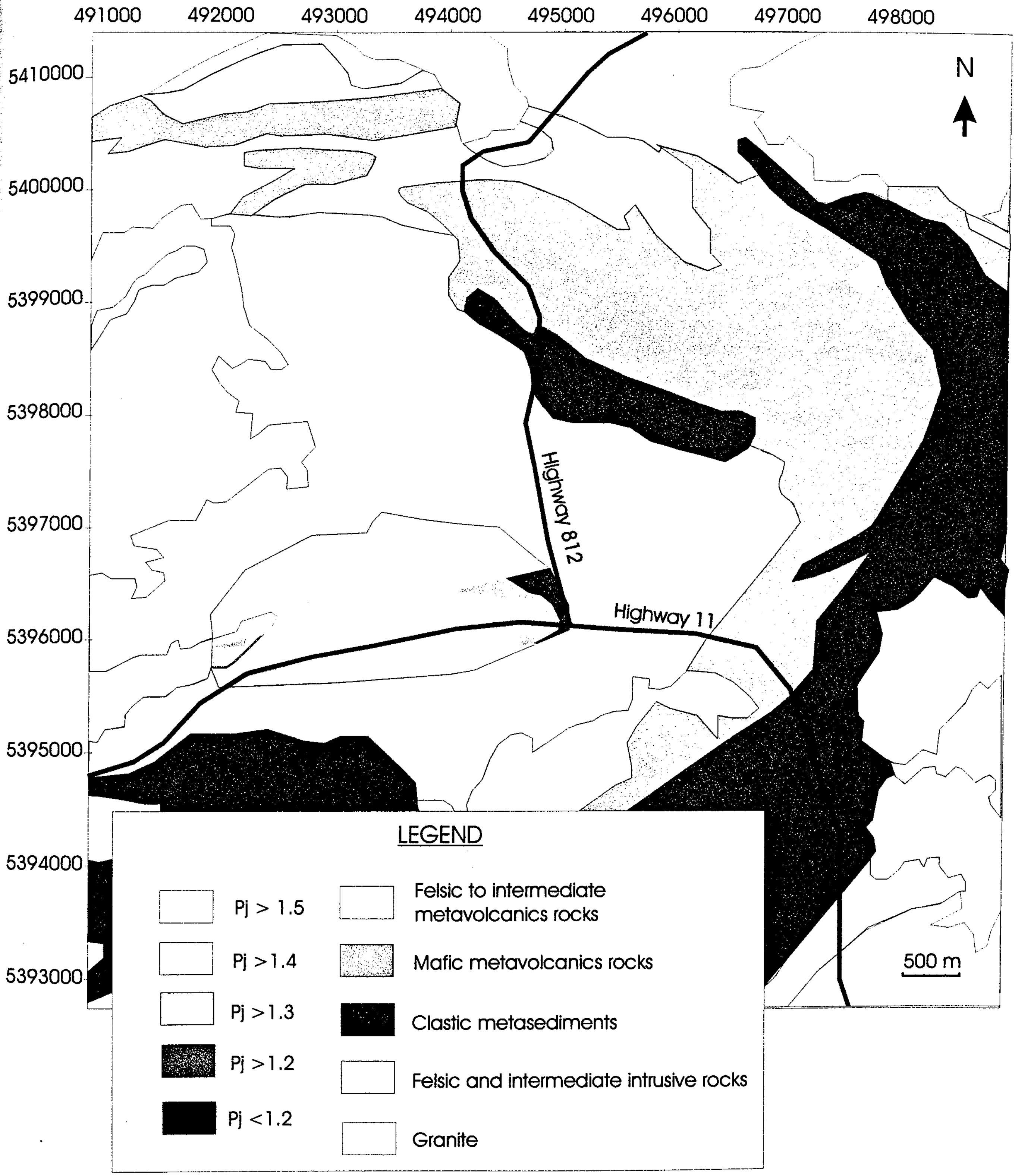

FigureVI.13. Map of AMS Pj of the Rice Bay dome.

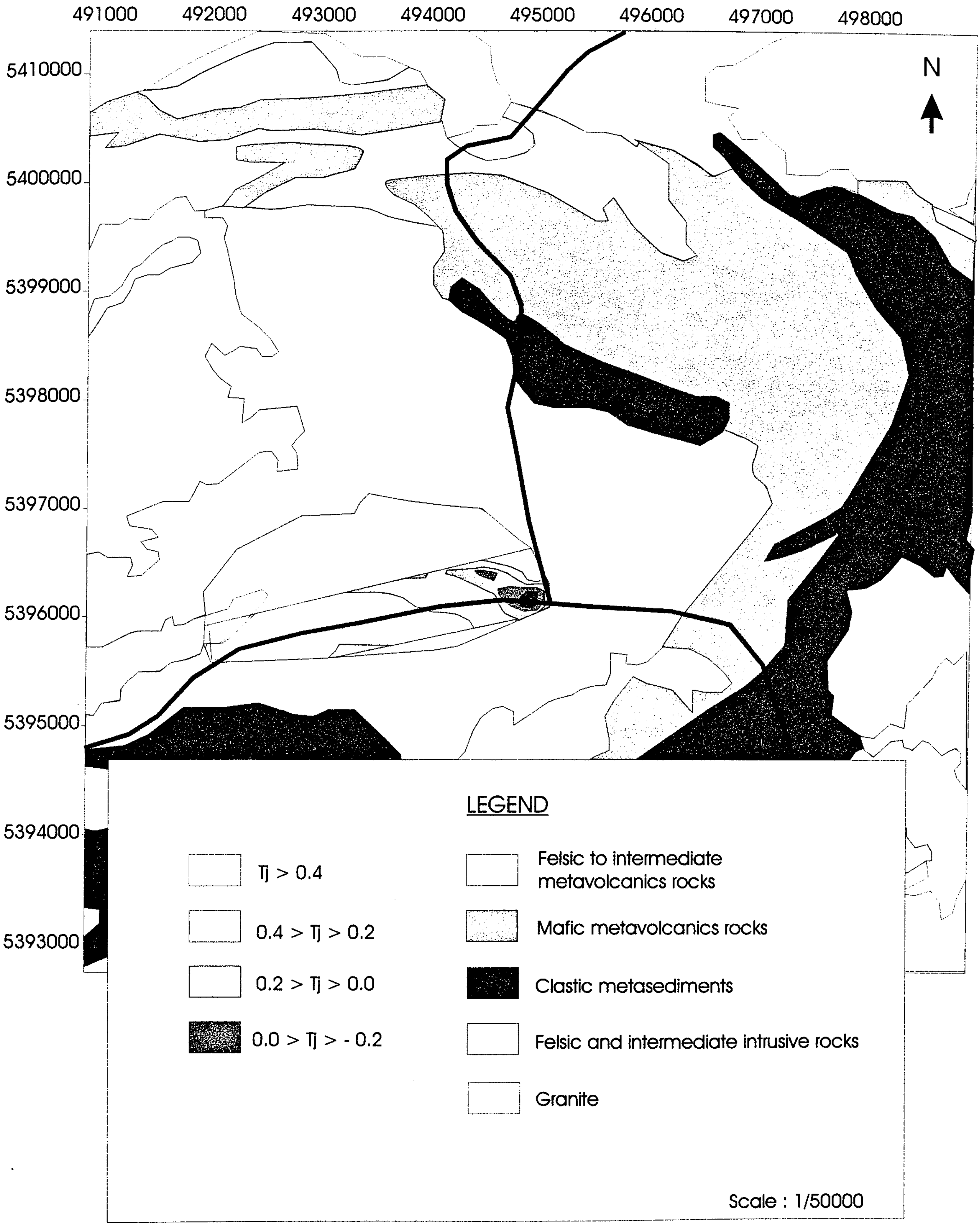

Figure VI.14. Map of AMS Tj of the Rice Bay dome.

VI.3. Conclusion

Rice Bay dome is composed of tonalitic gneiss. Two groups of specimens are differentiated: a first group with susceptibilities ≤ 100 μSI and a second group with susceptibilities > 2000 μSI. The specimens with susceptibilities ≤ 100 μSI are described by an oblate ellipsoid and an AMS Pj usually smaller than 1.5. The specimens with susceptibilities > 2000 μSI are described by a prolate ellipsoid and AMS Pj greater than 1.5. They both have prolate and oblate fabrics.

The orientation of k max axes corresponds to the mineral lineation although the ellipses tensors are described by an oblate ellipsoid. This observation is consistent with the regional deformation. The magnetic susceptibility could reflect a primary fabric related to the rise and the emplacement of the dome. The ellipse tensors show that the two groups have different behaviors and orientations and they both are non-coaxial: this is consistent with the transpressive context.

Orientations of k max. (ASM) are more or less horizontal and parallel to the axe of elongation of the dome and have a sigmoidal distribution: this suggests the syntectonic emplacement of the dome, concordant with the country rocks. The orientations of k_{min} are not well defined since their plungings are subvertical.

The Rice Bay dome gneiss has taken place under ductile conditions and therefore has risen by diapirism or gravity-driven undergoing regional transpressive deformation.

VI.4. Data of the Rice Bay dome

samples	dec.	inc.	k. min. (µSI)	dec.	inc.	k. int. (µSI)	dec.	inc.	k. max (µSI)	bulk k. (µSI)	Pj	Tj
RB001A	325	44	30	196	34	34	86	28	36	33	1.18	0.40
RB001B	297	54	32	172	23	34	70	26	36	34	1.12	-0.07
RB001C	312	46	33	151	43	36	52	10	38	35	1.15	0.06
RB002A	104	3	2935	10	52	3809	196	38	4252	3665	1.46	0.41
RB002B	70	12	1597	326	50	2111	169	37	2599	2102	1.63	0.15
RB003A	298	39	26	181	29	30	66	37	32	29	1.22	0.15
RB003B	293	14	28	141	75	33	25	7	34	31	1.21	0.52
RB004A	99	32	39	341	36	43	218	37	46	42	1.20	0.32
RB004B	106	26	38	329	57	42	206	20	44	41	1.17	0.22
RB005A	327	44	29	204	30	32	93	31	35	31	1.23	-0.02
RB005B	309	50	28	204	12	31	105	38	33	30	1.21	0.15
RB006A	139	50	10384	352	35	12191	250	16	17326	13300	1.69	-0.37
RB006B	133	54	9477	344	32	11001	244	15	15793	12090	1.70	-0.42
RB006C	155	54	9472	350	36	11009	255	7	15846	12108	1.70	-0.42
RB007A	270	19	33	128	66	39	5	14	42	38	1.27	0.41
RB007B	274	6	33	112	84	38	4	2	41	37	1.26	0.49
RB008A	99	51	38	310	35	39	209	15	40	38	1.05	0.38
RB008B	72	55	46	319	15	48	220	31	49	47	1.07	0.27
RB011A	74	27	12695	282	60	16594	171	12	23713	17667	1.88	-0.14
RB011B	89	26	12293	296	62	15721	184	11	21927	16646	1.79	-0.15
RB011C	91	28	13131	298	59	16949	187	12	24043	18041	1.84	-0.16
RB012A	168	11	4092	44	72	5265	261	15	7600	5652	1.87	-0.19
RB012B	2	22	8535	185	68	11554	93	1	15195	11761	1.79	0.05
RB012C	357	23	8718	181	67	12586	87	2	16309	12537	1.89	0.17
RB013A	188	28	9	23	61	13	282	6	13	11	1.50	0.83
RB013B	186	30	9	14	59	11	278	3	13	11	1.52	0.21
RB013C	180	34	7	358	56	10	89	1	12	9	1.78	0.16
RB013D	186	33	9	8	57	11	276	1	13	10	1.51	0.17
RB014A	272	48	9	16	13	9	117	39	10	9	1.13	-0.06
RB014B	16	87	10	251	2	14	161	3	15	12	1.51	0.53
RB014C	264	30	11	69	59	12	170	6	13	11	1.16	-0.14
RB014D	272	73	6	19	5	7	111	16	8	6	1.37	-0.01
RB015A	2	24	8	229	58	9	102	21	11	9	1.32	-0.33
RB015B	353	40	6	197	47	7	94	13	10	7	1.67	-0.29
RB015C	313	75	9	176	11	13	84	10	15	12	1.65	0.24
RB015D	325	65	8	192	17	9	96	17	12	9	1.56	-0.28
RB016A	340	63	20	171	27	20	79	5	22	20	1.09	-0.64
RB016B	16	9	20	282	25	21	123	63	23	21	1.12	-0.22
RB016C	345	54	20	192	33	21	93	13	23	21	1.15	-0.21
RB016D	332	39	17	191	44	18	80	21	18	17	1.07	-0.63

VII. The Sawbill dome

The Sawbill dome is located to the NE of Fort Frances (figure VI.1.). The N-S highway 512 going to Dryden crosses the dome along its length. The southern border of the dome is limited by the dextral Quetico fault. The western margin is limited by other tonalitic domes (from 2.5 to 2.9 Ga). The dome is surrounded by metavolcanic rocks (greenstones) (from 2.5 to 3.4 Ga). Greenstones show a syndeformation with the dome.

The dome composition is very heterogenous, composed of tonalitic and granodioritic rocks (quartz, plagioclases and biotites transformed into granodiorites with addition of K-feldspars). Only the SW part of the granite has been studied.

VII.1. Fabric study

52 cores from 12 locations have been collected. The bulk susceptibilities of the specimens vary from 26 to 8355 μSI, with mean susceptibility of 1718 ± 291 μSI. Sawbill dome has a multimodal frequency distribution of k. Two groups have been sorted (figure VII.1.).

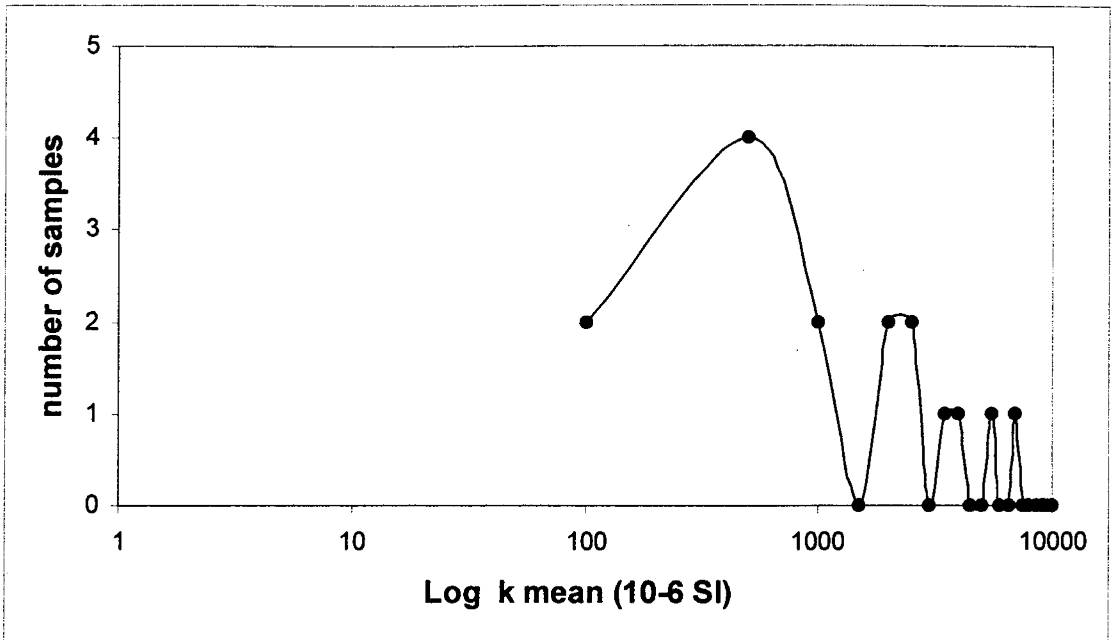

Figure VII.1. Frequency distribution of k mean of Sawbill dome's specimens. Two groups are differentiated: the gray circles correspond to a group whose specimens' mean susceptibilities ≤ 1000 μSI and the black circles correspond to a group with specimens' mean susceptibilities > 1000 μSI (n = 16).

The relationships between the susceptibility axes (k_{min}, k_{int} and k_{max}) and k are linear with high regression coefficients. The specimens bulk susceptibilities can be divided into two parts: the matrix (diamagnetic and paramagnetic minerals) whose calculated susceptibility is 203 ± 291 μSI and a ferromagnetic fraction.

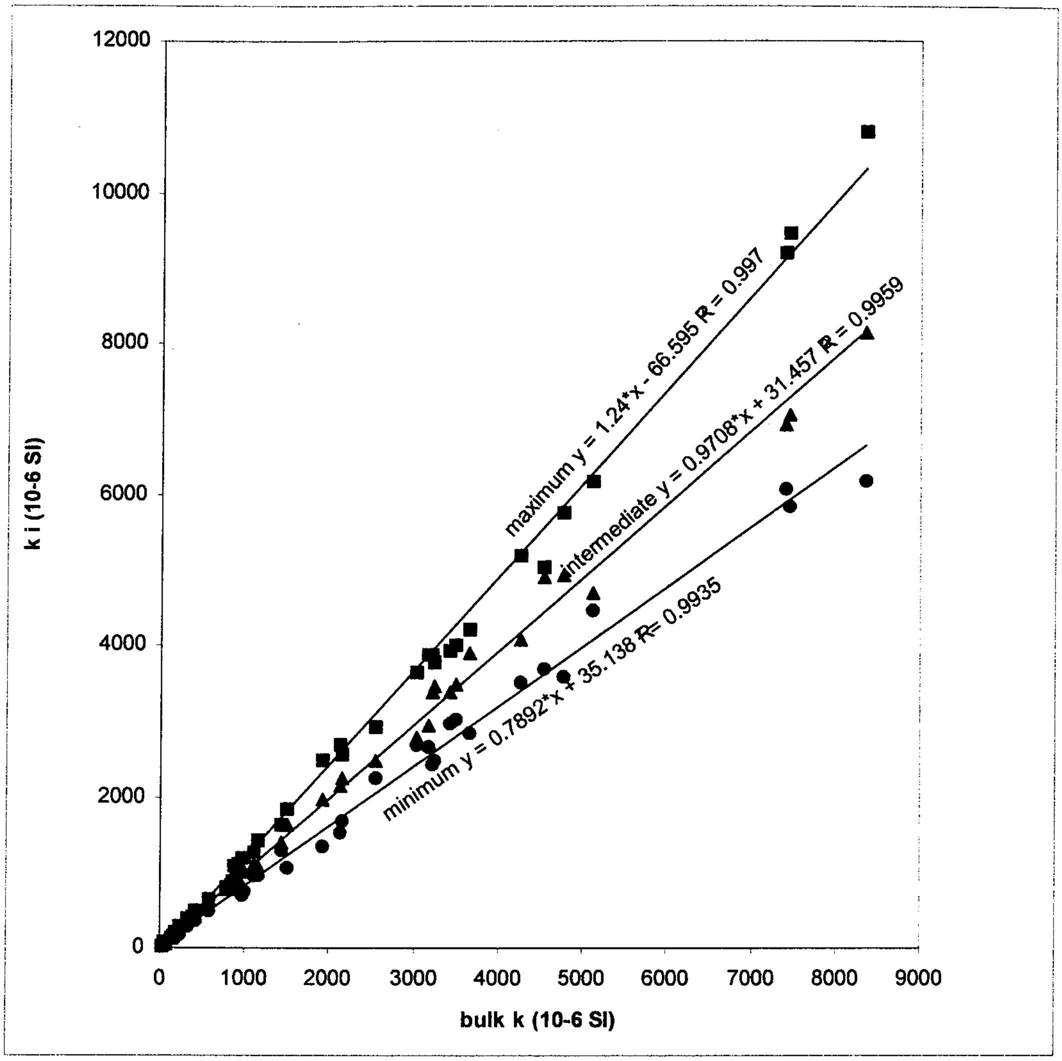

Figure VII.2. Relationship between axes susceptibility and the bulk susceptibility ((k max + k min + k int)/3) of the Sawbill dome (Henry, 1983). The black dots represent the relation between the minimum axis susceptibility and the bulk susceptibility. The gray dots represent the relation between the intermediate axis susceptibility and the bulk susceptibility. The white dots represent the relation between the maximum axis susceptibility and the bulk susceptibility (n = 52).

The points of intersections of two linear relations (Fig. VII.2), at 364 μSI (k max ∩ k int), at 226 μSI (k max ∩ k min) and 20 μSI (k min ∩ k int) are included in the range of susceptibilities given by the standard error. Again, this suggests the coaxiality of paramagnetic and diamagnetic minerals with the ferromagnetic minerals.

The AMS Pj vary from 1 to 1.9 with a uniform dispersion. Two areas with 5 % contours are differentiated: one with 1.3< Pj < 1.5 and 0.1< Tj < -0.2 and a second one with 1.4< Pj <1.6 and – 0.2 < Tj < -0.8. The Tj is also very dispersed. The specimens' Pj mean is 1.38 ± 0.03 and the Tj = 0.07 ± 0.07. The specimens are more located in the prolate area (Tj < 0).

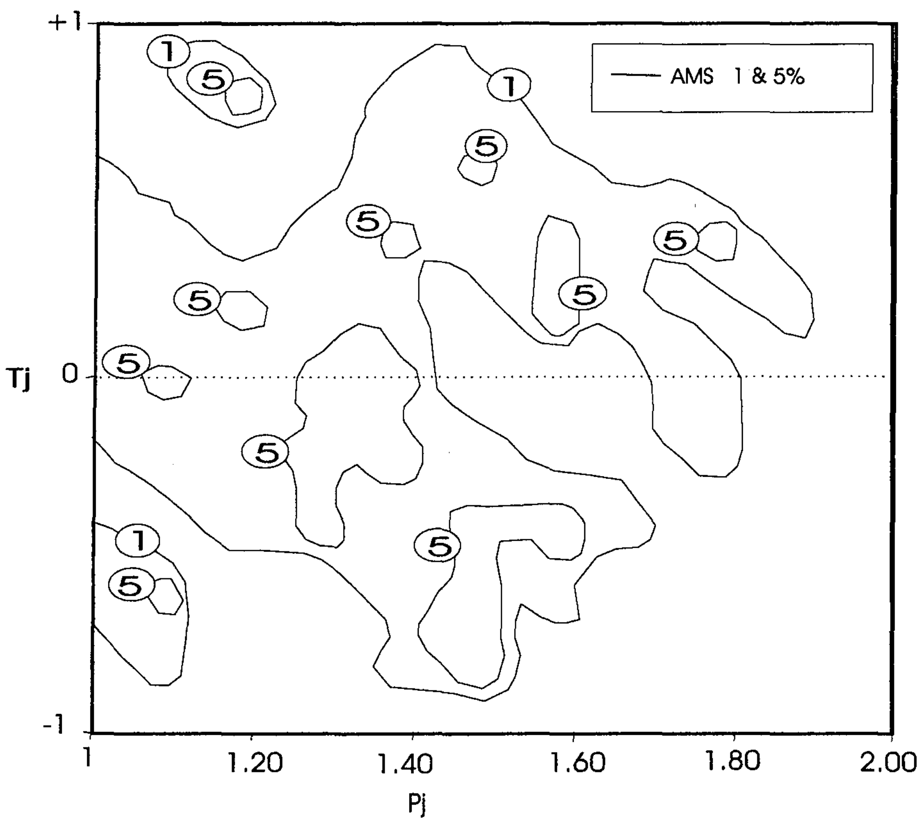

Figure VI.3. Diagram of Pj (sum of AMS Pj of all the specimens divided by their numbers) versus Tj (sum of AMS Pj of all the specimens divided by their numbers) of the Sawbill dome. The contours(1, 5, 10 and 15 %) correspond to the percentage of specimens (n = 52).

The relation between the bulk susceptibility and the Pj suggests the differentiation of two groups with two different Pj values: a group with k ≤ 1000 μSI with Pj < 1.5 and a group with k > 1000 μSI with 1.25 < Pj < 1.9. They both have prolate and oblate fabrics (figure VII.4.).

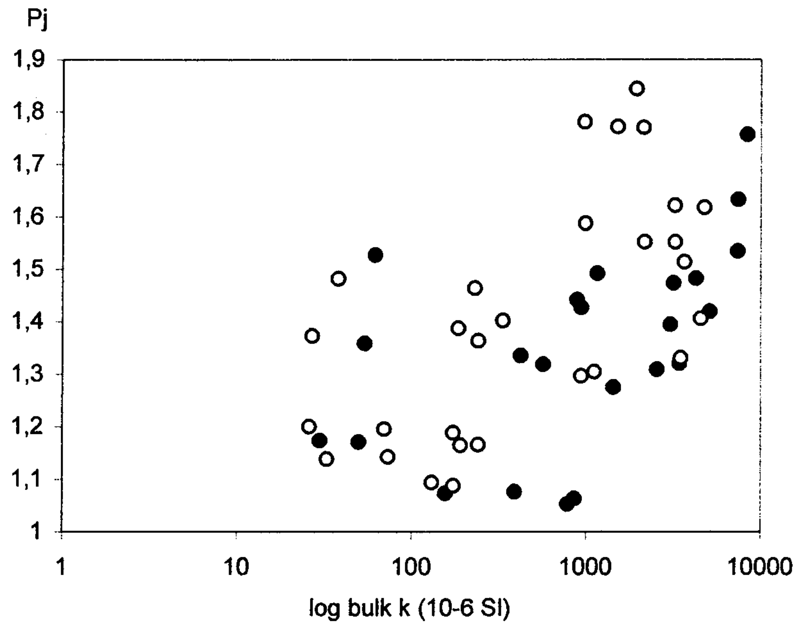

Figure VII.4. Relationship between the log bulk k ((k max + k int + k min)/3) with the Pj (intensity of anisotropy of the AMS ellipsoid) of the Sawbill dome. Black circles correspond to prolate (Tj < 0) fabrics and white circles are oblate fabrics (Tj > 0) (n = 52).

The relation of the bulk k and Tj (figure VII.5.) confirms this differentiation with a group of k ≤ 1000 μSI having more points into the oblate area (Tj > 0) and a group of k > 1000 μSI, which has more prolate fabrics (Tj < 0). The group with bulk k ≤ 1000 μSI has k mean of 342 ± 63 μSI, Pj mean of 1.29 ± 0.03 and mean Tj of 0.10 ± 0.08 (n = 30). The group with bulk k > 1000 μSI has k mean of 3594 ± 434, mean Pj of 1.52 ± 0.04 and a mean Tj of 0.02 ± 0.09 (n = 22).

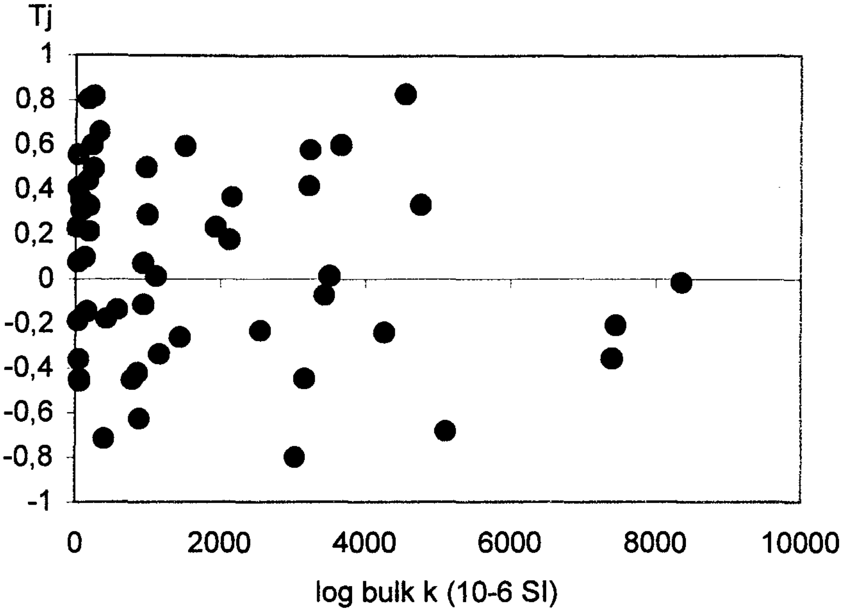

Figure VII.5. Relationship between log bulk k and Tj of the Sawbill dome (n = 52).

VII.2. Orientations-distribution of fabrics.

VII.2.1. **Stereonets**

The stereonets of orientations of AMS maximum, intermediate and minimum axes and the AMS normalized and non-normalized tensors are drawn in figure VII.6.. The orientations of k max are concentrated in two areas: a first one with very high density of directions oriented in the 33/59 direction corresponding to most of the specimens directions and another area with less density of points (260/36) corresponding to specimens affected by the movement of the Quetico fault in the South of the dome (see next chapter). The orientations of the k int are aligned along a plane oriented toward the southeast except some specimens concentrated in the 50/50 directions and probably related to the Quetico fault movement. The orientations of the k min are also concentrated along the same plane than the k int and therefore the orientations distribution of the susceptibility axes is described by an L-fabric (prolate ellipsoid). The dashed line drawn in the stereonet of orientations of k max represent the mineral foliation measured on the field. The magnetic ellipsoid is not oblate and the orientations of susceptibility axes do not correspond to the mineral foliations: therefore, the magnetic susceptibility do not describe the emplacement of the dome but another tectonic event.

The ellipses of cone of 95 % confidences of susceptibility axes correspond very well with the distribution of the susceptibility axes stereonets. The ellipse of orientations of k max is very little and consequently well defined. The ellipses of orientations of k int or k min are aligned and the ellipses symmetry is orthorhombic (for both normalized and non-normalized tensors): the orientations distribution of susceptibility axes is consequently described by a prolate ellipsoid and they are related to a coaxial deformation. The ellipses of susceptibility axes of non-normalized tensors are bigger than normalized tensors ones: the orientations of specimens having susceptibilities > 1000 μSI are consequently more dispersed than the orientations of specimens having susceptibilities ≤ 1000 μSI.

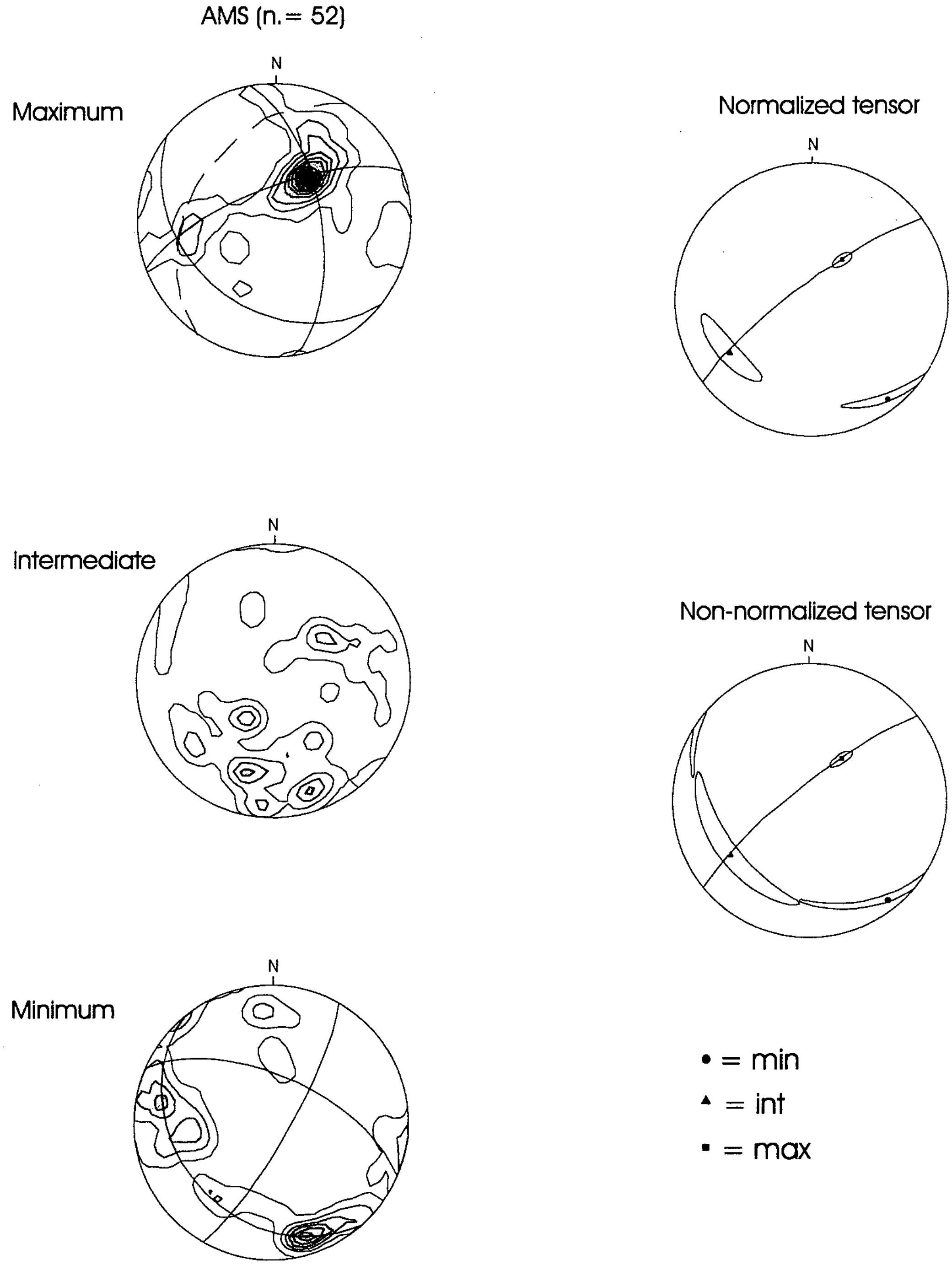

Figure VII.6. Stereonets of directions of specimens of the Sawbill dome (n = 52). Contours are multiple of the uniform density. The dashed line in the stereonet of orientations of AMS maximum axes is the mineral foliation measured on the field.

VII.2.2.2. **Maps**

The arrows representing the orientations of maximum and minimum AMS axes in the figures VII.7 and VII.8 have their azimuths and their length will be proportional to their inclination: the more the arrows are elongated and the more the inclination is subhorizontal. The orientations of maximum susceptibility axes of the Sawbill dome (figure VII.7.) can be divided in three groups. The first group is composed of the majority of the orientations of maximum susceptibility axes and its orientation is toward the NE. There is a variation of inclinations of the orientations of maximum susceptibility axes with vertical plunge of the directions in the South of the dome and they become more horizontal toward the center of the dome. This suggests that the magnetic fabrics have fossilized an event related to the movement of the suture of the Quetico subprovince (in the South of the Quetico fault) and the Wabigoon subprovince (in the North of the Quetico fault). The second group of orientations is located in the middle of the dome and their directions is parallel to the first group but their plunge is opposed and therefore they are competing the first group orientations: their origin is difficult to analyze and no explanation have been found. The third group of orientations is located in the southwestern border of the dome: the orientations are E-W and the plunge of orientations is horizontal. The third group directions are parallel to the Quetico fault movement and therefore they are affected by the dextral movement of the Quetico fault (figure VII.7.).

The orientations of minimum susceptibility axes of the Sawbill dome (figure VII.8) are in majority oriented in the E-W direction except in the south of the dome and in the middle of the dome. Their plunge is more or less horizontal. The southern area of the dome has minimum susceptibility axes orientations in the NNW-SSE direction and a plunge relatively horizontal: this group of specimens is affected by the Quetico fault movement. In the middle of the dome, a group of specimens has a N-S direction and relatively horizontal (figure VII.8.).

The map of bulk susceptibility ((k max + k int + k min)/3) (figure VII.9.) of the Sawbill dome is very heterogenous with two areas with different behaviors. The group of specimens with susceptibilities ≤ 1000 μSI located in the middle of the dome and specimen with susceptibilities > 1000 μSI are located in the western border of the dome. No relations between the orientations of maximum and minimum susceptibility axes and the k mean have been found (figure VII.9.).

The map of Pj (intensity of anisotropy of the AMS ellipsoid) of the Sawbill dome (figure VII.10.) is also divided in two parts; the Pj is lower in the middle of the granite and increase toward the western border of the dome. One area where Pj is greater than 1.4 coincide with the maximum mean susceptibility. The other area where Pj is the greatest is in the Southwestern border of the dome: this area corresponds to the region affected by the movement of the Quetico fault in the map of orientations of maximum susceptibility axes (figure VII.10.).

The map of Tj (shape parameter of the AMS ellipsoid) of the Sawbill dome (figure VII.11.) shows that the middle of the dome with susceptibilities smaller than 1000 μSI and Pj smaller than 1.3 has a Tj smaller than 0 and therefore tha fabrics are prolate. The Tj tend to increase toward the western border of the dome and become greater than 0 (oblate fabrics). Although the area where the susceptibility is the highest corresponds to a Tj smaller than 0 (prolate fabric) (figure VII.11.).

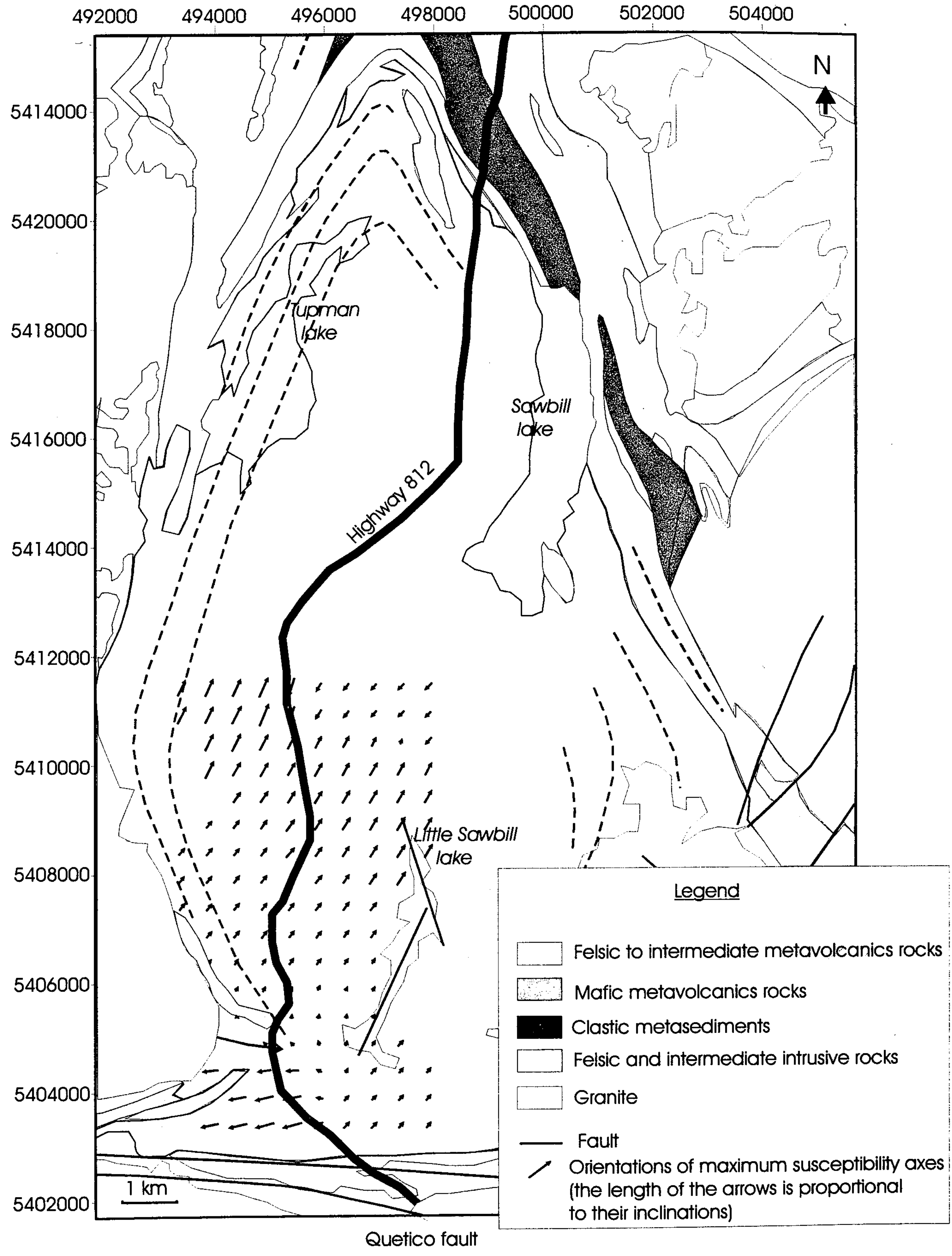

Figure VII.7. Map of orientations of AMS maximum axes of the Sawbill dome.

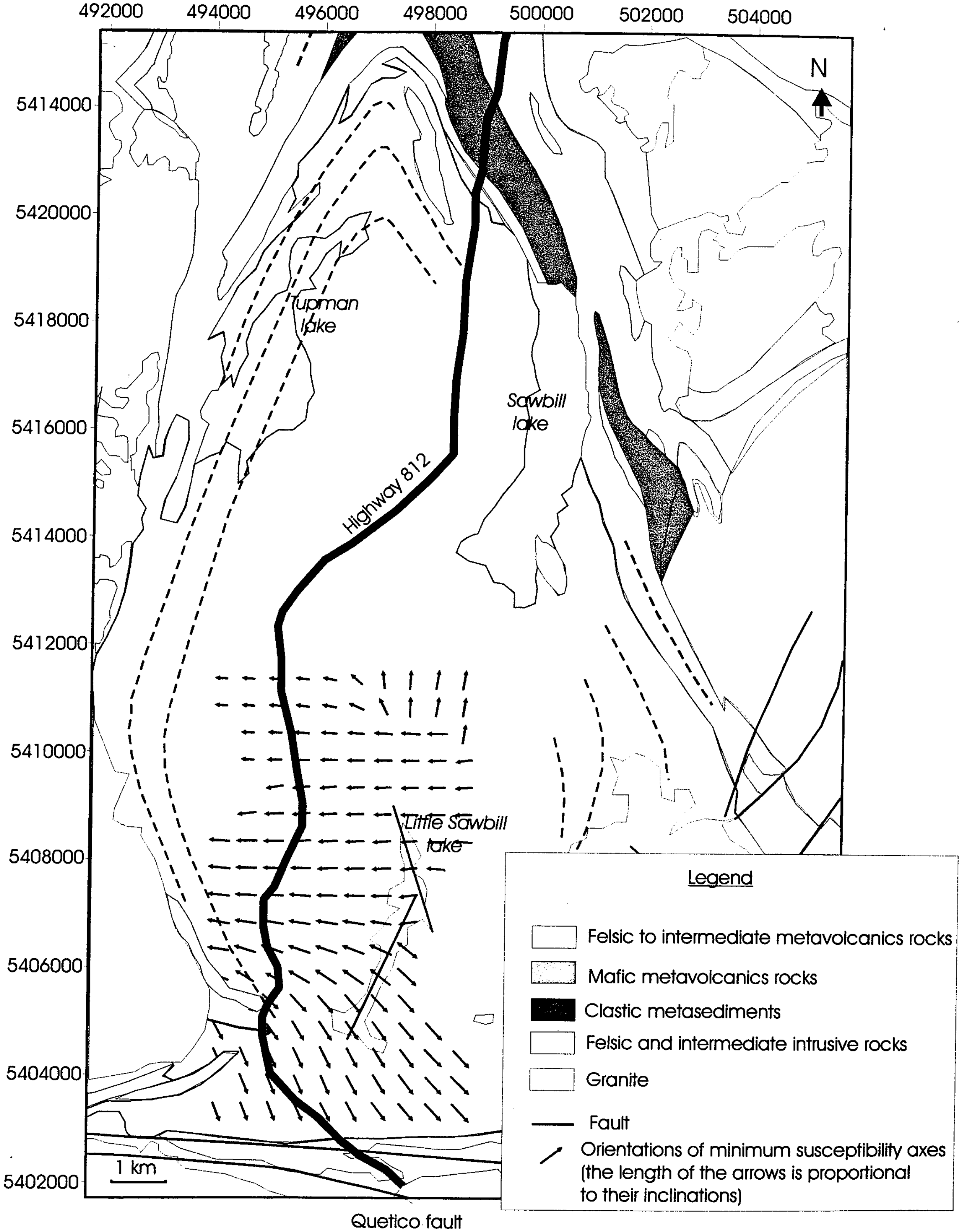

Figure VII.8. Map of orientations of AMS minimum axes of the Sawbill dome.

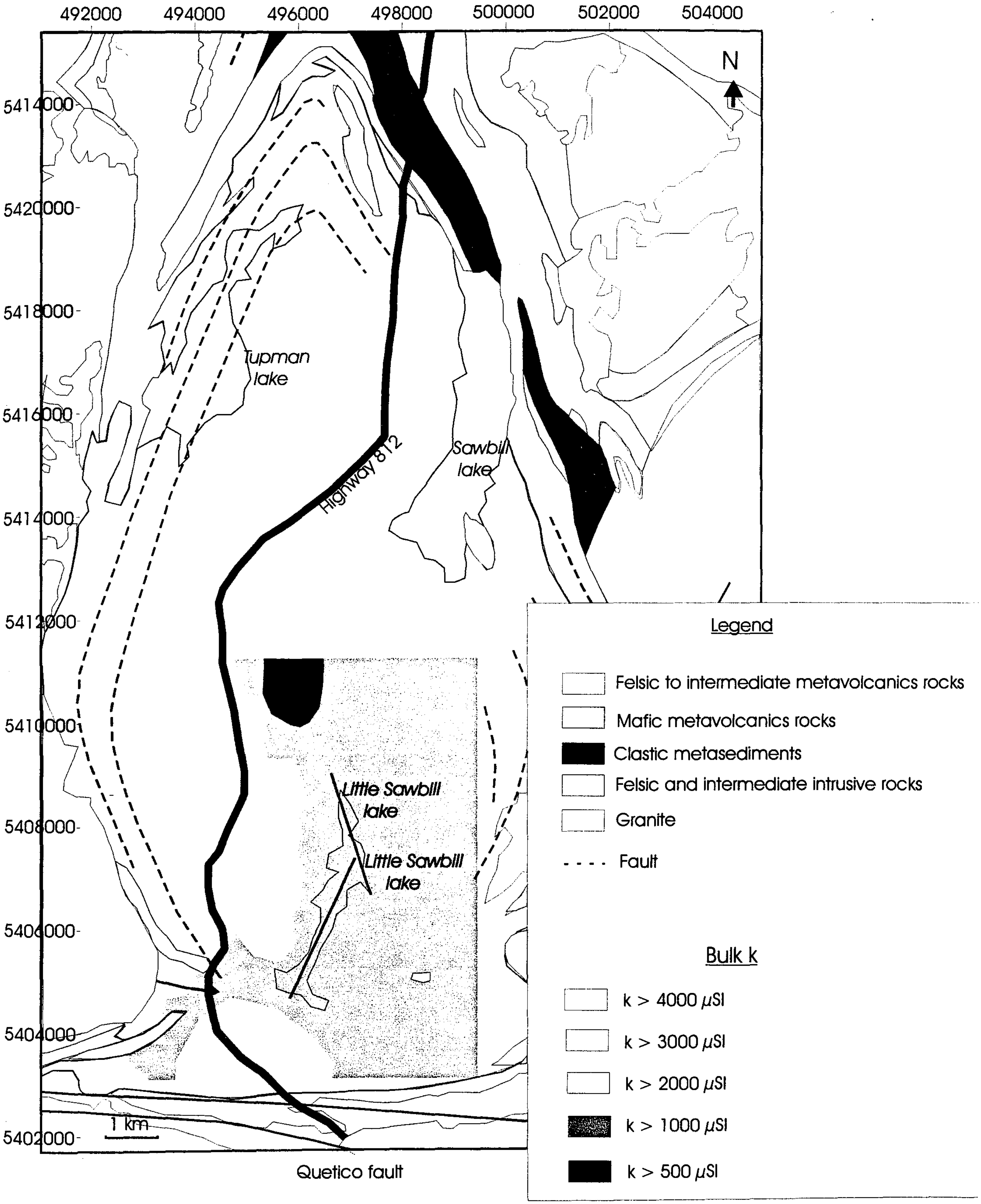

Figure VII.9, Map of bulk susceptibility ((k max + k int + k min)/3) of the Sawbill dome.

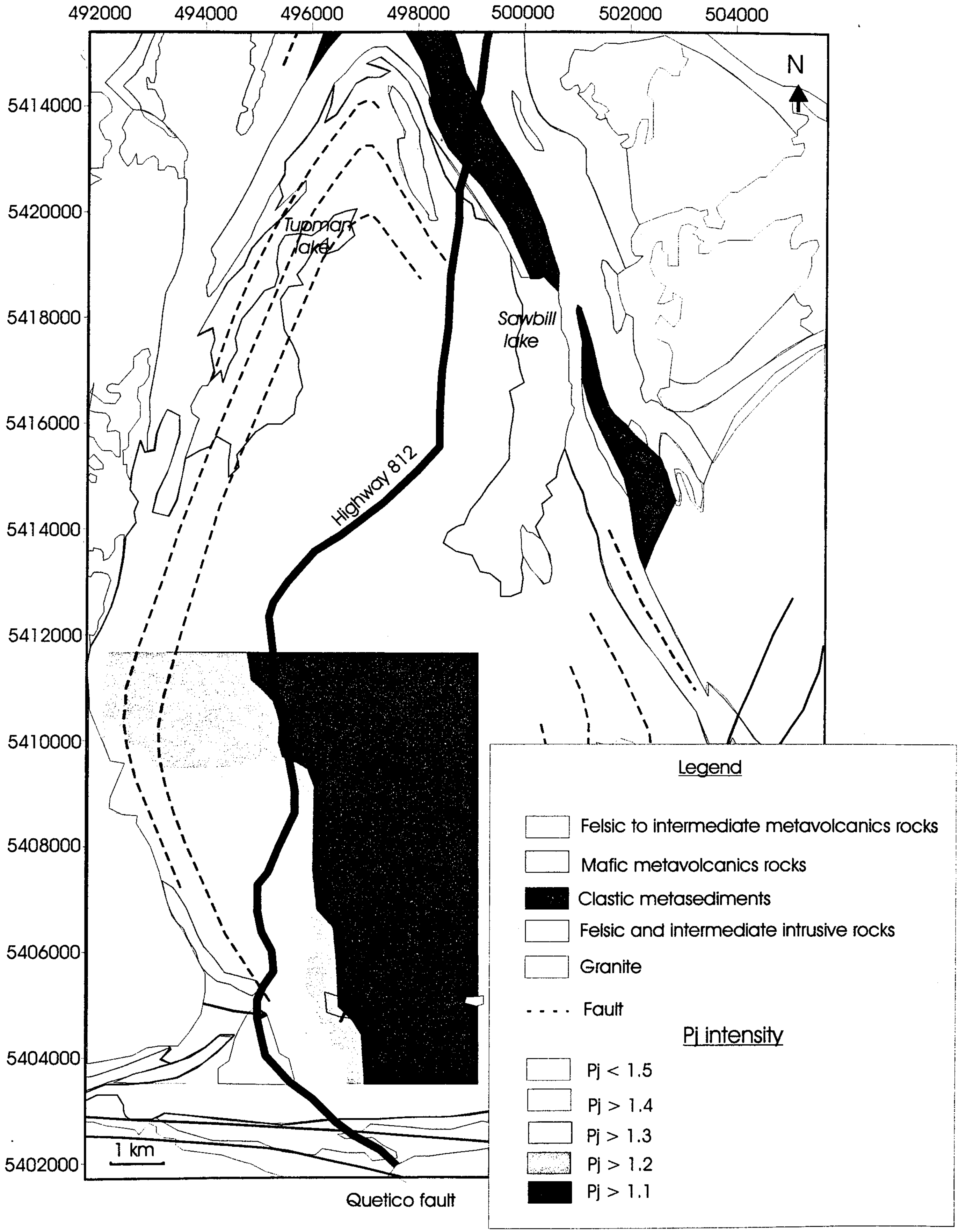

Figure VII.10. Map of AMS Pj (intensity of anisotropy of the AMS ellipsoid) of the Sawbill dome.

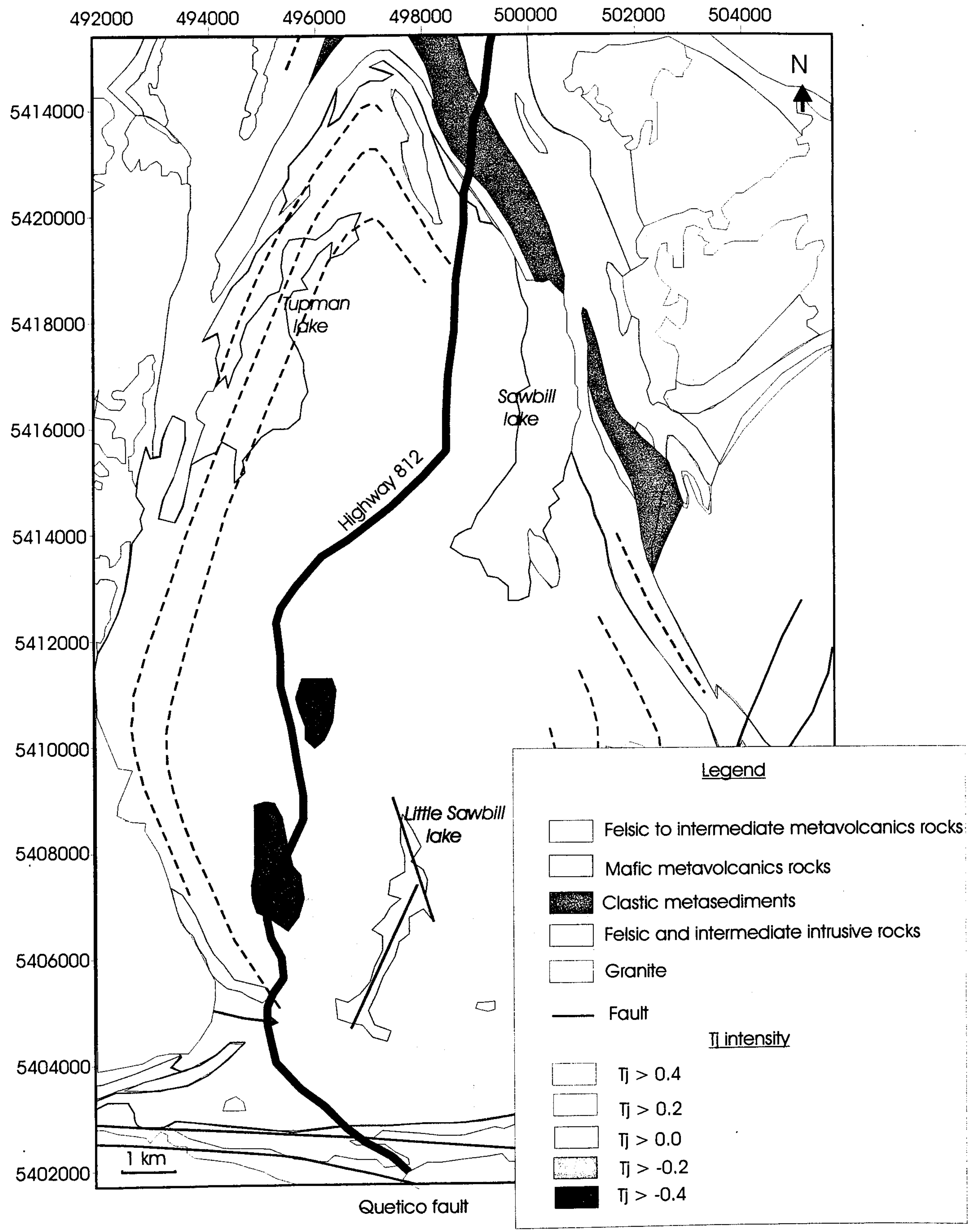

Figure VII.11. Map of AMS Tj (shape parameter of the AMS ellipsoid) of the Sawbill dome.

VII.3. Conclusion

Two groups of specimens have been differentiated: a first group with susceptibilities smaller than 1000 μSI having oblate fabrics and lower Pj. This group is located in the middle of the dome. The second group has susceptibilities greater than 1000 μSI with orthorombic fabrics and higher Pj: these specimens are located to the western border of the dome. The orientations-distribution of susceptibility axes are described by a prolate ellipsoid with a very well define magnetic lineation. This magnetic lineation does not correspond to the mineral foliation measured on the field. The tensors ellipses have an orthorhombic symmetry and therefore the orientations-distribution of the susceptibilities is related to a coaxial deformation. In the southern border of the dome, the specimens' fabrics and orientations have been affected by the movement of the Quetico fault. The majority of orientations of k max is horizontal in the southern margin of the dome and become more and more horizontal toward the middle of the dome.

VII.4.AMS Data of the Sawbill dome

samples	dec.	inc.	k. min. (μSI)	dec.	inc.	k. int. (μSI)	dec.	inc.	k. max (μSI)	bulk k. (μSI)	Pj	Tj
GBR008A	273	41	176	3	0	193	93	49	205	191	1.17	0.21
GBR008B	287	39	221	143	45	251	33	19	254	242	1.17	0.82
GBR008C	256	50	157	84	40	181	351	4	184	174	1.19	0.80
GBR009A	10	24	380	108	17	384	230	60	407	390	1.08	-0.72
GBR009B	356	13	835	92	24	850	240	62	887	857	1.06	-0.42
GBR009C	94	21	766	345	40	776	204	43	805	783	1.05	-0.45
GBR0010A	261	33	52	102	55	58	357	10	78	63	1.53	-0.46
GBR0010B	218	33	47	311	5	50	48	57	55	51	1.17	-0.36
GBR0010C	227	33	64	135	2	72	42	57	76	71	1.20	0.36
GRB0011A	204	41	6161	304	12	8118	47	47	10788	8355	1.76	-0.02
GBR0011B	189	40	3012	293	16	3483	40	46	4008	3501	1.33	0.02
GBR0011C	174	34	2665	279	20	2955	34	49	3875	3165	1.47	-0.45
GBR0012A	297	9	48	201	34	52	40	55	65	55	1.36	-0.45
GBR0012B	256	36	202	160	9	252	59	53	272	242	1.36	0.50
GBR0012C	287	20	69	183	34	75	42	49	78	74	1.14	0.31
GBR0013A	270	46	153	154	23	157	46	35	164	158	1.07	-0.14
GBR0013B	265	43	166	170	5	177	74	47	181	175	1.09	0.44
GBR0013C	254	44	126	149	16	132	44	42	138	132	1.09	0.10
GBR0014A	152	16	496	251	27	559	35	58	654	570	1.32	-0.14
GBR0014B	144	2	2236	235	23	2477	50	67	2920	2544	1.31	-0.23
GBR0014C	290	11	1280	195	28	1400	39	60	1630	1437	1.28	-0.26
GBR0015A	165	15	3696	21	71	4897	258	11	5029	4541	1.41	0.83
GBR0015B	158	10	2851	49	60	3900	254	28	4215	3655	1.77	0.60
GBR0015C	163	10	1066	4	80	1638	253	4	1826	1510	1.51	0.60
GBR0016A	169	18	690	59	46	1043	275	39	1197	977	1.78	0.50
GBR0016B	160	16	1354	50	49	1965	263	36	2473	1931	1.84	0.24
GBR0016C	152	14	1533	43	54	2137	251	33	2696	2122	1.77	0.18
GBR0016D	150	14	758	44	49	1016	252	38	1193	989	1.59	0.29
GBR0017A	164	11	155	72	12	192	295	73	214	187	1.39	0.33
GBR0017B	165	18	30	65	29	40	283	55	44	38	1.48	0.56
GBR0017C	166	12	274	67	34	356	273	53	375	335	1.40	0.66
GBR0017D	166	14	183	61	46	245	267	40	263	230	1.46	0.60
GBR0018A	134	8	766	229	27	817	29	62	1080	888	1.44	-0.63
GBR0018B	135	2	960	226	26	1093	40	64	1420	1158	1.49	-0.34
GBR0018C	139	12	780	237	34	913	34	53	1112	935	1.43	-0.11
GBR0019A	293	5	1669	201	25	2238	35	65	2562	2156	1.55	0.37
GBR0019B	98	1	2420	188	10	3374	5	80	3866	3220	1.62	0.42
GBR0019C	276	14	2486	185	6	3451	71	75	3767	3234	1.55	0.58
GBR0019D	272	3	966	181	13	1106	17	77	1261	1111	1.31	0.01
GBR0020A	279	3	367	188	15	413	18	75	490	423	1.34	-0.18
GBR0020B	257	6	816	165	16	938	7	73	1057	937	1.30	0.07
GBR0020C	278	18	3593	179	27	4920	38	56	5754	4755	1.62	0.33

samples	dec.	inc.	k. min. (µSI)	dec.	inc.	k. int. (µSI)	dec.	inc.	k. max (µSI)	bulk k. (µSI)	Pj	Tj
GBR0021A	278	20	2694	174	34	2776	32	50	3642	3037	1.40	-0.80
GBR0021B	286	1	2979	196	32	3391	17	58	3933	3435	1.32	-0.07
GBR0021C	142	17	3511	253	49	4071	39	36	5182	4255	1.48	-0.24
GBR0022A	280	29	28	147	51	30	24	24	33	30	1.17	-0.19
GBR0022B	317	5	23	219	60	28	50	29	31	27	1.37	0.41
GBR0022C	281	25	32	165	43	34	31	37	36	34	1.14	0.08
GBR0022D	282	17	24	171	49	26	25	36	28	26	1.20	0.23
GBR0023A	260	25	4458	162	16	4696	42	60	6175	5110	1.42	-0.68
GBR0023B	260	20	6054	164	16	6929	39	64	9200	7394	1.54	-0.36
GBR0023C	254	19	5822	157	19	7056	26	62	9454	7444	1.63	-0.21

The study of the Koenigsberger and the theoretical Koenigsberger ratio shows that the induced magnetization (the bulk susceptibility (sum of the AMS axes values divided by three) multiply with the constant of the Earth magnetic field) of the specimens is very often greater than their remanent magnetization (whether the natural remanent magnetization (NRM) in the case of the Koenigsberger ratio or the anhisteretic anisotropy of remanent magnetism (AARM) in the case of the theoretical Koenigsberger ratio): this result agree with the results of Pilkington and Percival (1999). The Koenigsberger ratio is less well defined than the theoretical Koenigsberger ratio in all the studied cases: this is true when the specimens are coming from specific complexes (plutons such as Trout lake, Barnum lake or McKenzie granite or gneissic domes such as the Sawbill dome) or when they are coming from granitic rocks of a region (Wabigoon belt or Minto Block). The relationship between the induced magnetization and the remanent one is characterized by a power law curve. This power law relation is better defined when the specimens have a wide range of remanent and induced magnetizations. The Koenigsberger ratio and the theoretical Koenigsberger ratio will first increase to tend to a maximum value when the induced magnetization and the remanent magnetization are small and will second gradually decrease when this maximum value (point of inflexion of the power law curve) is passed. Consequently, in each studied cases (except in Barnum lake granite case), the remanent magnetization and the induced magnetization relation is different before and after this point of inflexion. The induced magnetization is only dependent on the bulk susceptibility and the relation between the ARM intensity (sum of AARM axes divided by three) and bulk susceptibility (sum of AMS axes divided by three) is studied in the case of the McKenzie granite. It shows that they are also related to one another by a power law curve. As ARM intensity (sum of AARM axes divided by three) and the bulk susceptibility of the McKenzie granite are dependent on the ferromagnetic content of the specimens, this power law relation between the ARM intensity and the bulk susceptibility and its influence on the theoretical Koenigsberger ratio is due to a variation of magnetic property of the magnetite. This variation of property is not related to a difference of structure of the magnetite but probably to the interaction of magnetite grains' magnetic field with one another.

The McKenzie granite has a mean susceptibility (sum of all the bulk susceptibility divided by their numbers) greater than 2000 μSI and susceptibility of the specimens is consequently controlled by ferromagnetic minerals, which are magnetite. Three groups of specimens can be differentiated: one with bulk susceptibilities smaller than 500 μSI, a second one with bulk susceptibilities smaller than 6000 μSI and a third one with susceptibilities greater than 6000 μSI. The first group of specimens is found in the southern part of the granite. The second group of specimens is located preferentially in the northeastern part of the granite and in the southern part. The third group is located in the middle of the granite and in the western part. No real differences of fabric behaviors (shape and intensity of anisotropy of the AMS ellipsoid) between the three groups have been found. Although, AMS Pj is clearly proportional to the logarithm of the bulk susceptibility ((k max + k int + k min)/3) of the specimens. This relation between Pj and log bulk k is typical of granites controlled by their ferromagnetic content. The orientations-distribution of the AMS axes is defined by a prolate (L > S) ellipsoid with subvertical orientations of the AMS minimum axes and subhorizontal orientations of AMS maximum axes. The maps of AMS Tj and orientations of AMS minimum axes of the McKenzie granite permit to differentiate two groups of fabrics: specimens of areas where the orientations of AMS minimum axes are subhorizontal and oriented in the North-South direction have oblate fabrics; specimens of areas where the orientations of the AMS minimum axes are subvertical have prolate fabrics. The AMS non-normalized mean tensor, the orientations-distribution of the AARM axes and the AARM mean tensors (normalized and non-normalized) are described by an oblate ellipsoid (L<S). This result and the differenciation of two groups of fabrics shown by the AMS Tj map and the orientations of AMS minimum axes suggest that fabrics are divided in two groups. Both the AMS and the AARM orientations-distribution of axes are non-coaxial. The axes orientations cannot be used as kinematic indicators possibly because the orientations-distribution of AMS and AARM axes is non-coaxial and because a secondary fabric (metamorphic one) has overprinted a primary one (probably magmatic). The McKenzie granite is elongated in the NNE-SSW direction and is limited in the North by a fault suggesting that it is a concordant pluton emplaced in transcurrent context (the Southern part of the granite cannot be seen because it is submerged by the Lake Superior). No minerals fabrics can be clearly seen on the field: granitic look massive.

The Rice Bay dome bulk susceptibilities of specimens are clearly divided into two groups: a first group with very low bulk susceptibility (bulk $k \leq 100$ μSI) and a second group of specimens with bulk susceptibilities greater than 2000 μSI. The first group of specimens has a smaller intensity of anisotropy of AMS ellipsoid ($Pj < 1.5$) and the shape of their fabrics is preferentially described by an oblate ellipsoid (L<S). The second group

of specimens has a greater intensity of anisotropy of AMS ellipsoid (Pj > 1.5) and their fabrics have more a prolate shape (L>S): this group is controlled by its ferromagnetic content. The orientations-distribution of AMS axes of the Rice Bay dome are described by a prolate ellipsoid (L>S) with the not very well defined orientations of the AMS minimum axes and orientations of the maximum axes consistent with the orientations of the mineral lineations measured on the field: the magnetic fabrics reflect consequently the mineral fabric and the emplacement of the gneissic dome. The AMS mean tensors are described by an oblate fabric and the orientations-distribution of AMS and AARM axes is non-coaxial. The result of the mean tensors is consistent with the regional tectonic while the Rice Bay dome is elongated and has taken place in a transpressive basin limited in the North by the Quetico fault and in the South by the Seine River fault. The maps of the Rice Bay dome are very consistent with one another except for the map of orientation of AMS minimum axes showing a sigmoidal orientations of AMS maximum axes parallel to the axes of elongation of the dome. There is a decrease of the Pj from the center to the borders: these variations of Pj form elliptical areas whose the axis of elongation is more or less parallel to the orientation of the AMS maximum axes. The Tj (shape parameter of the AMS ellipsoid) is describes by a prolate ellipsoid in the center of the dome and tend to be more oblate in the Southwestern and Northeastern borders of the dome: these variations of Tj are also very similar to the directions of AMS maximum axes. This map is very similar to the bulk susceptibility map with smallest susceptibilities located in the center of the dome and tending to increase toward the Southwestern and Northeastern margins of the dome. The studied area of the Rice Bay dome is the apex of the dome. The orientations of the AMS maximum axes are very similar to theoretical model in figure

III.5. and as the dome has risen into ductile material, it can only be a diapir but this diapir have been clearly affected by regional stress and was still under ductile conditions when it has undergone the regional transpressive deformation. It is difficult to define if the diapir has risen and has undergone transpressive regional deformation under ductile conditions during two different tectonic events or if the rise of the gneiss is syntectonic with the transpressive regional deformation. Only one family of fabrics has been found and this suggests that the second hypothesis is more probable.

The Sawbill dome specimens are divided in two groups: a first group with bulk susceptibilities smaller than 1000 μSI with an oblate fabric and a smaller AMS Pj (around 1.3) and a second group with bulk susceptibilities greater than 1000 μSI with an orthorhombic ellipsoid ($L \approx S$) and a greater AMS Pj (around 1.5). This division in two groups can also be seen in the map of bulk susceptibility with the group of bulk susceptibilities smaller than 1000 μSI located in the center of the dome and the group of bulk susceptibilities greater than 1000 μSI in the border of the dome. The orientations-distribution of AMS axes is described by a prolate ellipsoid and is coaxial. The orientations of AMS maximum axes are very well defined and are subvertical and oriented toward the SW-NE and become more horizontal toward the center of the dome. In the southern border of the dome, fabrics of specimens are affected by the movement of the Quetico fault. The gradual decrease of inclination of the AMS maximum axes from the southern margin of the dome toward its center suggest that fabrics are due to an event related to the movement of the Quetico fault. The magnetic fabrics are not related to minerals fabrics (mineral foliation measured on the field) and therefore, the magnetic fabrics do not reflect the emplacement of the dome. The Sawbill dome is highly alterated and has undergone a granodiorization. The magnetic fabrics could reflect this granodioritization. The Sawbill dome has taken place under ductile conditions and therefore has risen by diapirism and has been affected by the emplacement of the adjacent domes.

References.

Arkani-Hamed, J., and Jolly, W. T., 1989. Generation of Archean tonalite. Geology, 17: 307-310.

Arth, J. G., and Hanson, G. N., 1975. Geochemistry and origin of the Early Precambrian crust of the north-eastern Minnesota. Geochim. Cosmochim. Acta, 39: 325-362.

Arth, J. G., Barker, F., Peterman, Z. E., and Friedeman, I., 1978. Geochemistry of the gabbro-diorite-tonalite-trondhjemite suite of south-west Finland and its implications for the origin of tonalite and trondhjemite magmas. J. Petrol., 19: 289-316.

Bonin, B., 1982. Ring complex granites and anorogenic magmatism. North Oxford Academic, 200 p.

Borradaile, G. J., 1988. Magnetic susceptibility, petrofabrics and strain – a review. Tectonophysics, 156: 1-20.

Borradaile G. J., and Werner T., 1994. Magnetic anisotropy of some phyllosilicates. Tectonophysics, 235: 233-248.

Borradaile, G. J., and Kehlenbeck, M. M., 1996. Possible cryptic tectono-magnetic fabrics in 'post-tectonic' granitoid plutons of the Canadian shield. Earth and Planet. Sci. Letters, 137: 119-127.

Borradaile, G. J., and Henry, B., 1997. Tectonic applications of magnetic susceptibility and its anisotropy. Earth Sci. Rev., 42: 49-93.

Borradaile, G. J., and Lagroix, F., 2001. Magnetic fabrics reveal Upper Mantle flow fabrics in the Troodos Ophiolite complex, Cyprus. J. of Struct. Geol., 23: 1299-1317.

Borradaile, G. J., 2001. Magnetic fabrics and petrofabrics: their orientation distributions and anisotropies. J. of Struct. Geology, 23: 1581-1596.

Bouchez, J. L., 1997. Granite is never isotropic: an introduction to AMS studies of granitic rocks. Kluwers Academic Publishers, pp. 95-112.

Bouhallier, H., Chardon, D., and Choukroune, P., 1995. Strain patterns in Archaean dome-and-basin structures: the Dharwar craton (Karnataka, South India). Earth and Planet. Sci. Letters, 135: 57-75.

Bowen, N. L., 1922. The behavior of inclusions in igneous magmas. J. of Geology: 30: 513-570.

Butler, R. F., 1992. Paleomagnetism: magnetic domains to geologic terranes. Dept. Geol., Univer. Arizona, Blackwell Scientific Publications, Boston: 319 p..

Castro, A., 1987. On granitoid emplacement and related structures: a review. Geol. Rundschau, 76: 101-124.

Card, K. D., 1990. A review of the Superior Province of the Canadian shield, a product of Archaean accretion. Precamb. Research, 48: 99-156.

Card, K. D., and Ciesielski, A., 1986. Subdivisions of the Superior Province of the Canadian shield. Geosci. Canada, 12: 5-13.

Chappell, B. W., and Stephens, W. E., 1988. Origin of infracrustal (I-type) granite magmas. Trans. of Roy. Soc. of Edimb. Earth Sci., 79: 71-86.

Clarke, D. B., 1992. Granitoid rocks. Department of Earth sciences, Dalhousie University, Halifax, Canada, Chapman and Hall: 279 p.

Clemens, J. D., and Mawer, C. K., 1992. Granitic magma transport by fracture propagation. Tectonophysics, 204: 339-360.

Collins, W. J., Beams, S. D., White, A. J. R., and Chappell, B. W., 1982. Nature and origin of A-type granites with particular reference to Southeastern Australia. Contrib. Mineral Petrol., 80: 189-200.

Condie, K. C., 1997. Contrasting sources for upper and lower continental crust: the greenstone connection. J. of Geology, 105: 729-736.

Creaser, R. A., Price, R. C., and Wormald, R. J., 1991. A-type granites: assessment of a residual–source model. Geology, 19: 163-166.

Cruden, A. R., 1988. Deformation around a rising diapir modeled by creeping flow past a sphere. Tectonics, 7: 1091-1101.

Cruden, A. R., 1990. Flow and fabric development during the diapiric rise of magma. J. of Geol., 98: 681-698.

Defant, M. J., and Kepezhinskas, P., 2001. Evidence suggests slab melting in arc magmas. Eos, Trans., Am. Geophy. Union, 82, n. 6: 1-68-69.

De Saint Blanquat, M., Tikoff, B., Teyssier, C., and Vigneresse, J. L., 1998. Transpressional kinematic and magmatic arcs. In: Continental transpressional and transtensional tectonics, J. Geol. Spec. Pub., 135: 327-340.

De Saint Blanquat, M., Law, R. D., Bouchez, J. L., and Morgan, S. S., 2001. Internal structure and emplacement of the Papoose flat pluton: an integrated structural, petrographic, and magnetic susceptibility study. GSA bulletin, 113 n.8: 976-995.

Eby, G. N., 1990. The A-type granitoids: a review of their occurrence and chemical characteristics and speculations on their petrogenesis. Lithos, 26: 115- 134.

England, R. W., 1990. The identification of granitic diapirs. J. of Geol. Soc. of London, 147: 931-933.

Flinn, D., 1956. On the deformation of the Funzie conglomerate, Fetlar, Shetland. J. Geol., 64: 480-505.

Guineberteau, B., Bouchez, J. L., and Vigneresse, J. L., 1987. The Mortagne granite pluton (France) emplaced by pull- apart along a shear zone: structural and gravimetric arguments and regional implication. Geol. Soc. of Am. Bull., 99: 763-770.

Grégoire, V., de Saint Blanquat, M., Nédélec, A., and Bouchez, J. L., 1995. Shape anisotropy versus magnetic interactions of magneite grains: experiments and application to AMS in granitic rocks. Geophys. Res. Letters, 22: 2765-2768.

Henry, B., 1983. Interpretation quantitative de l'anisotropie de susceptibilite magnetique. Tectonophysics, 91: 165-177.

Hudleston, P. J., Schultz-Ela, D., and Southwick, D. L., 1988. Transpression in an Archean greenstone belt, northern Minnesota. Can. J. of Earth Sci., 25: 1060-1068.

Johannes, W., and Holtz, F., 1996. Petrogenesis and experimental petrology of granitic rocks. Mineral and rocks, Springer-Verlag (eds), 335 p.

Kilpatrick, J. A., and Ellis, D. J., 1992. C-type magmas: Igneous charnokites and their extrusive equivalents. Trans. of the Royal Soc. of Edinburgh: Earth Sci., 83: 155-164.

Kimura, G., Ludden, J. N., Desrochers, J.-P., and Hori, R., 1993. A model of ocean-crust accretion for the Superior province, Canada. Lithos, 30: 337-355.

King, J., Banerjee, S. K., Marvin, J., and Ozdemir, O., 1982. A comparison of different magnetic methods for determining the relative grain size of magnetite in natural materials: some results from lake sediments. Earth and Planet. Sc. Letters, 59: 404-415.

Lagroix, F., and Borradaile, G. J., 2000. Magnetic fabric interpretation complicated by inclusions in mafic silicates. Tectonophysics, 325: 207-225.

Leblanc, D., Gleizes, G., Lespinasse, P., Olivier, P., and Bouchez, J. L., 1994. The Maladeta granite polydiapir, Spanich Pyrenees: a detailed magneto-structural study. J. Struct. Geol., 2: 223-225.

Mac Caffrey, K. J. W., 1992. Igneous emplacement in a transpressive shear zone: Ox mountain igneous complex. J. Geol. Soc. of London, 149: 221-235.

Marre, J., 1986. The structural analysis of granite rocks. North Oxford academic, 123 p.

Marsh, B. D., 1982. On the mechanics of igneous diapirism, stoping and zone melting. Am. J. Sci., 282: 808-895.

Martin, H., 1994. The archaean grey gneisses and the genesis of continental crust. Archean Crustal Evolution, K. C. Kondie (editor), Dev. In Precambrian Geol., 11: 205-259.

Miller, R. B., and Paterson, S. R., 1999. In defense of magmatic diapirs. J. of Struct. Geol., 21: 1161-1173.

Nédélec, A., Nsifa, E. N., and Martin, H., 1990. Major and trace element geochemistry of the Archaean Ntem pluotnic complex (South Cameroon): petrogenesis and crustal evolution. Precambrian Res., 47: 35-50.

Olivier, P., De Saint Blanquat, M., Gleizes, G., and Leblanc, D., 1997. Homogeneity of granite fabrics at the metre and dekametre scales. Granite: From segregation of melt to emplacement fabrics, Kluwer Academic Publishers, J. L. Bouchez, D. H. W. Hutton and W. E. Stephens (eds.): 113-128.

Park, R. G., 1983. Foundations of structural geology. Chapman and Hall, Blackie, 135 p.

Paterson, S. R., and Vernon, R. H., and Tobish, O. T., 1989. A review of criteria for the identification of magmatic and tectonic foliation in granitoid. J. of Struct. Geol., 11: 349-363.

Paterson, S. R., and Vernon, R. H., 1995. Bursting the buble of ballooning plutons: a return to nested diapir diapirs emplaced by multiple processes. Geol. Soc. of Am. Bull., 197: 1356-1380.

Patino-Douce, A. E., 1999. What do experiments tell us about the relative contributions of crust and mantle to the origin of granitic magmas? Understanding granites: integrating new and classical techniques, J. Geol. Spec. Pub., 168: 55-75.

Percival, J. A., and Williams, H. R., 1989. Late Archean Quetico accretionary complex, Superior Province, Canada. Geology, 17: 23-25.

Petford, N., and Atherton, M. P., 1991. Granitoid emplacement and deformation along a major crustal lineament: the Cordillera Blanca, Peru. Tectonophysics, 205: 171-185.

Petford, N., 1995. Segregation of tonalitic-trondhjemitic melts in the continental crust: the mantle connection. J. Geophys. Res., 100: 15735-15743.

Pilkington, M., and Percival, J. A., 1999. Crustal magnetization and long-wavelength aeromagnetic anomalies of the Minto block, Quebec. 104,n. B4: 7513-7526.

Pitcher, W. S., 1979. The nature, ascent and emplacement of granitic magma. J. Geol. Soc. Lond., 136: 627-662.

Poulsen, K. H., Borradaile, G. J., and Kehlenbeck, M. M., 1980. An inverted Archean succession at Rainy lake, Ontario. Can. J. Earth Sci., 17: 1358-1369.

Ramberg, H., 1981. Gravity, Deformation and the Earth's crust. 2nd ed., Academic press, London: 452 p..

Rapp, R. P., Watson, E. B., and Miller, C. F., 1991. Partial melting of amphibolite/eclogite and the origin of Archaean trondhjemites and tonalities. Precambrian Res., 51: 1-25.

Rochette, P., 1987. Magnetic susceptibility of the rock matrix related to magnetic fabric studies. J. of Struct. Geol., 9: 1015-1020.

Rogers, J. A., 1979. The Southeastern margin of the MacKenzie granite, Northwestern Ontario. HBsc. Lakehead University, 68p..

Roman-Berdiel, T., Gapais, D., and Brun, J. P., 1995. Analogue models of laccolith formation. J. of Struc. Geol., 17: 1337-1346.

Sanderson, D. J., and Marchini, R. D., 1984. Transpression. J. of Struct. Geology, 6: 449-458.

Sasaki, A., and Ishihara, S., 1979. Sulfur isotopic composition of the magnetite-series and ilmenite-series granitoids in Japan. Contr. Min. Petro., 107: 107-115.

Shand, S. J., 1947. Eruptive rocks. Their genesis, composition, classification, and their relation to ore-deposit. 3rd ed. J. Wiley and sons, New York: 488 p.

Schwerdtner, W. M., 1989. Structural tests of diapir hypotheses in Archean crust of Ontario. Can. J, of Earth Sci., 27: 387-402.

Schwerdtner, W. M., Stott, G. M., and Sutcliffe, R. H., 1983. Strain of crescentic granitoid plutons, Ontario. Can. J. Earth Sci., 5: 419-430.

Shirey, S. B., and Hanson, G. N., 1986. Mantle heterogeneity and crustal recycling in Archean granite-greenstone belts: evidence from Nd isotopes and trace elements in the Rainy Lake area, Superior Province, Ontario, Canada. Chim. et Cosmochim. Acta, 50: 2631-2651.

Smithies, R. H., 2000. The Archaean tonalite-trondhjemite-granodiorite (TTG) series is not an analogue of Cenozoic adakite. Earth and Planet. Sci. Letters, 182: 115-125.

Stephenson, A., Sadikun, S., and Potter, D. K., 1986. A theoretical and experimental comparison of the anisotropies of magnetic susceptibility and remanence in rocks and minerals. Geoph. J. of the Royal Astronomical Society, 84, 185-200.
Stern, C. R., and Hanson, G. N., 1991. Archaean high-Mg granodiorite: a derivative of Light rare Earth enriched monzodiorite of mantle origin. J. Petrology, 32: 201-238.

Tarling, D.H., Hrouda, F., 1993, The magnetic anisotropy of rocks. Eds Chapman & Hall. 217 pp.

Werner, T., and Borradaile, G. J., 1996. Paleoremanence dispersal across a transpressed Archean terrain: deflection by anisotropy or by late compression? J. of Geoph. Research, 101-B3: 5531-5545.

White, A. J. R., and Chappell, B. W., 1983. Granitoid types and their distribution in the Lachlan fold belt, Southeastern Australia. In Roddick, J. A. (ed.) Circum-Pacific Plutonic terranes, Mem. Geol. Soc. Am., 159: 21-34.

White, A. J. R., and Chappell, B. W., 1988. Some supracrustal (S-type) granites of the Lachlan fold belt. Trans. of Roy. Soc. of Edimb. Earth Sci., 79: 169-181.

Williams, H. R., 1989. Subprovince accretion tectonics in the south-central Superior Province. Can. J. Earth Sci., 27: 570-581.